A.I. Alikhanyan National Science Laboratory
(Yerevan Physics Institute)

Hazaravard M. Ghumaryan

Pythia8 Monte Carlo Generator Tuning for the Belle II Experiment

Thesis

for acquiring the degree of candidate of physico-mathematical sciences in division 01.04.16. "Nuclear, elementary particles and cosmic ray physics"

Supervisor: Dr. Gevorg A. Karyan

YEREVAN - 2024

List of Figures

List of Tables

Contents

Chapter 1

Introduction

The Belle II experiment [1], conducted at the High Energy Accelerator Research Organization (KEK) in Japan, represents a major advancement in the field of particle physics. Building upon the legacy of the original Belle experiment, Belle II aims to explore rare and previously unobserved phenomena in particle physics, including violations of CP symmetry and potential signals of new physics beyond the Standard Model. To achieve these ambitious goals, Belle II relies on a sophisticated array of detectors and a high-luminosity accelerator, which together generate an extensive dataset of high-precision particle collisions. Central to the analysis of this data is the use of Monte Carlo (MC) simulations [2], which model the complex interactions and behaviors of particles in high-energy collisions. The Pythia8 Monte Carlo generator [3] is one of the most widely used tools in particle physics for such simulations. It provides theoretical predictions by simulating the particle interactions according to various models and parameters. The accuracy of these simulations, however, is contingent upon the precision of the model parameters, which must be carefully tuned to match experimental data. The tuning of Pythia8 parameters is a critical process in ensuring that the simulations accurately reflect real-world particle interactions. This involves adjusting the generator's parameters to achieve the best possible agreement between the simulated data and the experimental observations. Proper tuning not only enhances the accuracy of the simulations but also ensures that subsequent data analyses and interpretations are reliable. The Pythia8 Monte Carlo generator is a pivotal tool in the field of high-energy physics, widely utilized for simulating particle collisions and interactions in various experimental settings. Developed by Torbjörn Sjöstrand and collaborators, Pythia8 is the latest version of the Pythia series, which has been a cornerstone in event generation for over four decades. Its primary role is to model the outcomes of high-energy particle collisions by providing theoretical predictions that can be compared with experimental data. Pythia8 is renowned for its extensive capabilities in simulating a range of physical processes that occur in particle collisions. These processes include the production and decay of particles, parton showers, and hadronization. The generator employs a variety of theoretical models and parameterizations to simulate these phenomena, making it a versatile tool for analyzing different aspects of particle interactions. At the heart of Pythia8's functionality is its ability to handle complex event generation through a combination of multiple sub-models. The generator incorporates a range of physics processes, including hard scattering events, multiple parton interactions, and underlying event simulation. These processes are governed by parameters that describe the underlying physical theories and experimental observations. Accurate tuning of these parameters is crucial for ensuring that the generated events closely match real experimental data. Pythia8 includes several key features that enhance its utility for high-energy physics research. It provides detailed models for parton distribution functions, which describe the distribution of quarks and gluons inside hadrons. The generator also includes sophisticated algorithms for simulating the evolution of parton showers, which are essential for modeling the complex fragmentation processes that occur after high-energy collisions. Additionally, Pythia8 incorporates hadronization models that convert partons into hadrons, reflecting the final state of particle interactions. One of the strengths of Pythia8 is its flexibility and configurability. Researchers can adjust numerous parameters to refine the simulation and tailor it to specific experimental conditions. This ability to customize the simulation makes Pythia8 an invaluable tool for a wide range of experiments, from collider studies to fixed-target experiments. In the context of the Belle II experiment, Pythia8 plays a crucial role in providing theoretical predictions for particle collisions at the SuperKEKB accelerator. The Belle II experiment aims to explore rare decay processes and phenomena beyond the Standard Model, requiring accurate simulations to interpret complex data. By using Pythia8, researchers can generate event samples that help in understanding particle interactions, testing theoretical models, and extracting meaningful results from experimental data. The tuning of Pythia8 parameters is an essential aspect of using the generator effectively. To ensure that the simulations align closely with experimental data, parameters must be carefully adjusted based on sensitivity analyses and comparisons with actual experimental results. This tuning process helps to minimize discrepancies between simulated and observed data, thereby improving the accuracy and reliability of the simulations. In this thesis, the tuning of the Pythia8 Monte Carlo generator for the Belle II experiment was conducted using the Professor2 package [4], a sophisticated tool designed for optimizing complex models in high-energy physics. The Professor2 package offers advanced capabilities for parameter optimization, which are essential for aligning Monte Carlo simulations with experimental data. The Professor2 package is an integral part of the tuning process due to its ability to handle multi-parameter optimization efficiently. The tuning process begins with the initialization of parameters within the Professor2 framework. This involves setting up the parameters that will be optimized and conducting a sensitivity analysis to identify which parameters have the most significant impact on the simulation results. Sensitivity analysis is a critical step as it helps to prioritize the parameters that require adjustment, allowing the tuning process to focus on the most influential variables. Once the parameters are initialized, Professor2 employs a range of optimization algorithms to explore the parameter space. These algorithms include grid search, gradient-based optimization, and evolutionary methods. Each of these techniques is used to iteratively adjust the parameters, with the goal of minimizing discrepancies between the simulated data and experimental observations. The grid search method systematically varies parameters within predefined ranges, while gradient-based methods use information about how parameters affect the simulation outcomes to make more targeted adjustments. Evolutionary algorithms apply principles of natural selection to explore the parameter space and identify optimal values. As parameters are adjusted, the impact on simulation results is continuously evaluated through comparisons with experimental data. Professor2 provides tools for assessing the quality of the fit between simulated and observed data, helping to determine whether further adjustments are needed. This iterative evaluation process involves refining the parameters until the simulations achieve a high degree of agreement with the experimental results. The optimized parameters are then integrated into the Pythia8 Monte Carlo generator, and new simulations are performed using these refined values. This step is crucial for validating the effectiveness of the tuning process [5], as it ensures that the adjustments lead to improvements in simulation accuracy. The results of these simulations are analyzed to confirm that the tuned parameters have achieved the desired alignment with the experimental data. The primary goal of using Professor2 in the tuning process is to enhance the precision and accuracy of the Monte Carlo simulations for the Belle II experiment. By optimizing the Pythia8 parameters, the tuning process aims to reduce discrepancies between simulated and experimental data, improve the overall quality of the simulations, and support the exploration of rare phenomena and theoretical models.

1.1 Motivation

The motivation for tuning the Pythia8 event generator for the Belle II experiment arises from the necessity to accurately describe model-dependent processes such as hadronization, parton showers and etc. This tuning aims to identify the minimum set of free parameters required to effectively represent these processes, ensuring that the selected parameters possess sufficient sensitivity to capture the relevant physics observables of interest. By minimizing the number of parameters in the tuning list, we aim to avoid complications in the optimization stage, which may arise due to correlations between parameters. However, it is essential that the chosen parameters retain enough sensitivity to accurately describe the physics observables. To achieve this, correlations between parameters are examined using Belle II data. This analysis helps identify parameters that have significant impact on the observables while minimizing redundancy. Comparison between experimental data and Monte Carlo simulations is performed using statistical tests [6] such as the Kolmogorov-Smirnov and Student's t-tests. These tests help assess the agreement between the simulation and experimental data. Preliminary sensitivity checks are conducted using the Professor2 package, focusing on parameters' impact on specific observables, such as η meson multiplicities. These studies aid in identifying the most sensitive parameters that should be included in the tuning list. Similar sensitivity studies should be conducted for other physics observables to ensure comprehensive tuning. It is crucial to compare the results obtained from different statistical tests systematically. Any differences between the tests should reflect the sensitivity of each method, providing confidence in the chosen parameter set's ability to accurately describe the physics observables of interest. Historically, the process of constraining free parameters in multi-parameter models has relied on the "change-check" method. This approach involves altering parameters individually and assessing their impact on the desired physics observables. However, as systems grow more complex with an increasing number of free parameters, this method becomes impractical and fails to consider parameter correlations effectively. In contemporary research, the state-of-the-art approach involves parameterizing the generator behavior by simultaneously adjusting multiple parameters. This is achieved through fitting the generator response with polynomials for each physics observable included in the tuning process. This advanced methodology offers a more comprehensive understanding of the interplay between parameters and their collective influence on the simulated outcomes. In high-energy physics, the parameterization of Monte Carlo (MC) simulations plays a crucial role in accurately modeling complex physical processes. This process allows researchers to fine-tune the simulations to align with experimental data, thereby enhancing the reliability of the predictions made by the MC generators. Effective parameterization enables the identification of the most influential parameters, which can significantly impact the results and interpretations of particle collision events. In this thesis, we delve into this modern approach, exploring its applications and implications for refining Monte Carlo simulations in high-energy physics, with a specific focus on enhancing the accuracy and efficiency of the tuning process for complex systems like the Belle II experiment.

$$MC_b(p) \approx f^b(p) = \alpha_0^b + \sum_i \beta_i^{(b)} p'_i + \sum_{i \leq j} \gamma_{ij}^{(b)} p'_i p'_j \tag{1.1}$$

In Equation (1.1), MC_b represents the true response of the Monte Carlo (MC) generator within a specific bin b, while $f^b(p)$ denotes a collection of functions modeling the true MC response for each bin b, contingent upon changes in the parameter vector $\mathbf{p}$. The parameter vector $\mathbf{p}'$, defined as $\mathbf{p}' = \mathbf{p} - \mathbf{p}_0$, represents the deviation of the parameter vector from its nominal value $\mathbf{p}_0$. To ascertain the optimal, or "tuned," values of the parameters, the response function is subjected to minimization with respect to a reference sample. This minimization process is achieved through χ^2 minimization, as delineated in equation (2). This approach entails minimizing the discrepancy between the observed outcomes and the expected outcomes predicted by the model, thereby refining the parameter values to best align with the experimental data.

$$\chi^2(p) = \sum_O \omega_O \sum_{b \in O} \frac{(f^b(p) - R_b)^2}{\Delta_b^2} \tag{1.2}$$

where R_b is the reference value for bin b, Δ_b is the total uncertainty of the bin b and ω_O is a statistical weight for each observable. Recent experimental findings have sparked increased modeling endeavors within the theoretical community, driving efforts to refine existing models and parameters. Despite Pythia's extensive validation against data from the LHC, Belle, and Belle II experiments, its calibration against e^+e^- colliders has remained unchanged since 2009. This reliance on an undocumented tuning process, facilitated by the Professor tool, necessitates reevaluation. In this study, we tackle this challenge by employing the Pythia8 Monte Carlo event generator within the Belle II analysis framework, aiming to update and enhance its constraints for e^+e^- colliders. The thesis involved different stages and studies, addressing both technical issues and physics, that contributed to fine-tuning the Pythia8 Monte Carlo generator. The technical part included implementing and automating the necessary packages, developing algorithms for the desired studies while handling multiparameter files, and writing custom bash scripts to automate and link all the code together. In terms of physics, the work involved conducting Monte Carlo studies using both Pythia6 and Pythia8 generators. These studies were compared with experimental data to ensure accuracy. The analysis was performed at both the generator level, where detector effects were not considered, and the reconstruction level, where the impact of detectors on the data was accounted for. This comprehensive approach ensured a robust understanding and validation of the physics involved in the tuning process. It should be noted that, until now, no dedicated tuning has been performed for electron-positron beams, which would best represent the fit between Monte Carlo simulations and experimental data. Comparisons were made between the published tuning results of the Old Belle experiment, as well as references in internal notes, and the experimental data. These comparisons showed that the expected improvements were not evident, highlighting the importance of achieving proper tuning specifically for electron-positron beams. Multi-parameter tuning in high-energy physics experiments presents significant challenges, particularly in terms of computational resources and the complexity of inter-parameter relationships. The tuning process, which involves optimizing multiple parameters simultaneously to fit experimental data, is computationally intensive, requiring substantial CPU time and disk space. As the number of parameters increases, the complexity grows exponentially, leading to a combinatorial explosion of possible configurations that need to be evaluated. This not only increases the time required for each tuning iteration but also places considerable demands on storage for intermediate and final results. Moreover, the correlations between parameters add another layer of difficulty. Parameters are often interdependent, meaning that changes in one parameter can affect others in non-linear and non-intuitive ways. This makes it challenging to isolate the impact of individual parameters and can lead to local minima in the optimization process, where the tuning algorithm may converge on suboptimal solutions. The presence of strong correlations requires more sophisticated techniques, such as global optimization methods, to properly explore the parameter space and achieve accurate tuning. These challenges necessitate the development of efficient algorithms and strategies to manage computational resources effectively while ensuring that the tuning process converges to the correct global minimum. To address challenges related to disk space and CPU time, the multi-parameter tuning was performed using a global grid network. This network connects many computers around the world, allowing the workload to be distributed across multiple systems. This approach significantly reduces the strain on any single computer and helps manage the large volume of data involved in the tuning process. The algorithms were designed to generate the smallest possible files to minimize data storage and transfer needs. This optimization is crucial for efficient use of the grid network, which has limitations on both bandwidth and storage. By keeping file sizes small, we can ensure faster data transfers and reduce the demand on network resources. Additionally, the data statistics were selected to fit within the grid's traffic constraints. This careful selection ensures that the amount of data generated and transmitted does not exceed the grid's capacity, which helps avoid potential bottlenecks and ensures smoother operation. Overall, these strategies allow the tuning process to be conducted efficiently within the global grid network's constraints. In preparation for the main tuning phase, a series of Pythia8 parameter sensitivity tests were performed. These tests aimed to identify which parameters had the greatest impact on the simulation outcomes. By focusing on these sensitive parameters, the tuning process could be streamlined to target the most influential factors. The next step involved comparing Monte Carlo data generated with the default Pythia8 parameter settings to experimental data.

This comparison revealed discrepancies between the simulation and observed results, highlighting areas where tuning was necessary. Following this initial assessment, the results obtained with the default Pythia8 settings were compared to those from previous Belle tuning parameters. This comparison was critical for evaluating whether the previous parameter adjustments provided any improvements in fitting the variables of interest. Analyzing these differences helped determine whether the existing tuning parameters needed further refinement. To validate the accuracy of the Pythia8 simulations, adjustments were made based on reference data. This validation process involved checking the consistency of the simulation results with known reference values to ensure reliability. Additionally, the role of various quark types was examined by analyzing stacked histograms. This analysis helped to understand how different quark interactions affected the simulation results and provided insights into the contributions of each quark type. Ultimately, the Pythia8 model was tuned based on the findings from the sensitivity tests, comparisons with previous parameters, and validation against reference data. The tuned model was then compared with experimental data to evaluate the effectiveness of the adjustments. This final comparison aimed to ensure that the simulation results aligned more closely with observed data, thus improving the overall accuracy of the Pythia8 model in replicating experimental conditions. All results included in this thesis were regularly presented at Collaboration meetings. These presentations facilitated ongoing discussions and feedback from fellow researchers. To further validate the tuning, Monte Carlo files were generated based on the results and distributed to all members of the collaboration. Each member tested these files with their own variables of interest, ensuring a comprehensive evaluation of the findings across different research perspectives. The collaborative approach not only helped to validate the results but also enriched the analysis by incorporating diverse insights and expertise from various members of the research team. The impact of the Monte Carlo files on different variables was carefully examined, contributing to a robust and well-rounded assessment of the tuning process. Detailed accounts of these collaborative efforts, including feedback received and subsequent refinements, are thoroughly documented in the thesis.

Chapter 2

Belle II Experiment

2.1 SuperKEKB Colider

SuperKEKB, an asymmetric-energy electron–positron double-ring collider, represents a groundbreaking advancement in particle physics research. Its construction involved the upgrading of the renowned KEKB B-Factory [7], which had previously operated from 1998 to June 2010. During its operational tenure, KEKB achieved the remarkable feat of attaining the world's highest luminosity, reaching an impressive value of $2.11 \times 10^{34}\,\mathrm{cm}^{-2}\mathrm{s}^{-1}$. The culmination of this achievement was the accumulation of a total integrated luminosity of $1.04\,\mathrm{ab}^{-1}$ by the Belle detector. The design luminosity of SuperKEKB is set at $8 \times 10^{35}\,\mathrm{cm}^{-2}\mathrm{s}^{-1}$ a monumental leap of 40 times higher than its predecessor, KEKB. The primary objective is to accumulate an integrated luminosity of $50\,\mathrm{ab}^{-1}$, thus laying the groundwork for groundbreaking discoveries and advancements in particle physics research. The SuperKEKB collider complex comprises a 7 [GeV] electron ring, referred to as the high-energy ring (HER), and a 4 [GeV] positron ring, known as the low-energy ring (LER). Additionally, the complex includes an injector linear accelerator (linac) and a 1.1 [GeV] positron damping ring (DR), as illustrated in Fig. 1.

To achieve its exceptionally high luminosity, SuperKEKB underwent substantial upgrades to its HER, LER, and final-focus system, building upon the foundation laid by the KEKB accelerator. The asymmetric-energy design of SuperKEKB is aimed at measuring time-dependent CP violation in the B meson system. The Belle II experiment is the next step in a series of collider experiments focused on tudying B mesons. Located at KEK in Tsukuba, Japan, Belle II follows the original Belle

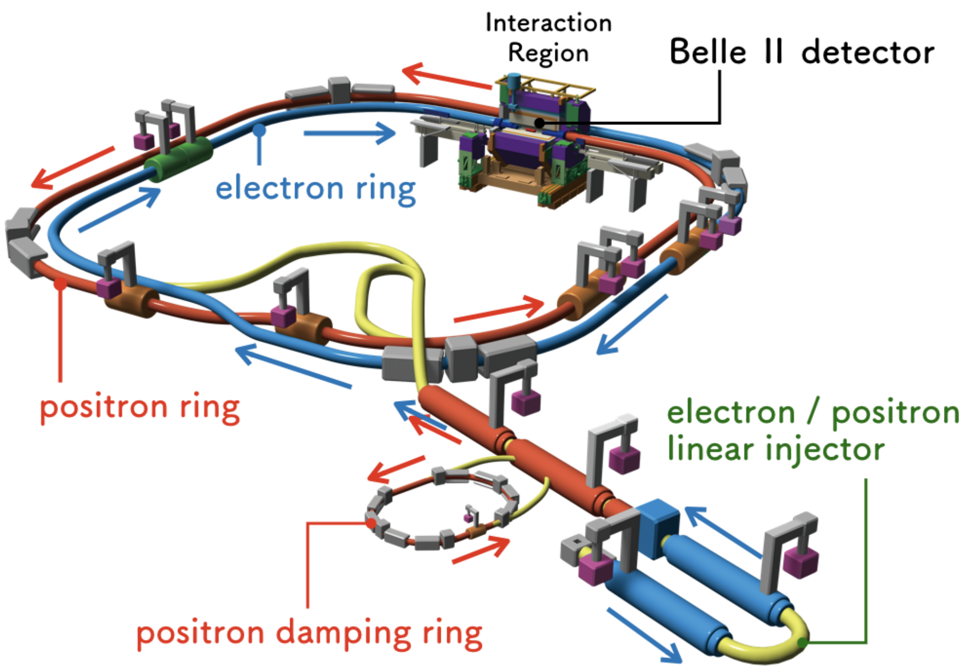

Figure 2.1: Schematic view of SuperKEKB: electron and positron rings.

experiment and works with the SuperKEKB accelerator. This advanced facility features an asymmetric electron-positron collider, with a High Energy Ring (HER) for electrons at 7 [GeV] and a Low Energy Ring (LER) for positrons at 4 [GeV]. With a goal to achieve a peak luminosity of $\mathcal{L} = 4.71 \times 10^{34}$ cm^{-2} s^{-1} [8], Belle II aims to surpass the capabilities of its predecessor, i.e. KEKB, by a factor of 40.
The main characteristics of the Belle II detector can be outlined as follows:

- Exceptional vertex resolution of approximately 50μm.
- Very high reconstruction efficiencies for charged particles, accommodating momenta as low as a few hundred [MeV/c], with enhanced efficiency for those down to 50 [MeV/c].
- Outstanding momentum resolution spanning the entire kinematic spectrum of the experiment, up to approximately 8 [GeV/c].
- Precise measurement capabilities for photon energy and direction across a range from a few tens of [MeV] to around 8 [GeV], with effective detection starting from 30 [MeV].

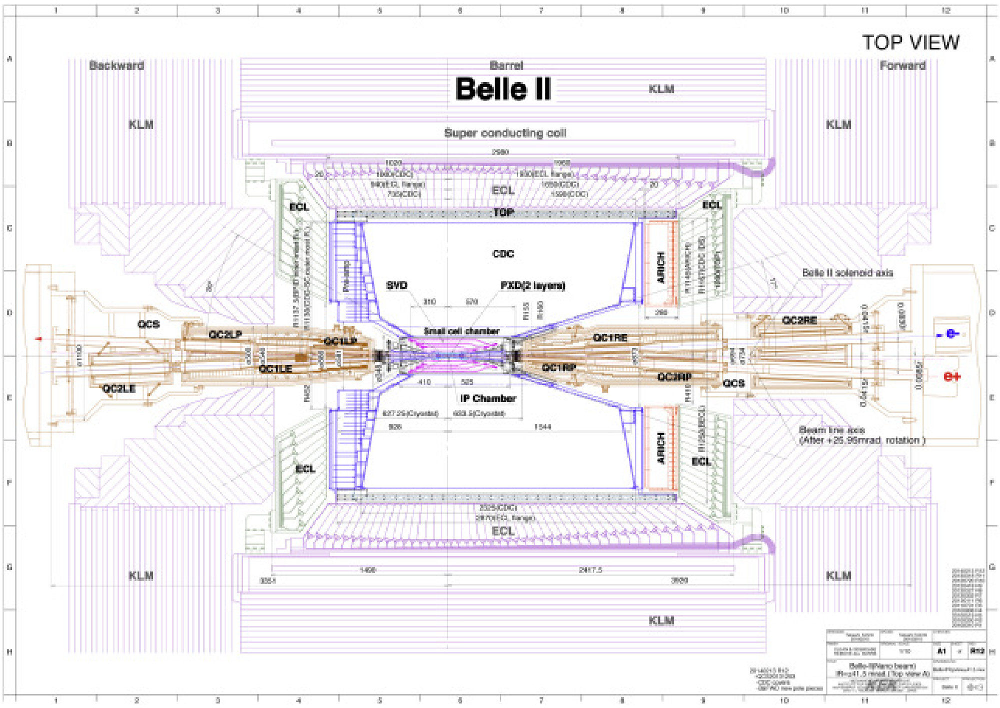

Figure 2.2: Top view of the Belle II spectrometer.

- A highly efficient particle identification system capable of discerning pions, kaons, protons, electrons, and muons throughout the experiment's kinematic range.
- Comprehensive coverage of (almost) the entire solid angle.
- Swift and efficient trigger system implementation, coupled with a data acquisition system adept at handling substantial data volumes.

The z-axis asymmetry in Belle II detector design responds to the unique collision dynamics, where both the center-of-mass frame and the flight paths of produced B mesons are directed towards the forward part of the detector. This forward orientation causes a Lorentz boost to the B mesons, effectively elongating their flight paths within the detector. Consequently, longer flight paths result in enhanced resolution on lifetimes, enabling more accurate measurements. This arrangement prompts a division of the angular acceptance into three distinct regions based on polar angles: the Forward, Barrel, and Backward regions. Polar angle θ represents the angle in the (x, z)-plane concerning the z-axis. Specifically, the Forward region spans angles from 17° to 30°, the Barrel region covers angles from 30° to 125°, and the Backward region extends from 125° to 150°. Belle II is designed with a primary focus on capturing the decay products of B mesons, given their extremely short lifetimes. Its structure consists of cylindrical layers surrounding the Interaction Point (IP), where particle collisions occur. Within the Belle II detector, distinct sub-components serve specialized purposes in measuring various particle properties. Notably, the tracking sub-detectors are dedicated to determining particle momentum and identifying decay vertices accurately. Complementing these are particle identification sub-detectors, which classify particle types, and a calorimeter responsible for reconstructing photon and electron energies. The detector comprises a beam pipe and a series of sub-detectors arranged from the innermost to outermost layers, as depicted in Figure x. These sub-detectors include the Vertex Detector (VXD), which consists of the Pixel Vertex Detector (PXD) and the Silicon Vertex Detector (SVD). Following the VXD is the Central Drift Chamber (CDC), succeeded by the Time of Propagation Counter (TOP), the Aerogel Rich Detector (ARICH), the Electromagnetic Calorimeter (ECL), and finally, the KLong and Muon Detector (KLM). Each sub-detector fulfills a specific function, collectively providing vital data necessary for reconstructing B meson decays.

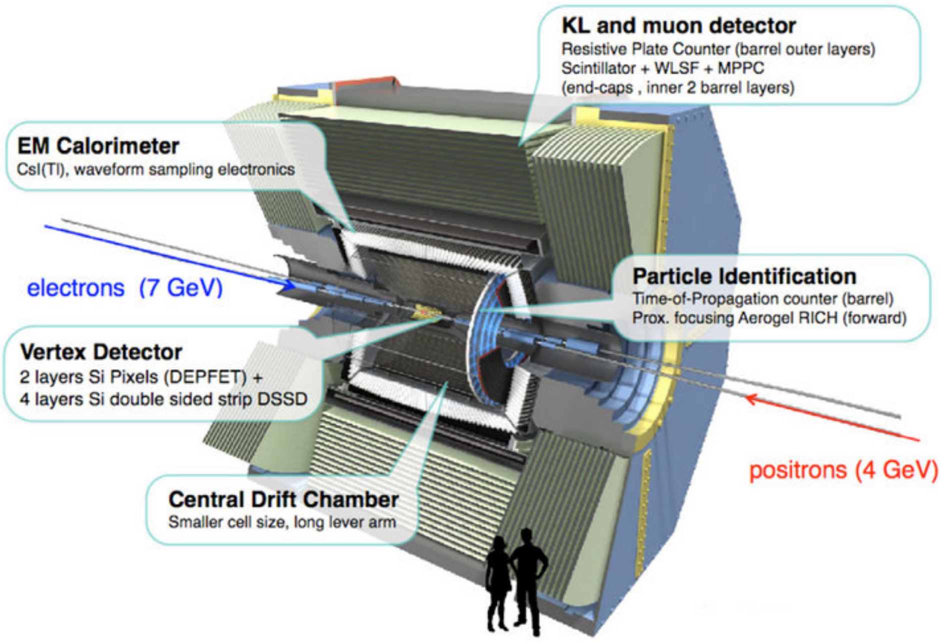

Figure 2.3: The Belle II detector.

2.2 Vertex detector (VXD)

After exiting the beam pipe, the particle enters the vertex detector, which consists of a pixel detector (PXD) [9] and a silicon vertex detector (SVD). The structure of the vertex detector [10] is illustrated in Figure.

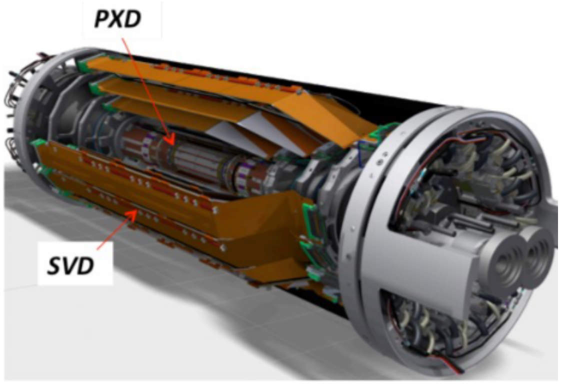

Figure 2.4: The structure of the vertex detector consists of an inner part, the PXD, which is surrounded by the outer SVD. Each component contains multiple layers.

The PXD comprises two layers of sensors with radii of 14 mm and 22 mm. To achieve high precision in vertex measurements within the innermost detector, the PXD uses pixel sensors rather than strips. DEPFET (DEPleted Field Effect Transistor) pixels are employed to detect track positions, allowing for extremely thin pixels, as thin as 50 microns. These thin pixels do not require additional air cooling because they are active only during the readout, when a particle is detected in the sensor. The SVD, which surrounds the PXD, consists of four layers of double-sided silicon strip detectors (DSSDs) as shown in Figure 3.5. Considering the large data volume and number of channels, it was more practical to use strip sensors for the outer part of the SVD rather than pixel sensors. The DSSDs form a ladder structure labeled L3 to L6, measuring the two-dimensional position of particles through the horizontal and vertical orientations of the strips on the sensor. The SVD can detect particles within the range of $17° < \theta < 150°$. Additionally, it can reconstruct particles with low transverse momentum, down to a few tens of [MeV/c].

2.3 Central Drift Chamber (CDC)

The CDC [11] is composed of 14336 sense wires arranged in 56 layers, with an inner radius of 160 mm and an outer radius of 1130 mm, and is filled with a 50:50

helium-ethane gas mixture (He-C_2H_6). It serves three key functions. First, it reconstructs charged tracks and measures their momenta with high precision. Second, it uses energy loss measurements within the gas volume for particle identification (PID). Third, it provides efficient trigger signals for charged particles. The CDC's data allows for the reconstruction of a complete 3D helical track, crucial for determining the momentum of charged particles. The charged particles ionize the helium atoms, producing free ions and electrons. The electrons accelerate and cascade until a measurable signal is detected by the sense wires. Ethane C_2H_6 is used in the gas mixture to localize the ionization cascade around the sense wires. Compared to Belle, the number of layers, sense wires, and the radius of the cylinder and sense wires have all been increased, while the gas mixture and diameter of the sense wires remain unchanged. The VXD and the CDC measure the position and momentum of charged particles by reconstructing their trajectories in a large phase space region under a 1.5 T magnetic field. The magnetic field is oriented in the direction of the electron beam (+z). Both the VXD and the CDC cover a polar angle acceptance from 17° to 150°.

2.4 The TOP Detector

In the Belle II experiment, the Time-of-Propagation (TOP) detector, along with the ARICH detector, is a key component of the particle identification (PID) system. The TOP counter [12], located in the barrel region after the Central Drift Chamber (CDC), consists of 16 quartz bar segments positioned at a radius of approximately 1200 mm. Each module is 275 cm long and 2 cm thick. This specialized Cerenkov detector [13] provides two-dimensional information of a Cerenkov ring image based on the time of arrival and impact position of Cerenkov photons at a photodetector located at one end of a 2.6 cm quartz bar. Particles crossing the TOP detector emit Čerenkov light when their speed exceeds the phase velocity of light in the quartz medium. The angle and energy of the emitted photons depend on the refractive index of the quartz and the momentum of the charged particle. The emission angle θ can be calculated by

$$\cos\theta = \frac{1}{\beta n} \quad \text{with} \quad \beta = \frac{v_p}{c}$$

where n is the refractive index, v_p is the speed of the charged particle, and c is the speed of light. In the TOP detector, emitted Cerenkov photons propagate through the quartz bars, where they are either reflected or absorbed by the walls upon collision. This propagation process, depicted in Figure 3.5, introduces uncertainty to the photon track with each reflection, leading to a probability distribution of detection values. Photons that successfully reach the photomultiplier tubes (PMTs) are used for particle identification. The TOP counter requires photo-sensors with a single-photon time resolution of about 100 ps, achieved using 16-channel Micro-Channel Plate (MCP) Photomultiplier Tubes (PMTs). For accurate particle identification, the particle production time must be known with a precision of approximately 50 ps. In the TOP, Cerenkov photons are captured in quartz, where they are reflected at the Cerenkov angle. Fast particles take a shorter path to reach the photon detectors, allowing the detector to reconstruct the particle's path in two-dimensional space (x, y) and time (t). By measuring the travel time of the photons in quartz, the TOP can determine the velocity of the particle, which enables it to deduce the particle's mass. The structure of the quartz bar is shown in Figure 2.5.

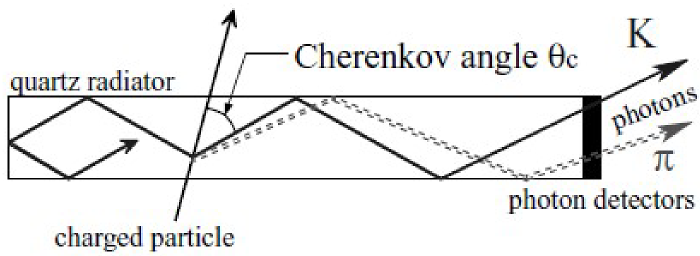

Figure 2.5: The Cherenkov photon travels through quartz, and its Cherenkov angle is measured. The angle's dependence on the particle's velocity results in different paths and times for the photon to reach the detector. This information allows for the distinction between Kaons and Pions based on their differing masses.

2.5 Aerogel Ring-Imaging Cherenkov detector(ARICH)

The Aerogel Ring Imaging Cherenkov (ARICH) detector is a proximity-focusing Čerenkov ring imaging detector with aerogel as the Čerenkov radiator, positioned in the forward endcap region of Belle II. Its primary function is to identify charged particles, specifically distinguishing between charged pions ($\pi^{\pm}$) and kaons ($K^{\pm}$), within a momentum range of approximately 0.4 [GeV/c] to 4 [GeV/c]. The ARICH detector achieves better than 4σ separation between kaons and pions in this range, operating above the pion momentum threshold for Čerenkov photon emission and below the region where Čerenkov angles of kaons and pions begin to overlap. To

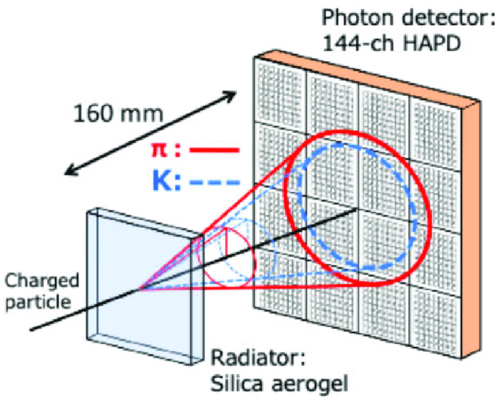

Figure 2.6: The principle of the particle identification of the ARICH counter.

enhance particle identification without compromising the Čerenkov angle resolution, the ARICH employs a novel technique with a double layer of aerogel, each layer having a different refractive index. This design provides a suitable compromise by allowing a refractive index that is above that of gaseous radiators and below that of solid ones, improving momentum coverage. In addition to kaon-pion separation, ARICH can also discriminate between pions, muons, and electrons in the region below 1 [GeV/c], which is essential for efficient heavy flavor tagging. Kaons and pions are common B meson decay products, so precise particle identification is critical for tagging and physics analyses. The main components of the ARICH system include a double layer aerogel radiator for Čerenkov photon emission, a region of empty space for the Čerenkov light cone expansion, and a segmented photon sensor plane with the readout system attached at the back. Together with the Time-of-Propagation (TOP) counter, which covers a polar angle acceptance from 31° to 128°, the ARICH (covering from 14° to 30°) plays a crucial role in particle identification, particularly for distinguishing $\pi^{\pm}$ and $K^{\pm}$ in the barrel and forward endcap regions, respectively.

2.6 The KL and Muon Detector (KLM)

The KLM detector [14], positioned beyond the superconducting coil that surrounds the ECL, is crucial in generating the Belle II magnetic field and is an integral part of the Belle II experiment setup. Its primary role is to detect and identify K^0_L mesons and muons while also serving as a magnetic flux return for the Belle II solenoid, thereby improving the effectiveness of the magnetic field in the setup. The KLM is divided into barrel and endcap sections, each with a unique design optimized for maximum detection efficiency. The barrel section consists of 4.7 cm thick iron plates alternated with Resistive-Plate Chamber (RPC) superlayers. This sandwich-like structure not only facilitates the magnetic flux return, enhancing the magnetic field's effectiveness, but also provides significant material density. This increased material density is crucial for improving the probability of interactions with K^0_L mesons, thus enhancing the detection and identification accuracy of these particles. Additionally, the active detector elements embedded within the layered structure are crucial to the KLM's functionality. The iron plates, combined with the RPCs that utilize glass-electrode technology, have demonstrated excellent performance during the extensive data-collection phase of the Belle experiment. This robust performance emphasizes the KLM's ability to withstand high background rates, particularly in certain regions of the Belle II KLM detector, such as both endcaps and the innermost layers of the barrel region. These areas are expected to encounter increased background rates mainly due to neutron production, which primarily results from electromagnetic showers initiated by background reactions like radiative Bhabha scattering. This aspect underscores the KLM's resilience and adaptability in handling background interference, highlighting its vital role in the Belle II experimental framework.

2.7 The Electromagnetic Calorimeter (ECL)

In the decay processes of B mesons, approximately 3% of the final state products consist of neutral particles, including pions, kaons, and photons. These neutral particles generate a substantial number of photons with energies spanning from 20 [MeV] to 4 [GeV]. Consequently, a high-resolution electromagnetic calorimeter (ECL) is a critical component of particle identification in the Belle II experiment. The ECL retains the majority of its components from the original Belle detector, with significant advancements made primarily to the readout system. For photon detection, the ECL employs scintillating cesium-iodide crystals doped with thallium (CsI(TI)). These crystals are coupled with photodiodes, and the resulting signals are digitized by flash analog-to-digital converters (ADCs) as part of the detection process. To address the more challenging background conditions in the end-cap regions, pure CsI crystals will be utilized. The ECL is constructed from a total of 8,736 crystals, distributed as follows: 1,216 in the forward region and 1,040 in the backward region. In addition to its primary function of detecting and distinguishing between electrons and photons, the ECL also serves as the primary trigger source for Belle II. The energy resolution of the ECL is anticipated to follow the formula:

$$\frac{\sigma_E}{E} = \sqrt{\left(\frac{0.066\%}{\sqrt{E/\mathrm{GeV}}}\right)^2 + \left(\frac{0.81\%}{4\sqrt{E/\mathrm{GeV}}}\right)^2 + (1.34\%)^2}$$

This relationship highlights the precision expected from the ECL in measuring photon energies, thereby enhancing the overall performance of the Belle II experiment.

2.8 Belle II Software Framework (basf2)

Similar to other High Energy Physics (HEP) belle II software framework (basf2) [15] was designed to handle extensive datasets with flexibility and configurability. This adaptability is attained by allowing users to customize the methods applied to the data. Each data processing method is encapsulated within a module, and these modules are organized in a defined linear sequence within a container known as a path. Users have the freedom to create any number of modules and paths, with the option to link multiple paths together to construct a comprehensive data processing chain.

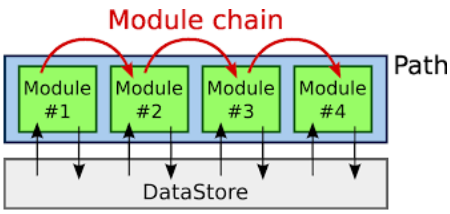

Figure 2.7: A simple data processing chain. One path contains 4 modules that exchange data with each other using the common Data-Store.

During the data processing phase, the framework operates by sequentially executing the modules within a path, commencing with the first module and progressing through the subsequent ones. These modules are executed individually, strictly adhering to the order in which they were arranged within the path. The data intended for processing by the modules is stored in a shared storage known as the DataStore (refer to Figure 2.7). Notably, basf2 allows the creation of multiple paths, thereby enabling the establishment of complex processing sequences. These paths can be interconnected through user-defined conditions. Each module has the capability to return an integer or boolean value. Based on these return values and the specified conditions set by the user, the processing flow can dynamically transition from one path to another (refer to Figure 2.8).

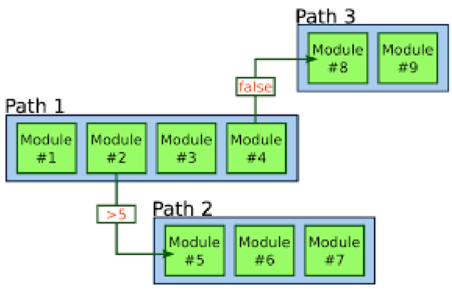

Figure 2.8: Multi path scheme in basf2: Three paths connected by conditions. Both possible condition types are shown: An integer value and a simple boolean value.

basf2 complete detector simulation relies on Geant4, the standard toolkit for simulating particle interactions with matter in HEP. To ensure accurate simulation, the TGeo geometry objects must be made accessible to Geant4.

Figure 2.9: The basf2 environment interface.

In the basf2 environment, the `generators.add_continuum_generator(path, finalstate, userdecfile='', *, skip_on_failure=True, eventType='')` function is employed to perform simulations using the Pythia8 generator. This function facilitates the inclusion of specific final states in the simulated events, with the option to specify custom decay files to further control the decay processes. In our analysis, this method was utilized to generate continuum events, which are critical for studying background processes and performing off-resonance analyses. In addition to Pythia8, our simulations incorporate the default continuum generators KKMC and Pythia. KKMC handles the simulation of initial-state and final-state radiation processes, while Pythia is responsible for modeling parton showers and hadronization. The default decay files associated with these generators are configured to represent the relevant decay channels, ensuring that the generated continuum events reflect the physical processes observed in the Belle II experiment. The Pythia settings are also tuned to align with the expected behavior of these events, with a particular focus on the production of light and charm quarks. By utilizing KKMC and Pythia alongside custom tuning of the Pythia8 generator, our simulations provide a robust framework for analyzing both on-resonance and off-resonance data. This approach allows for a comprehensive study of background processes, enabling us to effectively isolate signal events from the continuum background. The `reconstruction.add_reconstruction(path, components=None, pruneTracks=True, add_trigger_calculation=True, skipGeometryAdding=False, trackFitHypotheses=None, addClusterExpertModules=True, use_second_cdc_hits=False, add_muid_hits=False, reconstruct_cdst=None, event_abort=<function default_event_abort>, use_random_numbers_for_hlt_prescale=True, pxd_filtering_offline=False, create_intercepts_for_pxd_ckf=False, append_full_grid_cdc_eventt0=True, legacy_ecl_charged_pid=False, emulate_HLT=False, skip_full_grid_cdc_eventt0_if_svd_time_present=True)` function is utilized to add the standard reconstruction modules to a given processing path. This function orchestrates the full reconstruction process by integrating essential components such as clustering, tracking, and particle identification (PID) modules into a cohesive workflow. Each of these elements plays a critical role in transforming raw detector data into analyzable physics objects, such as tracks and clusters, and subsequently identifying the particles that generated them. The clustering module handles the aggregation of hits in subdetectors (such as the calorimeter or pixel detector) into clusters, representing the energy deposited by particles. The tracking module reconstructs particle trajectories from hits recorded in tracking detectors, such as the CDC (Central Drift Chamber). The PID module uses the reconstructed tracks and clusters to identify the particles by comparing their energy deposition patterns and track characteristics with expected values for different particle species. In our analysis, `reconstruction.add_reconstruction` was used in conjunction with `simulation.add_simulation` to generate simulated events and then reconstruct them, allowing us to study both the generator-level and reconstructed-level properties of the events. This two-step process ensures that the simulated events not only reflect the theoretical predictions but also incorporate detector effects, such as resolution and efficiency, which are essential for comparing with experimental data. This approach allows us to validate the performance of the detector and improve the accuracy of our Monte Carlo simulations, contributing to a deeper understanding of the underlying physics in the Belle II experiment.

Chapter 3

Pythia8 Monte Carlo Event Generator

The Pythia8 Monte Carlo Event Generator is a critical tool in modern particle physics research, providing comprehensive simulations of high-energy particle collisions. It simulates the outcomes of collisions by modeling various physical processes, such as particle generation, hadronization, and multiple parton interactions. This chapter delves into the intricate processes simulated by Pythia8, with a particular focus on its implementation of hadronization through the Lund String Model [16]. Pythia8 encompasses several core features essential for accurate event simulation: In our analysis, we conducted comparisons between two widely used versions of the Pythia Monte Carlo event generator: Pythia6 [17] and Pythia8.

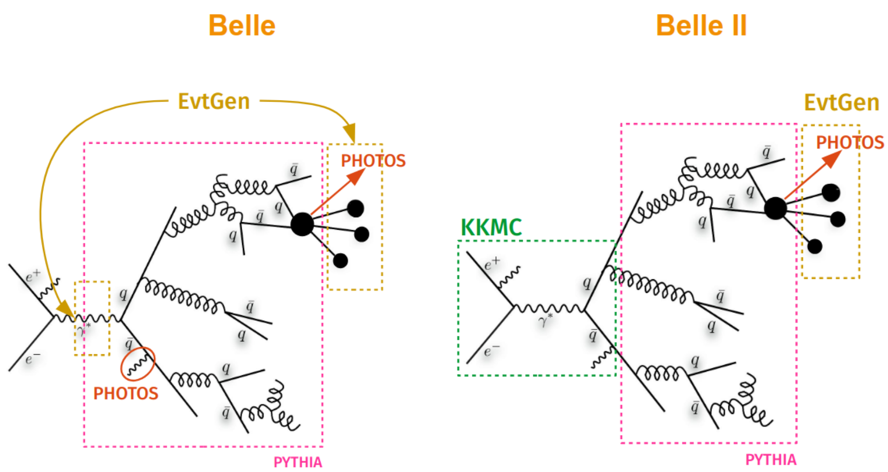

Figure 3.1: Diagram of the Monte Carlo simulation setup in Belle and Belle II, showing the different components used for particle generation and decay.

The Belle II Monte Carlo simulation framework consists of several components that work together to model e^+e^- collision events and particle decays:

- **KKMC:** KKMC is responsible for simulating the initial e^+e^- collision and generating γ^* events, accounting for radiative corrections and initial-state radiation. This is an essential first step in the simulation chain for events occurring in the Belle II environment.
- **Pythia:** The Pythia package is used to model the hadronization process. It takes quark pairs generated by KKMC and simulates the creation of hadrons.
- **EvtGen:** Once the hadrons are generated, EvtGen handles the decay of heavy particles, particularly those containing B mesons. It ensures that decays are modeled with the correct branching ratios and kinematic distributions.
- **PHOTOS:** PHOTOS is used for simulating final-state radiation (FSR) of photons in particle decays, allowing the model to account for additional photons emitted by charged particles. This is particularly important for precise measurements involving electromagnetic interactions.

This modular setup enables the Belle II simulation to accurately represent the physical processes from collision to final particle decay, with each package tailored to a specific part of the event generation process.

Understanding the key differences between these two versions is essential for interpreting the results of our comparisons and optimizing the accuracy of our simulations. Pythia6, written in Fortran, is based on a legacy codebase that has been widely used in particle physics for many years. Its procedural architecture, while functional, imposes certain limitations in terms of flexibility and ease of use. The physics models implemented in Pythia6, such as parton showers, hadronization, and multiple parton interactions (MPI), are based on older techniques that, although reliable, may lack the sophistication required for modern high-precision experiments. In contrast, Pythia8 represents a complete overhaul of the codebase, rewritten in C++ with a more modern object-oriented design. This new architecture allows for greater modularity and flexibility, making it easier to customize the generator for specific analyses and to interface with other software frameworks. Pythia8 also features more refined physics models, including advanced implementations of parton showers and MPI, and is optimized for better computational efficiency and event handling. These improvements make Pythia8 better suited for high-energy physics experiments like Belle II, where precise modeling of both signal and background processes is crucial. One of the major advantages of Pythia8 is its improved tuning and validation against more recent experimental data. While Pythia6 relies on older tunes, Pythia8 incorporates a broader range of tunes that have been optimized for modern collider environments, including those at the LHC and Belle II. This ensures that the generated events more accurately reflect the conditions observed in current experiments. Despite these advantages, Pythia6 still holds value, particularly for comparisons with older datasets or for validation against historical results. In our analysis, we used Pythia6 as a benchmark to compare with Pythia8, allowing us to assess the impact of the improvements in the newer version. These comparisons helped us identify potential discrepancies and validate the performance of Pythia8 in modeling the processes relevant to our study. The comparison between Pythia6 and Pythia8 was crucial in understanding the evolution of Monte Carlo simulations and their implications for our analysis. By leveraging the strengths of Pythia8, particularly its modern physics models and improved computational efficiency, we were able to achieve more accurate and reliable results, ultimately enhancing the quality of our simulations in the Belle II experiment.

3.1 Parameter Tuning and Customization

Pythia8 allows for extensive parameter tuning to match experimental data. Key parameters include:

- **Parton Distribution Functions (PDFs)**: Various models can be selected to represent the internal structure of hadrons.
- **Hadronization Parameters**: Adjustments to the string tension and fragmentation functions to improve the match with experimental observations.
- **MPI Parameters**: Settings that define the likelihood and impact of multiple interactions within a single collision.

The tuning process involves comparing simulated results with experimental data and iteratively adjusting parameters to minimize discrepancies. Fragmentation in Pythia is governed by the Lund String Model, originally developed by Andersson et al. . This model provides a comprehensive physics description of hadronization, which involves various interconnected aspects. Consequently, these aspects are split accordingly in the Pythia framework, reflecting the set of classes involved in the fragmentation mechanism. The variables associated with fragmentation cover a broad range of functionalities. Some are essential for any hadronization tuning exercises, while others are advanced parameters intended to be adjusted only by experts. Additionally, the fragmentation flavor-selection mechanism is shared with other parts of Pythia, notably particle decays, and is covered in the Flavour Selection documentation. Pythia offers several methods to reweight generated events based on fragmentation parameters. These methods enable users to adjust parameters efficiently, conduct parameter scans, and oversample rare event configurations, with reweighting applied to maintain correct cross-sections. Further documentation on these reweighting methods is available on the Hadronization Variations page. For scenarios involving Hidden Valleys, fragmentation is modeled similarly to standard string fragmentation but with a distinct parameter set tailored to the specific Hidden Valley configuration. The fragmentation function itself is handled by the `StringZ` class, which determines the longitudinal lightcone fraction z according to one of two possible shapes. For light quarks, the Lund symmetric fragmentation function is employed, defined as:

$$f(z) = \frac{1}{z}(1-z)^a \exp\left(-\frac{b\, m_T^2}{z}\right)$$

where a and b are the primary free parameters to be tuned to experimental data.

Hadronization is a fundamental process in particle collisions, wherein color-charged quarks and gluons transform into color-neutral hadrons. Pythia8 leverages the Lund String Model to simulate this phenomenon, based on the concept of color confinement in Quantum Chromodynamics (QCD).

$$V(r) = \sigma r, \tag{3.1}$$

where σ is the string tension. When the string length exceeds a critical value, it breaks, leading to the creation of new quark-antiquark pairs that form hadrons. The energy stored in the flux tubes dictates the masses and momenta of the resulting hadrons.

Chapter 4

Tuning Procedure

To tackle the complexities of multi-parameter optimization challenges, Professor2, a specialized package, has been created as an alternative to manual adjustment techniques. Professor2 employs a method called parametrization-based tuning. A key advantage of this package is its capability to manage correlations among various parameters, facilitating multivariate minimization within the parameter domain. The main aim of this approach is to identify the correlation function, or characteristic polynomial, aligning the Monte Carlo data with the reference data, thereby minimizing the multi-dimensional function. In our research, we employ the Pythia8 model to generate physics events. We conduct a comparison and fine-tuning of selected observables derived from reference data and the Belle II off-resonance Monte Carlo event generator. An essential part of the tuning process involves selecting the free parameters from the models that influence the observables we're interested in. This selection is made by conducting sensitivity checks, as detailed in Section 3.2. Once we have identified the sensitive parameters, we carry out the tuning process using the Professor2 toolkit. This involves generating samples with different combinations of these sensitive parameters. The Professor2 framework offers four types of parameter sampling methods: grid, uniform, Sobol, and Latin hypercube sampling. The "Sobol" and "Latin" hypercube distributions aim to evenly cover the parameter space, particularly useful for smaller sample sizes. For this study, we opted for "uniform" sampling with N = 1500 parameter points, as illustrated below.

```
prof2-sample -o output params.dat -n 1500
```

Figure 4.1: prof2-sample used to generate parameter samples for interpolation and tuning in Professor2.

The process involves creating 1500 sets of parameters within predefined intervals for each. These parameter sets are then used to generate Monte Carlo samples, which are later utilized to extract the observables of interest for tuning the model parameters. Detailed descriptions of the observables of interest can be found in Section 2.1. The resulting datasets were saved in ROOT file-format and subsequently analyzed to extract the distributions of interest in a binned (histogram) format. It's important to note that special attention is given to ensuring that the histograms do not contain any empty bins; in cases where empty bins are encountered, the corresponding weights are set to zero. To accommodate the multi-correlations among the parameters, the order of the polynomial can be adjusted accordingly. For this study, we've set the polynomial order to 5. As a result, the interpolation generates an "ipol.dat" file containing crucial interpolation results necessary for the tuning process. These results include the Monte Carlo (MC) response extracted for each observable, represented in terms of variations in bin content. To model the Monte Carlo (MC) response, we construct the characteristic polynomial from the generated Monte Carlo samples, as illustrated below:

```
prof2-ipol runsdir ipolfile=ipol.dat --order=5
```

Figure 4.2: 5th-order polynomial interpolation performed using the interpolation file "ipol.dat" with Professor2.

4.1 Observables for Tuning

SuperKEKB collides electrons with positrons at the centre-of-momentum energies corresponding to the Upsilon resonance masses. For instance, at the SuperKEKB accelerator, collisions are typically conducted at the energy of $\mathrm{E}_{\mathrm{res}}$ [GeV] to match the mass of the resonance particle being studied. However, this is not the only energy configuration available for data collection at Belle II. Standard collisions occur at the resonance energy of $\mathrm{E}_{\mathrm{res}}$ [GeV]. This energy precisely matches the mass of the resonance particle being studied. In addition to on-resonance collisions, the SuperKEKB accelerator also operates at other energy levels. Notably, there is an off-resonance dataset collected approximately 60 [MeV] below the resonance energy. At this lower energy, where the production of resonance mesons is suppressed, the focus shifts to studying continuum events, including the production of light and charm quark pairs. The cross section for such continuum processes is about σ_{cont} nb, which is more than three times larger than that for the production of resonance mesons. This off-resonance data is crucial for understanding the background contributions in hadron production. While Monte Carlo simulations can model these continuum processes, analyzing real data provides more accurate and effective insights. Typically, this off-resonance dataset is collected once or twice per year, providing a clean sample of continuum events, free from resonance mesons, known as the off-resonance (or continuum) sample. In our analysis, we focused on the off-resonance data. Although Belle II also collects on-resonance data, our primary interest was in the off-resonance dataset due to its value in studying background processes and continuum events that are critical for accurate meson analysis. In our investigations, a pivotal aspect

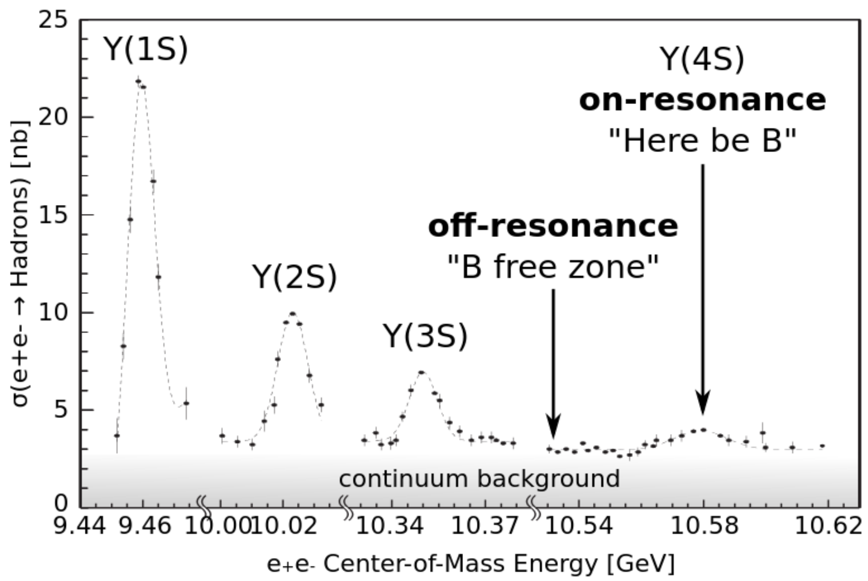

Figure 4.3: Cross section around the Υ resonances showing the difference between on- and off-resonance.

of understanding physics events lies in characterizing their "event shape," derived from the measured hadron yields. This characterization enables the discrimination of physics events originating from diverse physical processes. A widely utilized method for describing this "event shape" is through Fox-Wolfram moments, elucidated by Equation 2:

$$R = \sum_{i,j} P_i P_j \left(\frac{|\vec{p}_i||\vec{p}_j|}{E_{\text{vis}}^2} \right)^{n_i} \left(\frac{2}{E_{\text{vis}}} \right)^{n_i+n_j}$$

Here, P_i and P_j represent the momenta of particles i and j respectively, while E_{vis} denotes the visible energy in the event. The exponents n_i and n_j control the weighting of different energy components. Furthermore, another crucial observable utilized for event characterization is the Thrust variable, which quantifies the collimation of final-state particles along a common axis. It is expressed as:

$$T = \max_{\vec{n}} \frac{\sum_i |\vec{p}_i \cdot \vec{n}|}{\sum_i |\vec{p}_i|}$$

Here, $\vec{n}$ represents a unit vector pointing in the direction of the thrust axis. The Thrust variable T achieves its maximum value when the final-state particles are perfectly aligned along this axis, indicating a highly collimated event. These variables, Fox-WolframR2 and Thrust T, offer valuable insights into the underlying physics processes by quantifying the distribution of particle momenta and the degree of collimation within an event, respectively.

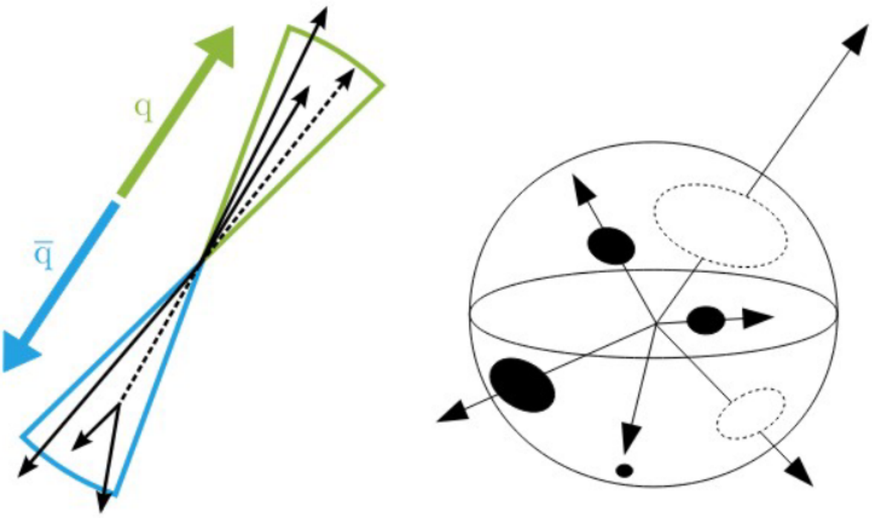

Figure 4.4: Thrust and foxWolfram.

In our analyses, we incorporated the variable "VisibleEnergyOfEventCMS" which represents the total energy of detectable particles produced in collision events within the center-of-mass (CMS) frame. This pivotal quantity offers insights into the available energy for particle interactions and production, aiding in the characterization of collision dynamics and the identification of particle types generated. The calculation of visible energy involves summing the energies of all detected particles, providing foundational information for understanding the physics processes underlying collider experiments. Let E_{vis} represent the visible energy of the event in the CMS frame. It can be calculated by summing the energies of all detected particles:

$$E_{\text{vis}} = \sum_i E_i$$

Here, E_i represents the energy of each detected particle in the event.
Another variable selected for inclusion in the tuning list is the "MissingEnergyOfEventCMS". The missing energy in the center-of-mass (CMS) frame refers to the energy that cannot be accounted for by detected particles in a collision event, as measured in the frame where the total momentum of the colliding particles is zero. This quantity is essential for identifying undetected particles, such as neutrinos or other weakly interacting particles, which may carry away energy. The presence of missing energy can indicate the occurrence of new, yet undetected, physics processes or particles. Let E_{miss} represent the missing energy of the event in the CMS frame. It can be calculated as the difference between the total initial energy of colliding particles and the sum of energies of all detected particles:

$$E_{\text{miss}} = E_{\text{initial}} - \sum_i E_i$$

Here, E_{initial} represents the total initial energy of the colliding particles, and E_i represents the energy of each detected particle in the event.
Another variable chosen for the tuning list is the "MissingMomentumOfEvent". The missing momentum of the event refers to the momentum vector that cannot be accounted for by detected particles in a collision event. Similar to missing energy, missing momentum indicates the presence of undetected particles or phenomena affecting momentum conservation. It is crucial for identifying processes involving particles that escape detection, such as neutrinos or other weakly interacting particles. Let $\vec{p}_{\text{miss}}$ represent the missing momentum of the event. It can be calculated as the negative vector sum of momenta of all detected particles:

$$\vec{p}_{\text{miss}} = -\sum_i \vec{p}_i$$

Here, $\vec{p}_i$ represents the momentum vector of each detected particle in the event.

4.2 Sensitivity Check

To identify the sensitive parameters for the chosen list of observables, parameter sensitivity checks are conducted using the normalized residuals obtained from two sample tests, as illustrated below:

$$r_i = \frac{n_i - N\hat{p}_i}{\sqrt{N\hat{p}_i \left(1 - \frac{N}{N+M}\right) \left(1 - \frac{n_i+m_i}{N+M}\right)}} \tag{4.1}$$

Where:

- r_i: The normalized residual for the i-th bin in the histogram of the observable of interest.
- n_i: The observed count or value for the i-th bin in the histogram of the observable of interest in the reference data.
- $N\hat{p}_i$: The expected count based on a model, where N is the total sample size, and $\hat{p}_i$ is the estimated probability for the i-th bin in the histogram. .
- $\sqrt{N\hat{p}_i \left(1 - \frac{N}{N+M}\right) \left(1 - \frac{n_i+m_i}{N+M}\right)}$: The standard deviation of the residuals, accounting for sample size corrections and the variance in the probability distribution.

In our analysis, we conducted a two-sample test to compare event and event shape variables. The resulting plots revealed deviations centered around zero. In cases where the difference between the two distributions lacked statistical significance, the deviations around zero tended to be less than 2. Conversely, deviations exceeding 2, particularly where $|r_i| > 2$ indicated statistically significant differences between the distributions for those bins. Additionally, if the residuals consistently shifted away from zero in one direction, it suggested the presence of a systematic shift between the two distributions.

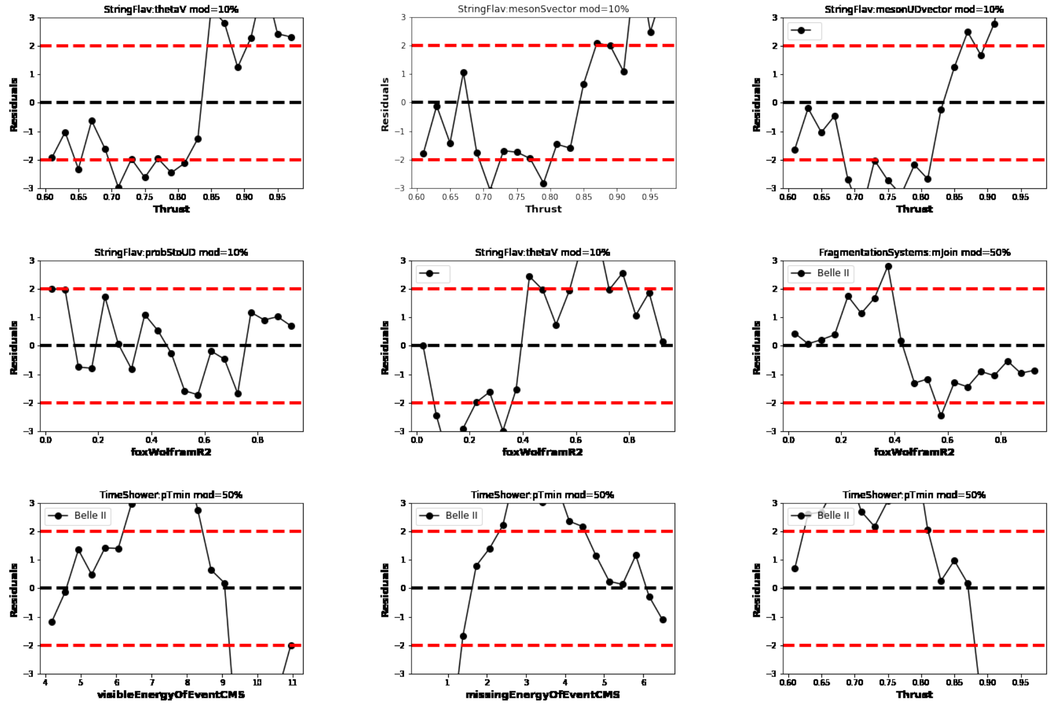

Figure 4.5: Sensitivity checks (varying parameters from their default values).

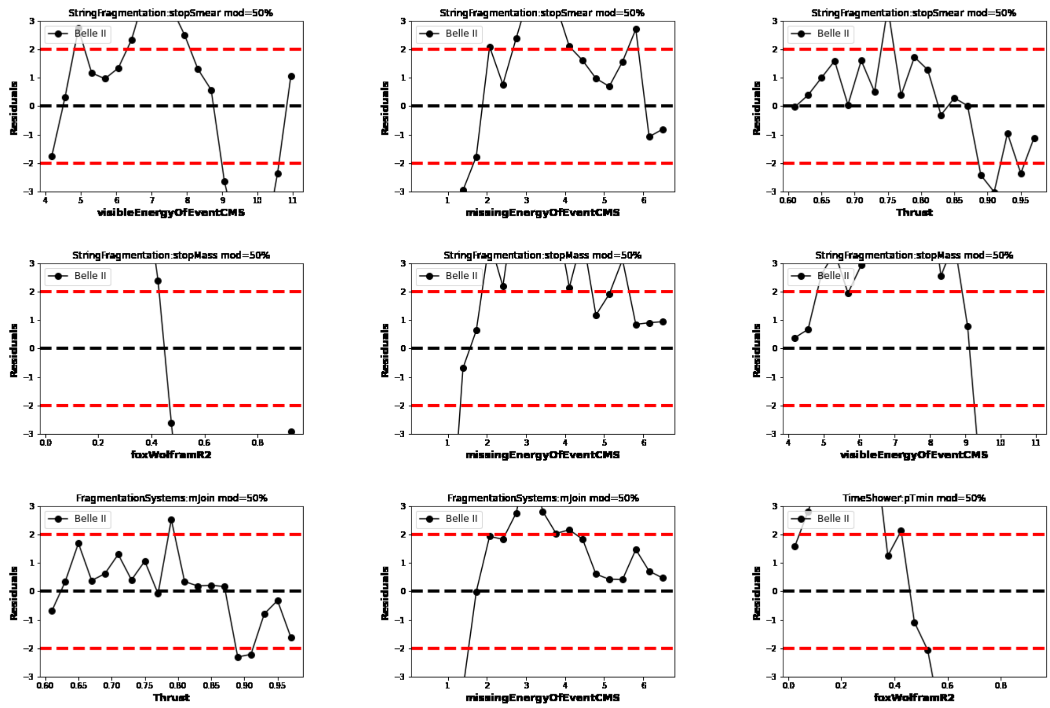

Figure 4.6: Sensitivity checks (varying parameters from their default values).

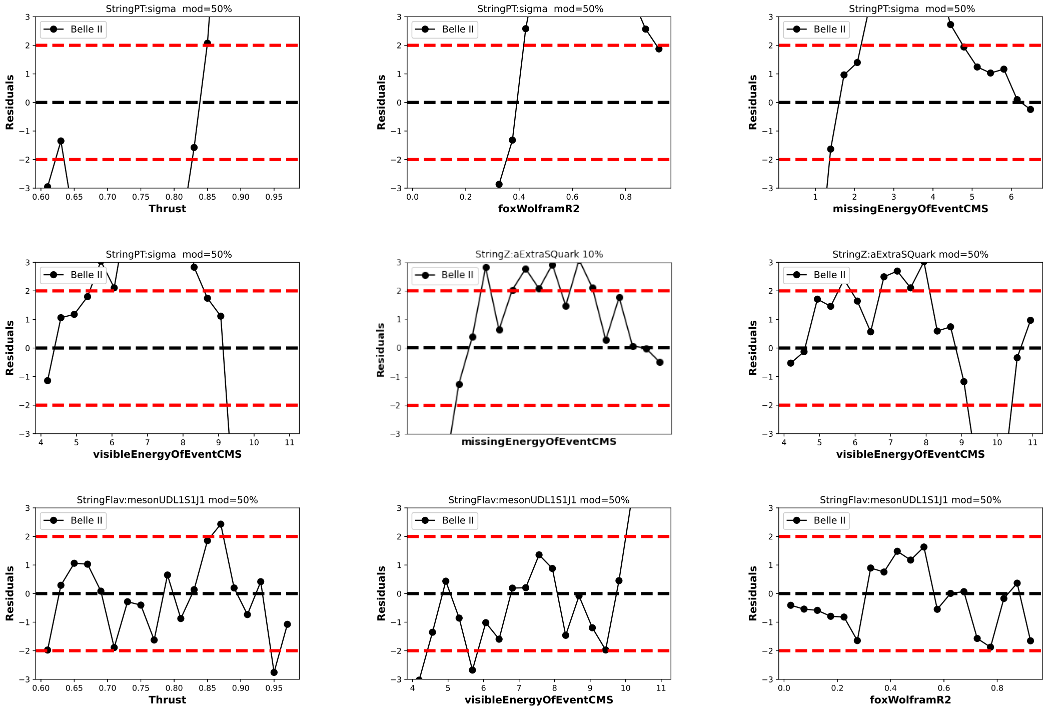

Figure 4.7: Sensitivity checks (varying parameters from their default values).

Based on the sensitivity checks the parameters below have been selected for the tuning.

- **StringFlav:mesonUDvector** (default = 0.50; minimum = 0.; maximum = 3.): the relative production ratio vector/pseudoscalar for light (u, d) mesons.

- **StringFlav:mesonSvector** (default = 0.55; minimum = 0.; maximum = 3.): the relative production ratio vector/pseudoscalar for strange mesons.

- **StringFlav:mesonCvector** (default = 0.88; minimum = 0.; maximum = 3.): the relative production ratio vector/pseudoscalar for charm mesons.

- **StringFlav:thetaPS** (default = -15.; minimum = -90.; maximum = 90.): gives the mixing angle thetaPS in the pseudoscalar meson sector (which is rather poorly determined), expressed in degrees.

- **StringFlav:thetaV** (default = 36.; minimum = -90.; maximum = 90.): gives the mixing angle thetaV in the vector meson sector (which is somewhat better determined), expressed in degrees.

- **TimeShower:alphaSvalue** (default = 0.1365; minimum = 0.06; maximum = 0.25): The alphastrong value at scale MZ2. The default value corresponds to a crude tuning to LEP data, to be improved.

4.3 Professor II Method

Historically, the primary methods for generator tuning have been manual "by eye" adjustments and extensive brute-force parameter space scanning. Tuning complex systems manually is clearly inefficient, yet it has been the most common method. This approach requires deep understanding of the algorithm's response to parameter changes and is inherently slow, often taking a day or more per iteration. Manual tuning is also limited, as humans struggle to optimize more than five parameters using a similar number of comparison plots. The method's responsiveness to new data or models is poor, often necessitating a complete restart for different generators, making it an unpopular task to repeat. These challenges highlight the need for automated tools like Professor. Parameterization-based tuning, which has a long history, involves modeling the generator's behavior. Since the fit function is complex and not easily parameterizable, an indirect method is used: a polynomial is fitted to the generator response, MC_b, for each observable bin b based on changes in the parameter vector $p = (p_1, ..., p_P)$. Once a suitable parameterization of the generator's response to the steering parameters for each observable bin is established, a goodness of fit (GoF) function is constructed and minimized. This yields a predicted parameter vector, (p_{tune}), which should closely match the best description of the tune data that the generator can provide, assuming the technique is robust. The runtime for parameterization-based tuning is mainly determined by the time required to run the generator and produce reference data points. With enough CPU resources to run several hundred Monte Carlo jobs in parallel, this takes at most a few days. Converting this data into a predicted set of optimal parameters takes only a few minutes and can also be parallelized for different configurations as a precaution. The Professor system uses this parameterization-based optimization approach. For

P	$N(2)$ (2nd order)	$N(3)$ (3rd order)
1	3	4
2	6	10
4	15	35
6	28	84
8	45	165
10	66	286

Table 4.1: Scaling of number of polynomial coefficients $N(P)$ for polynomials of second order ($n = 2$) and third order ($n = 3$).

a general polynomial of order n, the number of coefficients $N(P)_n$ is determined by counting only the independent components of the matrix term, given by:

$$N(P)_n = 1 + \sum_{i=1}^{n} \frac{1}{i!} \prod_{j=0}^{i-1} (P + j). \tag{3}$$

This formula (Equation 3) shows how the number of parameters scales with P for different polynomial orders. For instance, for a second-order polynomial ($n = 2$), the number of coefficients $N(2)$ increases as P increases. Similarly, for a third-order polynomial ($n = 3$), the number of coefficients $N(3)$ follows a different scaling pattern. Using a polynomial for the fit function offers general-purpose robustness. A key advantage is that the choice of p_0 is irrelevant; shifting the reference point simply redefines the coefficients $\{\alpha, \beta, \gamma\}$ while preserving the function's form. Therefore, a numerically stable value within each parameter's chosen range, such as the center of the hypercube $[p_{\min}, p_{\max}]$ as defined in the subsequent section, can be freely selected without loss of generality. We used a heuristic χ^2 function for evaluating goodness of fit (GoF), though other metrics are also applicable. The importance of different distributions in our dataset can vary. For instance, when there are 20 event shape distributions and one charged multiplicity, it might be necessary to increase the weight of the multiplicity by about 10 times to maintain its significance in the GoF evaluation. Therefore, we include weights w_O for each observable O in our definition of χ^2. The weighted χ^2 function is defined as:

$$\chi^2 = \sum_O w_O \left(\frac{d_O - m_O}{\sigma_O} \right)^2$$

where d_O represents the data value for observable O, m_O is the model prediction for the same observable, and σ_O is the uncertainty associated with d_O. The weight w_O is used to adjust the contribution of each observable O to the overall χ^2 value, ensuring that observables with different levels of importance or different numbers of events are appropriately considered in the goodness of fit assessment. The goodness of fit (GoF) function $\chi^2(p)$ is defined as:

$$\chi^2(p) = \sum_O w_O \sum_{b \in O} \left(\frac{f(b)(p) - R_b}{\Delta_b} \right)^2,$$

where R_b is the reference value for bin b, and Δ_b is the total uncertainty of the reference for bin b.This version maintains the technical details while providing a clearer explanation of the weighting rationale in the context of the goodness of fit function.

4.4 Beam Background Effect on the Observables

Beam background has a significant impact on the measurement of observables in particle physics experiments. In this section, we evaluate the influence of beam background by comparing off-resonance Monte Carlo (MC) simulations of *udsc* events without beam background (bg) to the official Belle II MC14rd *udsc* sample, which includes beam background effects. This comparison was conducted for four key observables: foxWolframR2, Thrust, Missing Energy in the CMS frame, and Missing Momentum. Each observable provides insight into the kinematic properties of events and how they are influenced by background.

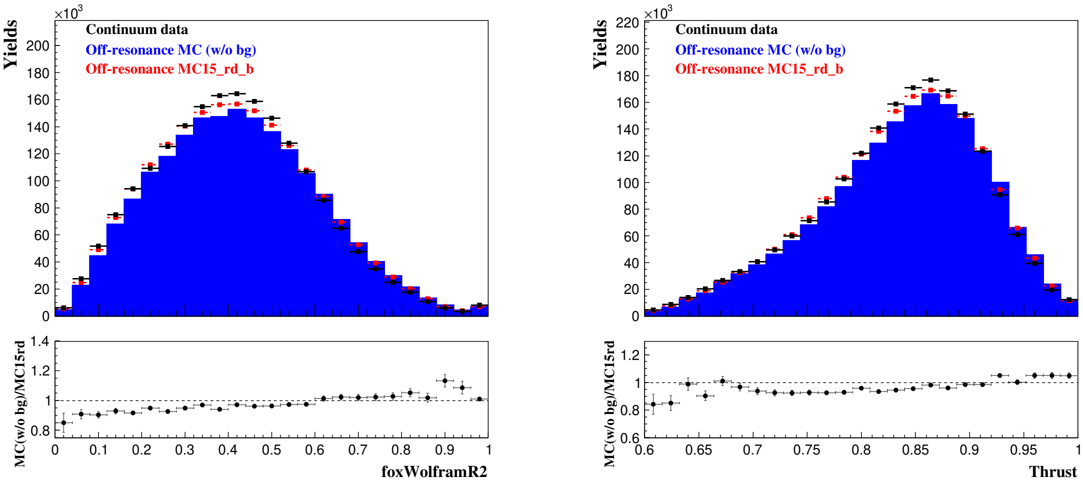

Figure 4.8: Comparison of foxWolframR2 and Thrust observables between MC(udsc) without beam background and MC14rd(udsc) for off-resonance data.

The comparison between the off-resonance MC(udsc) without bg and MC14rdd shows deviations mainly in the high-thrust region (close to 1), with the official MC including background effects having fewer events with high thrust. This suggests that beam background leads to an underestimation of thrust values due to the presence of additional soft particles from beam-induced interactions, which reduce the overall event collimation.

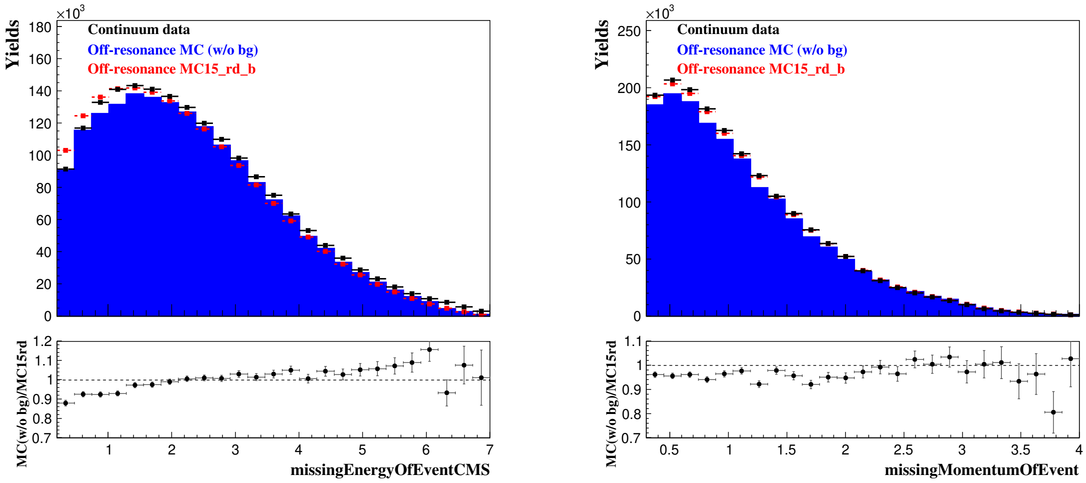

Figure 4.9: Comparison of missing energy and missing momentum observables between MC(udsc) without beam background and MC14rd(udsc) for off-resonance data.

The Missing Energy in the CMS frame provides an estimate of energy that is unaccounted for in the reconstructed event, typically indicating the presence of undetected particles, such as neutrinos. A comparison between the off-resonance MC(udsc) without bg and MC14rd reveals a systematic offset across the entire energy range. The missing energy in the CMS frame is consistently higher in the MC14rdd sample, which can be attributed to the influence of beam background. Beam background interactions introduce additional low-energy particles or tracks that may not be fully reconstructed, thus contributing to an apparent increase in the missing energy component. This systematic shift needs to be accounted for in precision analyses, particularly in searches for invisible particles or rare decays involving undetected final states. The Missing Momentum observable quantifies the total momentum imbalance in an event. A high missing momentum value typically indicates either poorly reconstructed tracks or the presence of invisible particles that escape the detector. The comparison shows a noticeable discrepancy at higher momentum values, where the MC14rdd sample exhibits significantly more missing momentum than the off-resonance MC without bg. This effect can be explained by the beam background introducing mismeasured tracks or undetected soft particles that contribute to the momentum imbalance. Such background-induced momentum fluctuations are particularly problematic in analyses aiming to measure particle momenta with high precision, such as in studies involving heavy-flavor quarks or in missing energy/momentum searches.

4.5 MC parameter sampling

The plot consists of two 2D scatter plots, with each axis corresponding to specific parameters within the Pythia8 generator. The left panel shows the relationship between the parameters ‘StringFlav:thetaV‘ and ‘TimeShower:alphaSvalue‘, while the right panel displays the parameters ‘StringFlav:mesonSVector‘ and ‘StringFlav:thetaV‘. The scattered points indicate the diversity of parameter values explored during the sampling phase. This initial sampling of the parameter space is essential to cover a broad range of possibilities, ensuring that the tuning process adequately explores the potential configurations that best describe the experimental data. The Professor2 package begins by sampling various combinations of parameters, as visualized in the plot. After events are generated for each sampled point, the simulation data is compared to experimental results. The parameters displayed in the plot, such as ‘StringFlav:thetaV‘, ‘TimeShower:alphaSvalue‘, and ‘StringFlav:mesonSVector‘, play a critical role in controlling the flavor and hadronization processes within Pythia8. These parameters directly influence the transition of quarks into hadrons, which affects the final state observables in the simulation. Therefore, a proper sampling and subsequent optimization of these parameters are crucial for enhancing the fidelity of the Monte Carlo simulation to match real-world data.

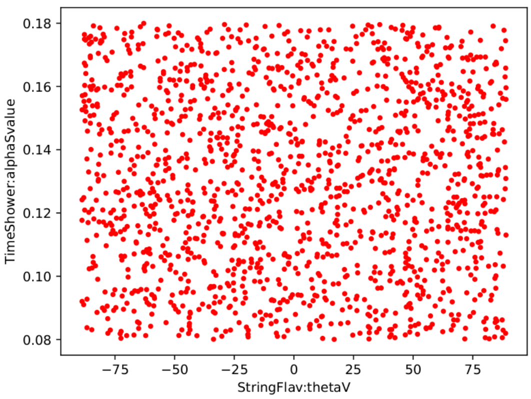

Figure 4.10: Sampling of the parameters ‘StringFlav:thetaV‘ vs ‘TimeShower:alphaSvalue‘, used to explore the interplay between hadronization and parton showering in Pythia8.

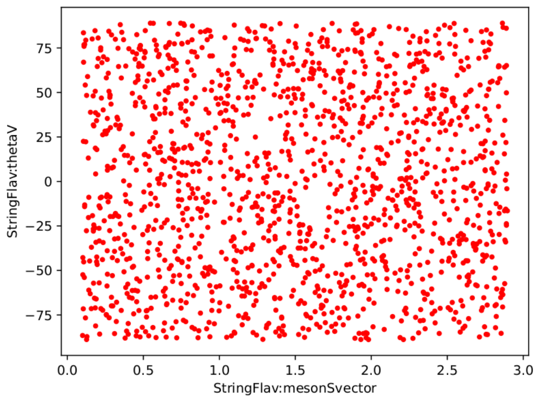

Figure 4.11: Sampling of the parameters ‘StringFlav:thetaV‘ vs ‘StringFlav:mesonSVector‘, used to study the impact of flavor parameters on meson production in Pythia8 simulations.

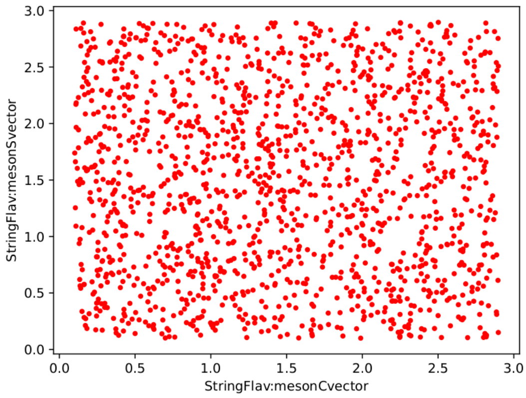

Figure 4.12: Sampling of the parameters ‘StringFlav:mesonCvector‘ vs ‘StringFlav:mesonSvector‘, focusing on meson production with varying vector parameters in Pythia8.

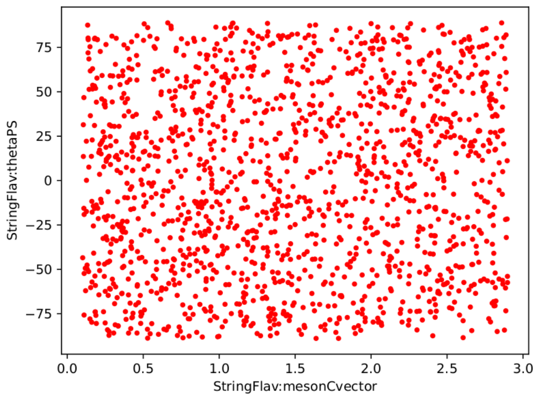

Figure 4.13: Sampling of the parameters ‘StringFlav:mesonCvector‘ vs ‘StringFlav:thetaPS‘, showing the impact of the ‘thetaPS‘ parameter on meson production in the Pythia8 generator.

4.6 Envelope Plots

Having determined the range of values for each parameter, we visualize the region of the distributions to assess its usefulness. This step is crucial before moving forward. We can accomplish this using the Professor2 tool by generating envelope plots with the command prof2-envelopes. These plots display an area encompassing the distributions, indicating the bin values the observables can take within the chosen parameter ranges. The results are presented in the following section.

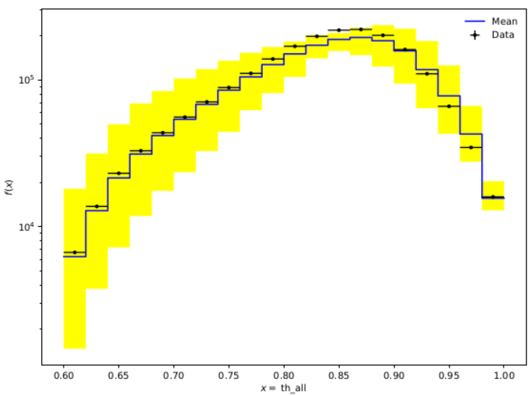

Figure 4.14: Envelope plot for Thrust distribution. This plot visualizes the range of observable values determined from the parameter tuning process, illustrating how well the envelopes encompass the reference data.

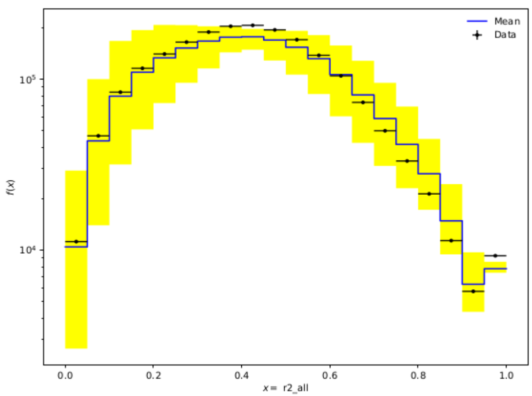

Figure 4.15: Envelope plot for Fox-Wolfram R_2. This visualization confirms the adequacy of the chosen parameter ranges, with the envelopes covering the reference data in most bins.

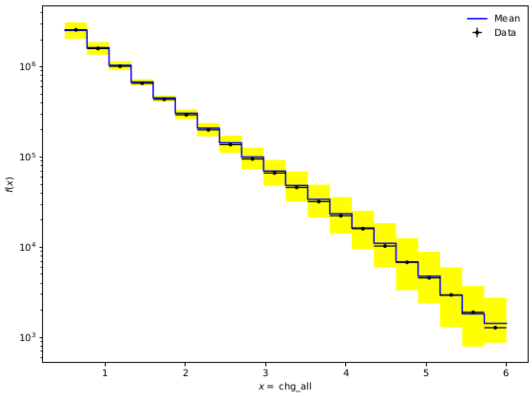

Figure 4.16: Envelope plot for multiplicity distributions. This plot assesses the parameter ranges for track multiplicity and charged particle multiplicity, showing good agreement with reference data.

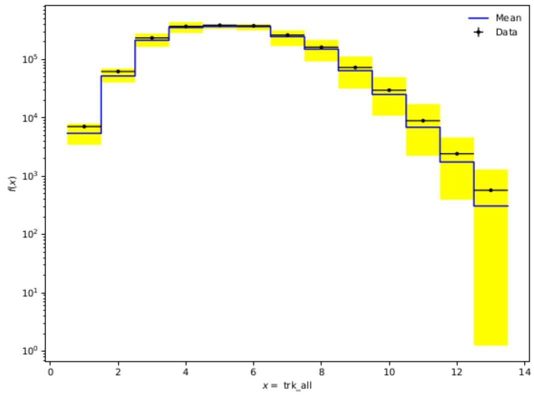

Figure 4.17: Envelope plot for the number of tracks in event distributions. This plot demonstrates how well the chosen parameter ranges capture the expected track multiplicities.

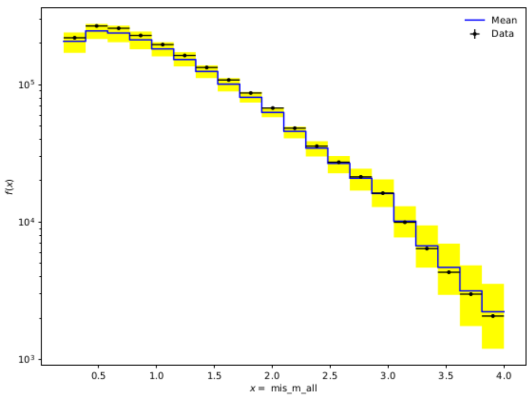

Figure 4.18: Envelope plot for missing momentum in event distributions. This visualization indicates the adequacy of the parameter ranges for this observable.

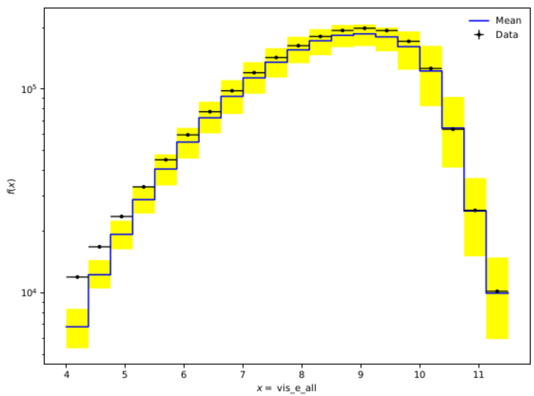

Figure 4.19: Envelope plot for visible energy in event distributions. This plot further assesses the tuning quality of the parameter ranges.

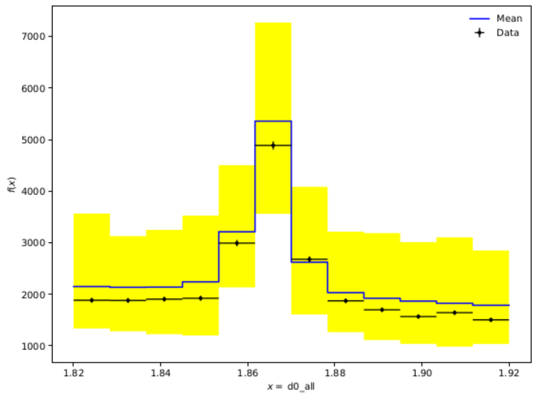

Figure 4.20: Envelope plot for D^0 meson distribution. This plot indicates the parameter ranges suitable for this meson observable, with the envelope closely matching the reference data.

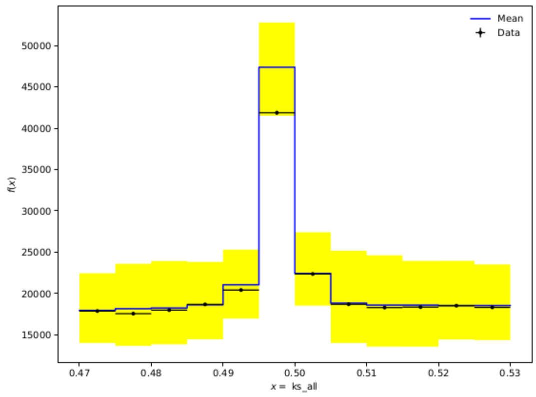

Figure 4.21: Envelope plot for K_S^0 meson distribution. This plot indicates the parameter ranges suitable for this meson observable, with the envelope closely matching the reference data.

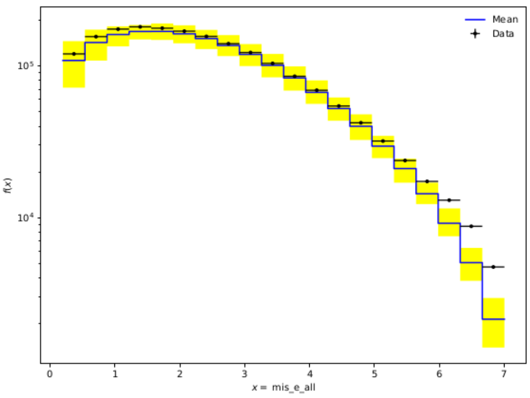

Figure 4.22: Envelope plot for missing energy in event distributions. This plot visualizes the range of values obtained from the tuning process, demonstrating how well the envelope aligns with reference data.

The figures demonstrate that the envelopes cover the reference data in nearly all bins, confirming that the chosen parameter ranges are suitable. As observed in Figure 7, the envelopes do not completely encompass the reference data at certain points. This limitation arises from reaching the maximum fit achievable with Pythia for this distribution. Therefore, we deem this acceptable for the scope of this report and will proceed with our selected parameter ranges. The weight file assigns weights to the distributions for tuning, which are manually adjusted based on our specific interests. In this project, a total of 9 distributions were initially assigned a default weight of 1 to obtain the Common Tune.

4.7 Pythia8 MC Tuning Validation Using the Professor2 Package

This section details the comprehensive Pythia8 tuning validation process conducted for the Belle II experiment using the Professor2 package. The tuning approach began with a comparative analysis of Monte Carlo events, examining quark flavor dependencies—$u\bar{u}$, $d\bar{d}$, $s\bar{s}$, $c\bar{c}$, and others, along with leptonic events (e^+e^-, $\mu^+\mu^-$, etc.)—displayed in stacked histograms to observe the influence of different quark contributions. Following this, an initial tuning stage was performed using three key parameters, after which a fourth parameter was incorporated to study parameter correlations and the impact of varying parameter counts on tuning accuracy. After these intermediate steps, a comprehensive six-parameter tuning was executed, using critical observables like thrust, charged particle momentum spectra, track counts, and visible energy in the CMS frame. The final tuning results demonstrate significant improvements in the alignment between tuned Monte Carlo spectra and reference data, providing a robust framework for refining model-dependent processes, including hadronization and parton showers. These results have been validated by Belle II collaborators using independently generated samples for their analyses and presented at general Belle II meetings, underscoring the reliability and broad applicability of this tuning approach within the Belle II physics program. The stacked histogram shown in the figure represents the contributions of various quark-antiquark pairs to the observed data distribution. The x-axis represents the observable of interest and the y-axis shows the yield, i.e., the number of events corresponding to each bin of the observable. Each colored region in the histogram corresponds to the contribution from a specific quark-antiquark pair:

- **Blue**: $u\bar{u}$ (up quark - anti-up quark)
- **Magenta**: $c\bar{c}$ (charm quark - anti-charm quark)
- **Red**: $d\bar{d}$ (down quark - anti-down quark)
- **Green**: $s\bar{s}$ (strange quark - anti-strange quark)
- **Cyan**: *Others*(e^+e^-, $\mu^+\mu^-$, *etc.*), which include contributions from more combinations .

The black data points with error bars represent the experimentally observed data. The error bars indicate the statistical uncertainties associated with each bin. In a stacked histogram, the contributions are layered on top of each other. The height of the top of the stack at any point represents the cumulative yield of all contributions at that particular bin of the observable. By comparing the stack's height to the black data points, one can evaluate how well the model (comprising these various quark-antiquark pairs) describes the experimental data.

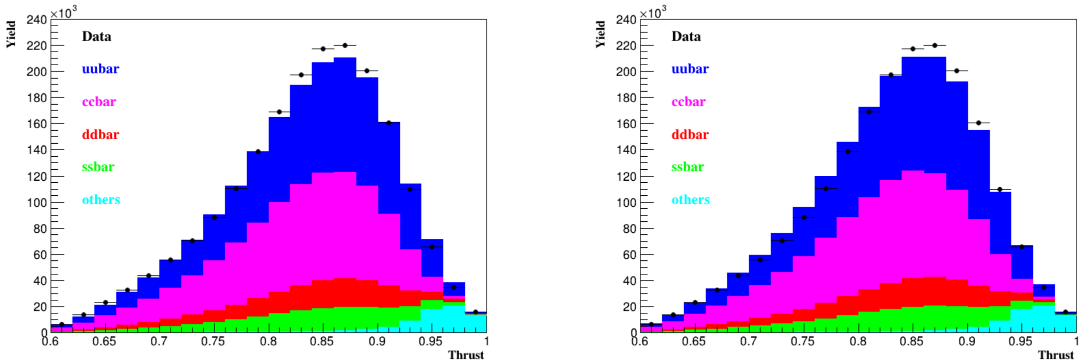

Figure 4.23: Comparison of quark-antiquark pair contributions to Thrust distributions before and after tuning.

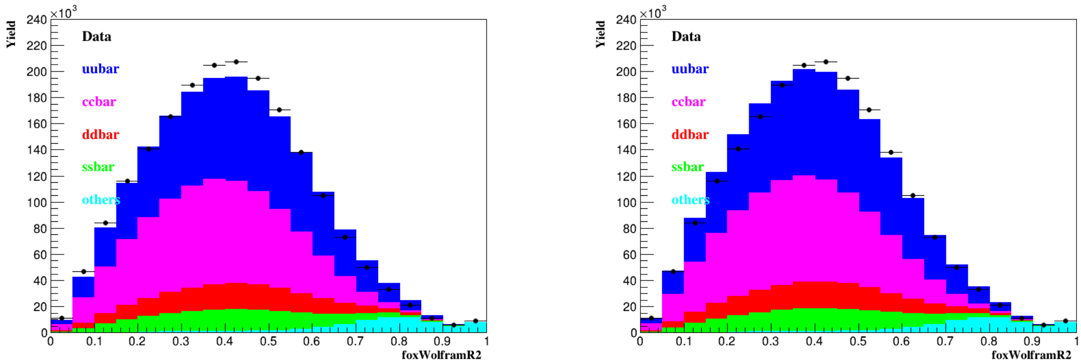

Figure 4.24: Comparison of quark-antiquark pair contributions to FoxWolframR2 distributions before and after tuning.

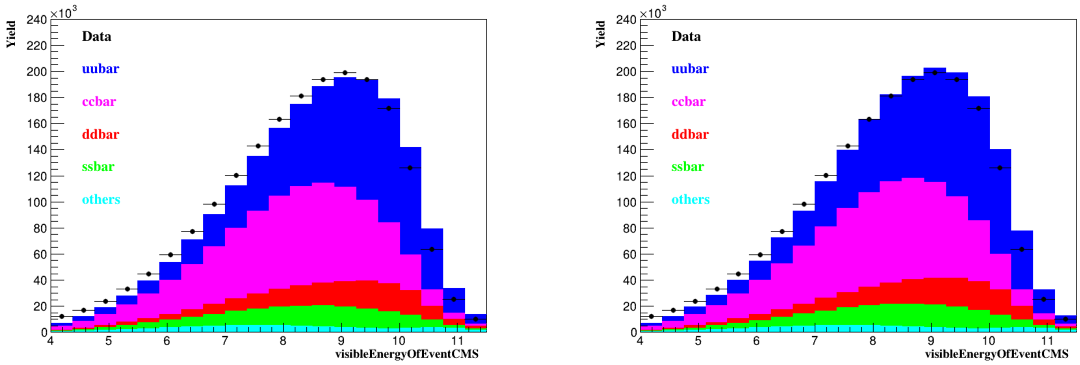

Figure 4.25: Comparison of quark-antiquark pair contributions to visible energy distributions before and after tuning.

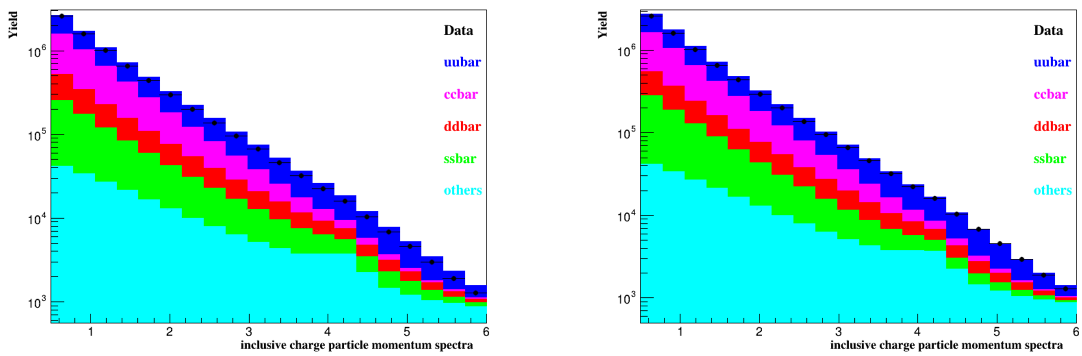

Figure 4.26: Comparison of quark-antiquark pair contributions to inclusive charge particle momentum distributions before and after tuning.

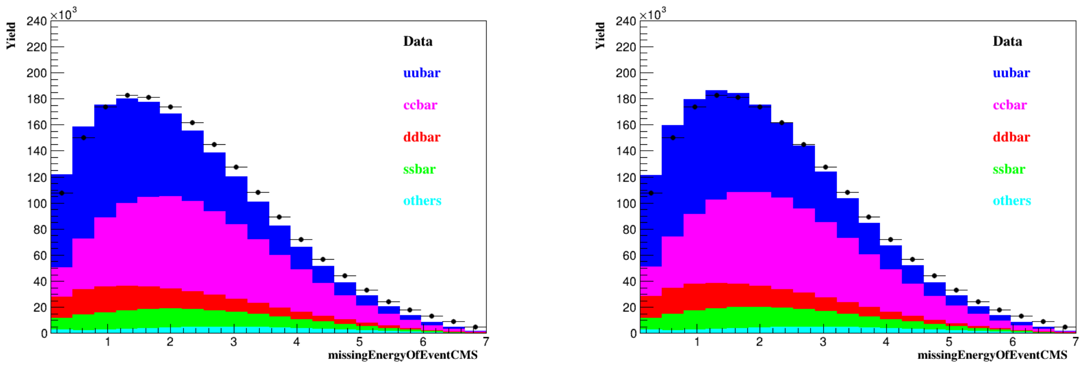

Figure 4.27: Comparison of quark-antiquark pair contributions to missingMomentumOfEvent distributions before and after tuning.

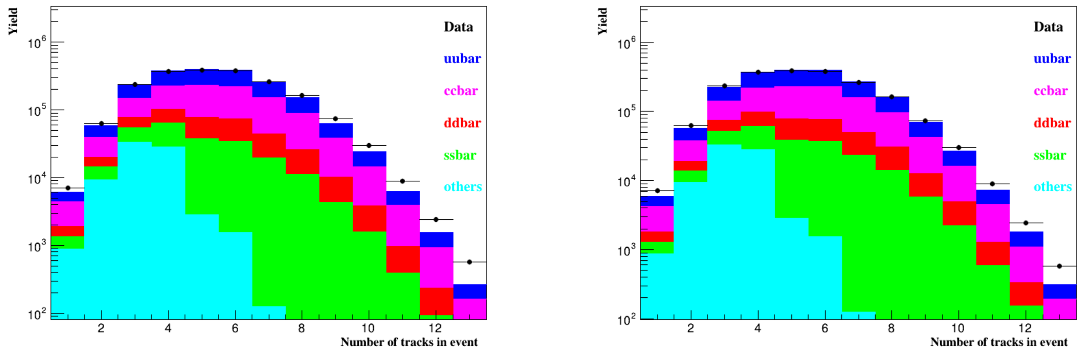

Figure 4.28: Comparison of quark-antiquark pair contributions to the number of tracks in event distributions before and after tuning.

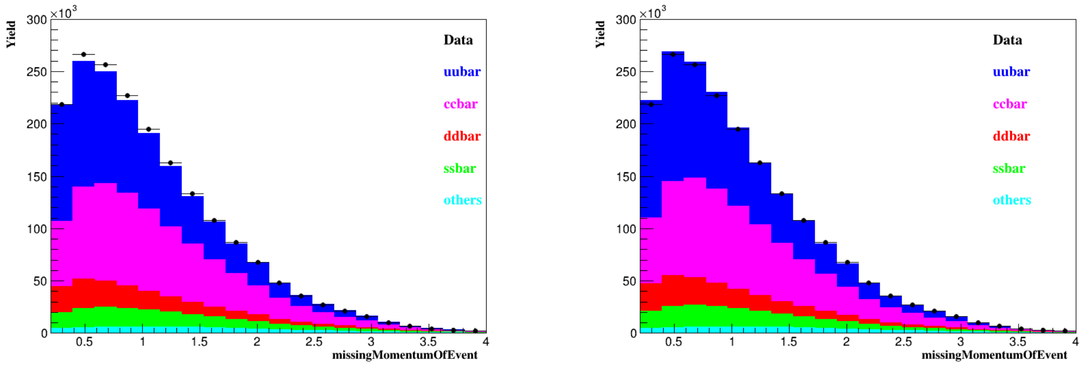

Figure 4.29: Comparison of quark-antiquark pair contributions to missingMomentumOfEvent distributions before and after tuning.

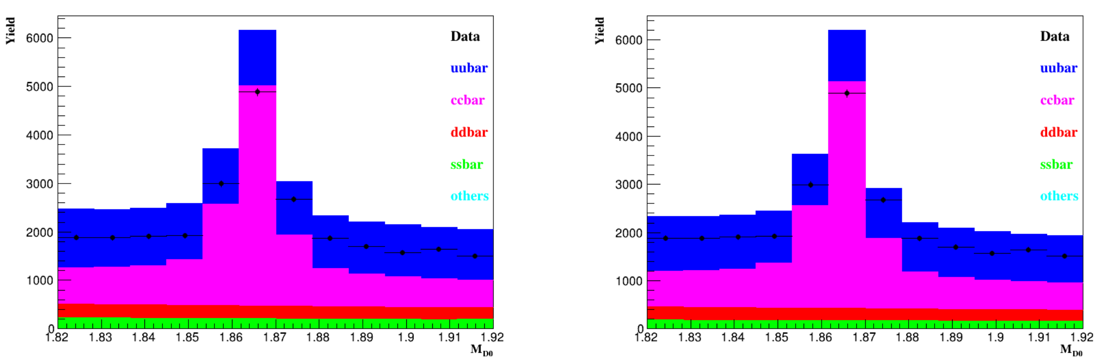

Figure 4.30: Comparison of quark-antiquark pair contributions to invariant mass of the D^0 distributions before and after tuning.

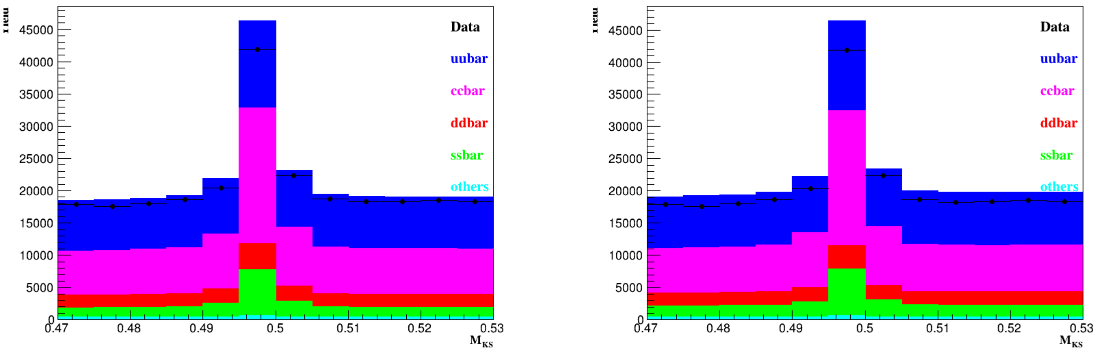

Figure 4.31: Comparison of quark-antiquark pair contributions to invariant mass of the K_S^0 distributions before and after tuning.

Before proceeding to the main stage of tuning, several algorithms were developed and automated. The initial tuning was validated using the Professor2 package [26]. At this stage, reference data was utilized to ensure accuracy and reliability.

4.7.1 Three-Variable Tuning

The variables (observables) utilized in the tuning procedure are detailed in Tables 1 and 2. The selection of each variable is driven by the specific goals of the tuning process, namely, which models the generator should constrain. This study involved a two-stage tuning process: initially, three variables of interest (listed in Table 1) were selected.

Table 4.2: Observables used for the first-stage tuning.

Thrust
Inclusive charge particle momentum spectra
Number of tracks in event

Our research highlights that the validation of the Pythia8 Monte Carlo (MC) tuning process using the Professor2 package is significantly influenced by statistical considerations, the number of generated samples, and the interdependencies among Pythia8 parameters. Effective control of these factors is essential for ensuring reliable and meaningful outcomes in Pythia8 simulations. Moreover, by increasing the statistical robustness and the quantity of MC samples generated for combinations involving u, d, s, and c quarks, and employing interpolation using a 5th order characteristic polynomial, we successfully replicate the distributions extracted from the reference sample, as illustrated in Figures. It is noteworthy that due to these correlations, the optimized parameter values may deviate from their default settings, despite achieving very close agreement between the spectra of observable quantities in the tuned and reference samples.

Table 4.3: Default and tuned values for the three-variable tuning stage.

Pythia8 parameters	Default	Tuned	Comment
StringFlav:mesonUDvector	=0.5	=0.444457	Light-flavour vector suppression
StringFlav:mesonSvector	=0.55	=0.434957	Strange vector suppression
StringFlav:mesonCvector	=2.8	=2.428458	Charm vector suppression
StringFlav:thetaPS	=-15	=-13.500045	Mixing angle θ_{PS}
StringFlav:thetaV	=36	=29.243306	Mixing angle θ_V
TimeShower:alphaSvalue	=0.1365	=0.135795	Effective $\alpha_S(m_Z)$ value

Table 4.4: MIGRAD errors for the three-variable tuning stage.

Pythia8 parameters	MIGRAD errors
StringFlav:mesonUDvector	=4.685612e-02
StringFlav:mesonSvector	=8.267797e-02
StringFlav:mesonCvector	=1.690820e-01
StringFlav:thetaPS	=7.967455e+00
StringFlav:thetaV	=8.819869e+00
TimeShower:alphaSvalue	=4.741711e-04

For three variables, the parameters' default and tune values were quite similar, considering the errors.

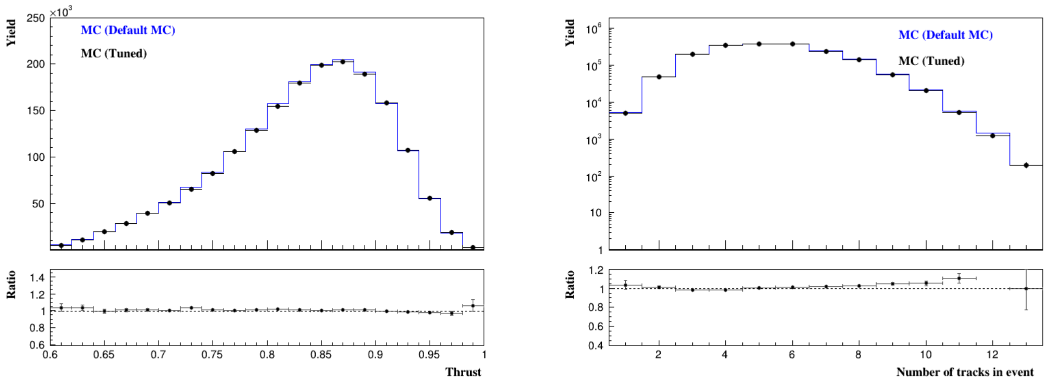

(a) (b)

Figure 4.32: Comparison of thrust and track in event distributions in events. The default Monte Carlo (MC) is represented in blue, while the tuned results are shown in black.

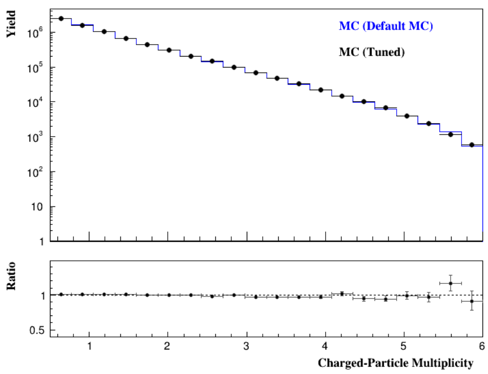

(a)

Figure 4.33: Comparing Inclusive charge particle momentum distributions: Default Monte Carlo (MC) in blue vs. tuned in black

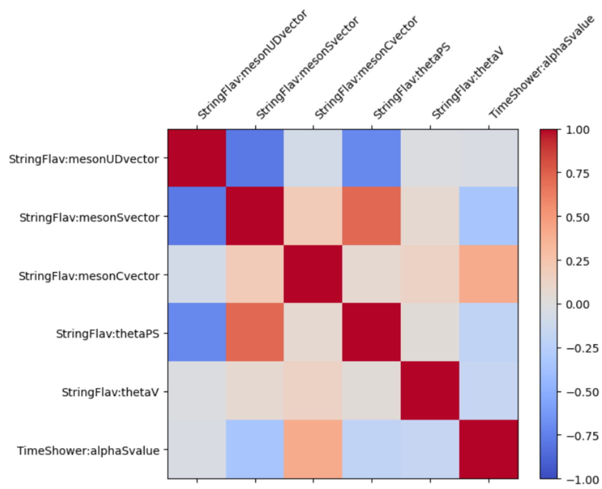

Figure 4.34: Correlations values of the parameters for the first stage tune.

4.7.2 Four-Variable Tuning

Next, we included the visibleEnergyOfEventCMS variable in our list of observables to study the impact of correlations when tuning with an increased number of variables. This tune was also performed with 5th-order polynomial to ensure the robustness for the minimization results.

Table 4.5: Observables used for the first-stage tuning.

Thrust
Inclusive charge particle momentum spectra
Number of tracks in event
visibleEnergyOfEventCMS

The comparison between tuned and reference samples for visibleEnergyOfEventsCMS observable is also a very good agreement.

Table 4.6: Default and tuned values for the four-variable tuning stage.

Pythia8 parameters	Default	Tuned	Comment
StringFlav:mesonUDvector	=0.5	=0.454673	Light-flavour vector suppression
StringFlav:mesonSvector	=0.55	=0.432484	Strange vector suppression
StringFlav:mesonCvector	=2.8	=2.388490	Charm vector suppression
StringFlav:thetaPS	=-15	=-14.416715	Mixing angle θ_{PS}
StringFlav:thetaV	=36	=32.127201	Mixing angle θ_V
TimeShower:alphaSvalue	=0.1365	=0.135604	Effective $\alpha_S(m_Z)$ value

The Default and tuned values for Pythia8 parameters. For four variables, the parameters' default and tune values were quite similar, considering the errors.

Table 4.7: MIGRAD errors associated with the tuned values for each Pythia8 parameter.

Pythia8 parameters	MIGRAD errors
StringFlav:mesonUDvector	=4.270846e-02
StringFlav:mesonSvector	=7.325382e-02
StringFlav:mesonCvector	=1.705115e-01
StringFlav:thetaPS	=6.570061e+00
StringFlav:thetaV	=6.979057e+00
TimeShower:alphaSvalue	=4.257399e-04

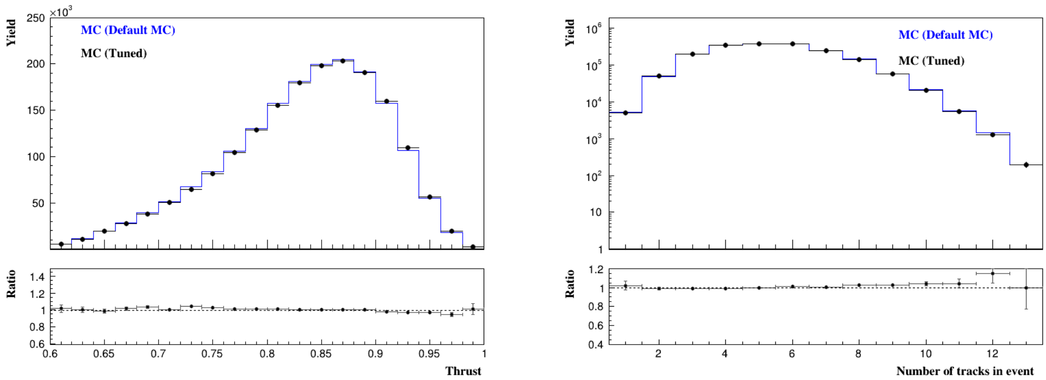

(a) (b)

Figure 4.35: Comparison of event distributions for thrust and track in event. Default Monte Carlo (MC) is shown in blue, while the tuned results are represented in black.

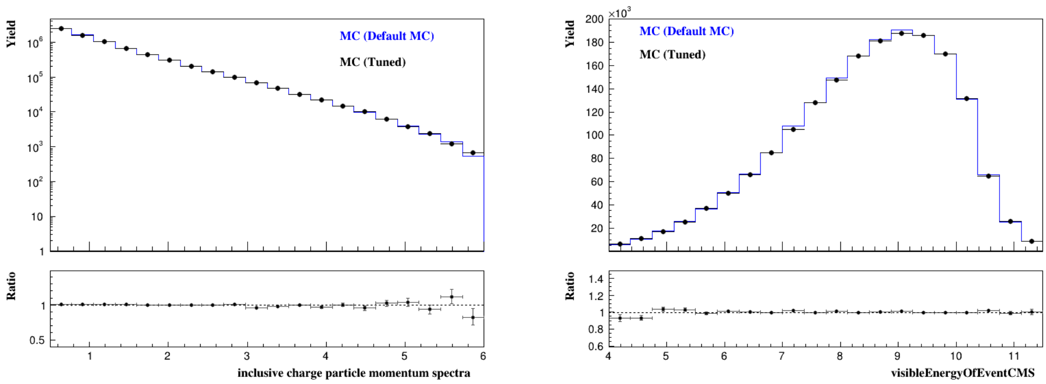

(a) (b)

Figure 4.36: Comparison of inclusive charged particle momentum and center-of-mass system (CMS) visible energy distributions. Default Monte Carlo (MC) is depicted in blue, with tuned results shown in black.

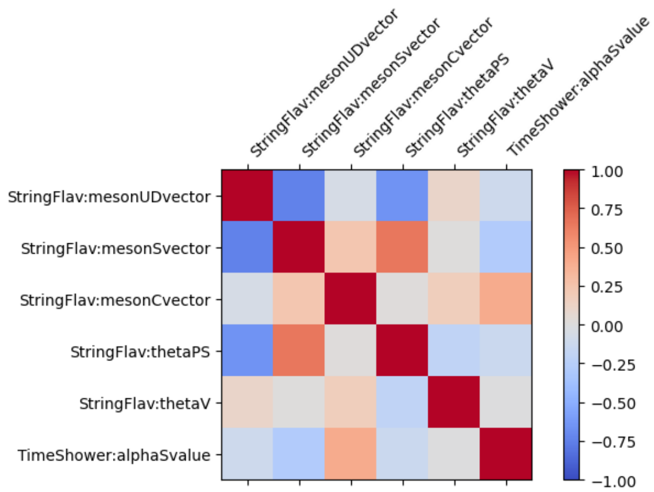

Figure 4.37: The correlation values of parameters obtained from the second-stage tuning.

The validation of the tuning procedure for a specific set of parameters in the Pythia8 Monte Carlo event generator utilizes the Professor2 package. This procedure concurrently tunes six Pythia8 MC parameters for both event and event shape variables. The results demonstrate excellent agreement between the spectra derived from the reference and tuned configurations. This methodology can be extended to constrain free parameters in any model using real experimental data.

Chapter 5

Dataset

For this analysis, we utilized the following dataset Data Sample (4Soffres):
`/belle/Data/release-06-00-12//proc13/prod00025341/e0008/4Soffres/*/all/mdst/`
The integrated luminosity for the data sample in the continuum (exp8 / proc13) was 0.806 fb^{-1}. The analysis utilized Monte Carlo (MC) samples generated through the GRID system , derived from an extensive dataset with integrated luminosities tailored to each quark combination. These MC samples, referred to as "generic" MC data, were prepared by the Belle II collaboration and encompass various quark pairs such as $u\bar{u}, d\bar{d}, s\bar{s}, c\bar{c}$. The weights assigned to these combinations are proportional to the respective cross-sections for $e^-e^+ \to q\bar{q}$ processes. The primary MC generator for simulating hadron interactions is the Pythia8 package, while the Geant4 package is employed for simulating charged tracks traversing through the detector system. All simulations are conducted within the Belle II Analysis Software Framework (basf2), ensuring detailed simulations of detector responses that consider calibration constants. The complete reconstruction of charged tracks, based on the hits in the corresponding detector, is accomplished using the Belle II tracking algorithm.

Table 5.1: MC samples and MC luminosity.

Data Sample	Process	MC Luminosity (fb^{-1})
MC15rd_b	uu	3.32
4S_offrs	dd	3.32
	ss	3.32
	cc	3.32
	$\tau^+\tau^-$	3.32
	$\mu^+\mu^-$	3.32
	$\gamma\gamma$	1.66
	e^+e^-	0.083
	e^+e^-	0.803
	$e^+e^-\mu^+\mu^-$	0.803
	l^+l^-XX	0.803
	h^+h^-ISR	0.830

In the framework of this work, a detailed comparison between the Belle II General Monte Carlo (MC) data and the experimental data was performed to understand the similarities and differences between these datasets. This comparison is crucial for validating the accuracy of the simulation models and for ensuring that the Monte Carlo simulations accurately reflect the real experimental conditions. For the purpose of tuning the Monte Carlo simulations, we developed and implemented custom algorithms. These algorithms were designed to adjust the parameters of the Monte Carlo simulations to better align with experimental observations. The tuning process involved generating Monte Carlo data using these algorithms, with particular emphasis on optimizing the simulation parameters to reflect the experimental data more accurately. To facilitate this process, we utilized the Professor2 package, which was employed to manage the multi-parameter optimization and comparison of observables. The key input files for the Monte Carlo generation were the parameter files (‘dat‘ files) and detector configuration files (‘det‘ files). Specifically, 1500 samples were generated using these files, which served as the primary input for our tuning procedures. The use of the Professor2 package allowed for a systematic and thorough evaluation of the simulation parameters, ultimately leading to improved agreement between the Monte Carlo simulations and the experimental data. In Table 5.2 lists the parameters used in the BASF2 environment for the simulation of light quarks (uds quarks) within the Belle II experiment. These parameters are crucial for generating the official Monte Carlo samples and are specifically tuned to accurately represent the behavior of light quarks under experimental conditions.

Table 5.2: Configuration settings.

Parameter	Value
StringFlav:etaSup	0.27
StringFlav:etaPrimeSup	0.12
StringFragmentation:stopMass	0.3
StringZ:aLund	0.32
StringZ:bLund	0.62
StringZ:usePetersonC	off
StringZ:usePetersonB	off
StringZ:usePetersonH	off
StringZ:rFactC	1.0
ParticleDecays:multIncrease	4.5
ParticleDecays:multIncreaseWeak	2.0
Control Radiation	
ParticleDecays:FSRinDecays	on
TimeShower:QEDshowerByQ	on

In contrast, a separate set of parameters is employed for the simulation of heavier quarks, such as the charm quark (‘c‘). These parameters are essential for accurately modeling the dynamics and interactions involving heavy quarks. The relevant parameters for heavy quarks are detailed in Table 5.3. The parameters listed for heavy quarks are designed to account for the distinct physical processes associated with their mass and interactions, which differ significantly from those of light quarks.

Table 5.3: Charm quark configuration settings.

Parameter	Value
StringFlav:etaSup	0.27
StringFlav:etaPrimeSup	0.12
StringFragmentation:stopMass	0.3
StringZ:aLund	0.32
StringZ:bLund	0.62
StringZ:usePetersonC	off
StringZ:usePetersonB	off
StringZ:usePetersonH	off
StringZ:rFactC	1.0
ParticleDecays:multIncrease	4.5
ParticleDecays:multIncreaseWeak	2.0
Control Radiation	
ParticleDecays:FSRinDecays	on
TimeShower:QEDshowerByQ	on
Modifications to Restore Excited D States	
New Charm Parameters	
StringFlav:mesonCL1S0J1	0.06
StringFlav:mesonCL1S1J0	0.1775
StringFlav:mesonCL1S1J1	0.1868
StringFlav:mesonCL1S1J2	0.1836
StringFlav:mesonCvector	2.8
New Strange Parameters	
StringFlav:probStoUD	0.286
StringFlav:probSQtoQQ	0.323
New Baryon Parameters	
StringFlav:probQQtoQ	0.133
StringFlav:probQQ1toQQ0	0.0468

5.1 Event Selection Criteria

The thesis employed the Professor2 package to optimize multivariate minimization problem efficiently, considering parameter correlations. Analysis scripts utilizing the Jupyter Notebook interface were developed for multivariate analysis of generated data, while statistical tests were conducted using the CERN ROOT package [19]. Experimental data, crucial for model tuning, was analyzed through the Belle2 Analysis Framework (basf2), and Monte Carlo samples were generated using a global GRID computing system [20]. Data selection criteria for the experimental data were meticulously defined.

In our analysis, we implemented several event selection criteria to ensure the quality and relevance of the data. Each criterion is designed to isolate significant physics events while reducing background noise and irrelevant interactions. Below, we detail each cut and its motivation:

- **good tracks: $p_{\perp}$ [GeV] > 0.1, |d0| [cm] < 1, |z0| [cm] < 2**
  - *Explanation*: The transverse momentum ($p_{\perp}$) cut of 0.1 [GeV] ensures that only tracks with sufficient momentum are considered, excluding low-momentum tracks that may be more susceptible to noise. The distance of closest approach (|d0|) cut of less than 1 cm ensures that tracks originate from the collision vertex, while the longitudinal impact parameter (|z0|) cut of less than 2 cm aligns tracks with the interaction point along the beam axis.
  - *Motivation*: These criteria help in selecting tracks that are likely to come from the primary interaction point, thereby improving the signal-to-noise ratio and focusing the analysis on genuine collision events.
- **Good Clusters:** Clusters not associated with charged track deposits, E_{lab} [GeV] > 0.1, clusters in the CDC acceptance ($0.296706 < \theta$ [rad] < 2.61799])
  - *Explanation*: Clusters not associated with charged tracks are considered to avoid double-counting energy deposits. Clusters are required to have an energy E_{lab} greater than 0.1 [GeV] to filter out low-energy noise. Clusters are restricted to the CDC acceptance range to ensure they are within the detector's effective region. The distribution of the cosine of the polar angle, $\cos\theta$, is also considered to focus on clusters with a well-defined angular distribution within the detector's acceptance, excluding regions with low detector sensitivity.
  - *Motivation*: These cuts ensure that selected clusters contribute to the visible energy of the event while excluding noise and energy deposits from irrelevant regions or charged particles. The inclusion of $\cos\theta$ helps select clusters with meaningful angular distributions, improving the accuracy and relevance of the energy measurements.
- **number of good tracks in an event** ≥ 3

  - *Explanation*: This criterion requires at least three good tracks to be present in the event. This ensures that the event has a significant amount of charged particle activity.
  - *Motivation*: Events with fewer than three tracks are likely to be less interesting or contaminated by noise. This cut helps in focusing on events with substantial particle activity that are more likely to be of interest.

- **number of good clusters in an event** ≥ 3
  - *Explanation*: At least three good clusters are required to ensure that the event has sufficient electromagnetic activity.
  - *Motivation*: This cut filters out events with minimal electromagnetic activity and focuses on those with significant photon or neutral particle energy, which are relevant for the analysis.

- $E_{\textbf{vis}}$ **[GeV]** $> \mathbf{4}$
  - *Explanation*: The visible energy (E_{vis}) is defined as the sum of the momenta of good tracks and the energy of good clusters. A threshold of 4 [GeV] is applied to ensure that only high-energy events are considered.
  - *Motivation*: This criterion helps in rejecting low-energy background events and selecting those with substantial energy deposits, indicative of more significant physics processes.

- **momentum balance** $0 < p_z$ **[GeV]** $< \mathbf{5}$
  - *Explanation*: The sum of the z-components of the momenta of good tracks and good clusters is required to be between 0 and 5 [GeV]. This ensures reasonable longitudinal momentum balance in the event.
  - *Motivation*: This cut helps in selecting well-reconstructed events with balanced longitudinal momentum, thus reducing the influence of beam-related background and improving the quality of the selected events.

These criteria collectively aim to improve the signal-to-noise ratio and ensure that the data analyzed are representative of significant physics processes. By applying these cuts, we enhance the reliability of the results and focus on events that contribute meaningfully to the study's goals.

5.2 Comparison of Event Shape Variables Extracted from Pythia6 and Pythia8 Monte Carlo Event Generators

Unlike the Belle2 experiment, which utilizes the Pythia8 Monte Carlo generator, the Belle experiment employed the Pythia6 version. Consequently, it was essential to investigate the differences between these generators and comprehend their impact on the physical variables. The transition from Pythia6 to Pythia8 involves updates and improvements in the modeling of hadronization and parton showers, as well as better handling of multiple parton interactions and more accurate event simulation. Understanding these differences is crucial for ensuring consistency and accuracy in the analysis of experimental data across the two experiments. In the initial phase, event shape variables were compared between the Pythia6 and Pythia8 Monte Carlo event generators using their default parameter values. This comparison aimed to identify any inherent differences in the event shape distributions produced by each generator. In the figures, we observe the parameters of Pythia8 and Pythia6, which have been adjusted to align with each other and create comparable tables. The Pythia6 generator is based on Fortran, whereas Pythia8 is based on C++. Many parameters do not have direct equivalents and often require recalculations. In our tables, the default values of Pythia6 and Pythia8 parameters differ, and this disparity is evident in the distributions, where we observe more than a 50 percent difference between them.

Table 5.4: Pythia6 and Pythia8 parameter equivalents and their default values.

Pythia 8.215	**Pythia 6.202**	**Pythia 8.215 Default values**	**Pythia 6.202 Default values**
StringZ:aLund	PARJ(41)	0.68	0.3
StringZ:bLund	PARJ(42)	0.98	0.58
StringPT:sigma	PARJ(21)	0.335	0.36
StringFragmentation:stopMass	PARJ(33)	1	0.8
StringFlav:etaSup	PARJ(25)	0.6	1
StringFlav:etaPrimeSup	PARJ(26)	0.12	0.4
TimeShower:pTmin	PARJ(82)	0.5	1
StringZ:aExtraDiquark	PARJ(45)	0.97	0.5
StringZ:rFactC	PARJ(46)	1.32	1
StringPT:enhancedFraction	PARJ(23)	0.01	0.01
StringPT:enhancedWidth	PARJ(24)	2	2
StringFragmentation:stopSmear	PARJ(37)	0.2	0.2
MiniStringFragmentation:nTry	MSTJ(17)	2	2
HadronLevel:mStringMin	MSTJ(14)	1	1
StringFragmentation:eBothLeftJunction	PARJ(49)	1	1
StringFlav:probStoUID	PARJ(2)	0.217	0.3
StringFlav:probQQtoQ	PARJ(3)	0.081	0.1
StringFlav:probSQtoQQ	PARJ(3)	0.915	0.4
StringFlav:probQQ1toQQ0	PARJ(4)	0.0275	0.05
StringFlav:mesonUDvector	PARJ(11)	0.5	0.5
StringFlav:mesonSvector	PARJ(12)	0.55	0.6
StringFlav:mesonCvector	PARJ(13)	0.88	0.75
StringFlav:mesonUDL1S0J1	PARJ(14)	0	0
StringFlav:mesonUDL1S1J0	PARJ(15)	0	0
StringFlav:mesonUDL1S1J1	PARJ(16)	0	0
StringFlav:mesonUDL1S1J2	PARJ(17)	0	0
StringFlav:decupletSup	PARJ(18)	1	1
StringFlav:popcornSpair	PARJ(6)	0.9	0.5
StringFlav:popcornSmeson	PARJ(7)	0.5	0.5
TimeShower:pTminChgQ	PARJ(83)	0.5	1
MultipartonInteractions:expPow	PARJ(83)	1.85	1
MultipartonInteractions:pT0Ref	PARP(82)	2.28	1.9
MultipartonInteractions:ecmPow	PARP(90)	0.215	0.16
MultipartonInteractions:coreRadius	PARP(84)	0.4	0.2

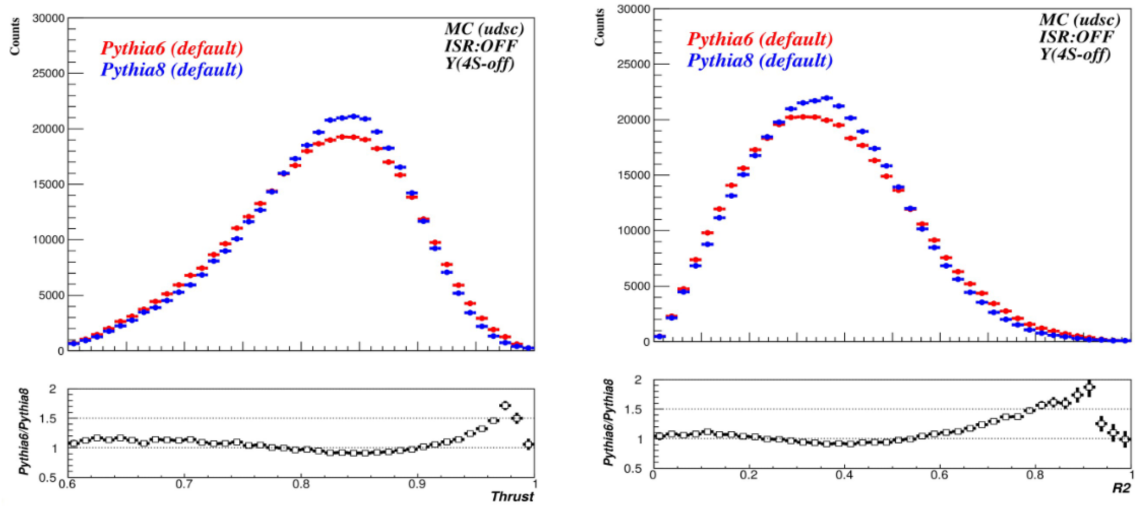

Figure 5.1: Comparison of Thrust and R2 variables: Pythia6 Default (Red) vs. Pythia8 Default (Blue)

To ensure consistency, a Table of Correspondence Parameters (ToC) was created. Monte Carlo events were generated with Pythia8 and Pythia6 using the ToC parameters. The comparison of event shape distributions showed that using ToC parameters improved the match between the two sets of distributions, compared to the default settings.

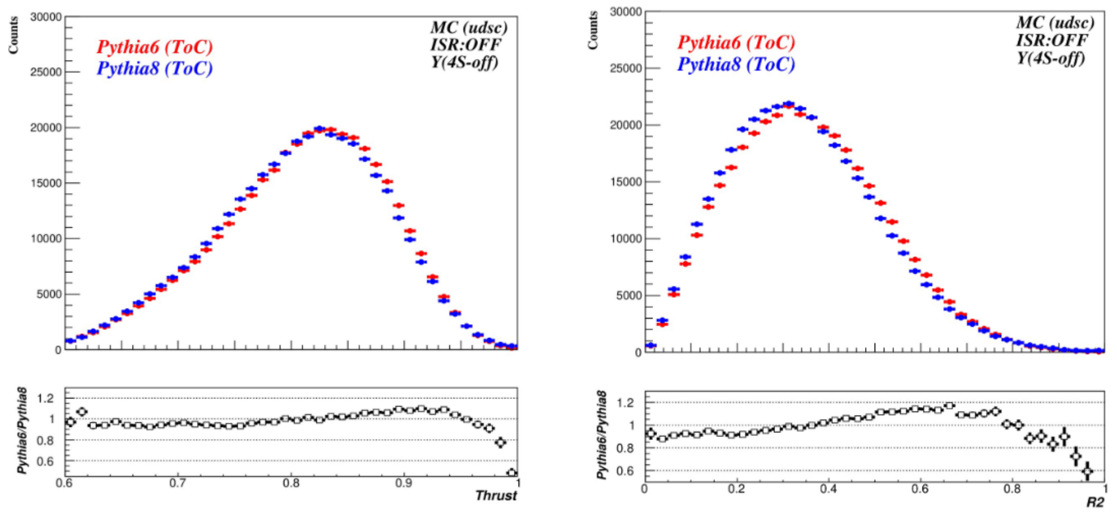

Figure 5.2: Comparison of Thrust and R2 variables: Pythia6 ToC (Red) vs. Pythia8 ToC (Blue)

Table 5.5: Comparison of parameters between Pythia 8.215 and Pythia 6.202.

Pythia 8.215	**Pythia 6.202**
StringFlav:mesonCvector=0.75	PARJ(13)=0.75
StringFlav:mesonUDL1S01=0	PARJ(14)=0
StringFlav:mesonUDL1S10=0	PARJ(15)=0
StringFlav:mesonUDL1S11=0	PARJ(16)=0
StringFlav:mesonUDL1S12=0	PARJ(17)=0
StringFlav:decupletSup=1	PARJ(18)=1
StringFlav:popcornSpair=0.5	PARJ(6)=0.5
StringFlav:popcornSmeson=0.5	PARJ(7)=0.5
TimeShower:pTminChgQ=1	PARJ(83)=1
MultipartonInteractions:expPow=1	PARJ(81)=1
MultipartonInteractions:pT0Ref=1.9	PARJ(82)=1.9
MultipartonInteractions:ecmPow=0.16	PARJ(90)=0.16
MultipartonInteractions:coreRadius=0.2	PARJ(84)=0.2
StringZ:aLund=0.32	PARJ(41)=0.32
StringZ:bLund=0.62	PARJ(42)=0.62
StringPT:sigma=0.42	PARJ(21)=0.42
StringFragmentation:stopMass=0.3	PARJ(33)=0.3
StringFlav:etaSup=0.27	PARJ(25)=0.27
StringFlav:etaPrimeSup=0	PARJ(26)=0
StringZ:aExtraDiquark=0.5	PARJ(45)=0.5
StringZ:rFactC=1	PARJ(46)=1
StringPT:enhancedFraction=0.01	PARJ(23)=0.01
StringPT:enhancedWidth=2	PARJ(24)=2
StringFragmentation:stopSmear=0.2	PARJ(37)=0.2
MiniStringFragmentation:nTry=2	MSTJ(17)=2
HadronLevel:mStringMin=1	MSTJ(14)=1
StringFragmentation:eBothLeftJunction=1	PARJ(49)=1
StringFlav:probStoUID=0.2	PARJ(2)=0.2
StringFlav:probQQtoQQ=0.1	PARJ(3)=0.1
StringFlav:probSQtoQQ=0.4	PARJ(3)=0.4
StringFlav:probQQ1toQQ0=0.05	PARJ(4)=0.05
StringFlav:mesonUDVecto=0.5	PARJ(15)=0.5
StringFlav:mesonSVector=0.6	PARJ(12)=0.6

5.3 Pythia6 (“Belle-Note-780”) vs. Pythia6 (“old Belle”) tunes

In our study, we used the "old Belle" tune parameters [21] for Pythia6 as defined in the article published in Physical Review D 101, 092004 (2020). By defining these parameters, we generated Monte Carlo events and compared our results with those obtained using the "Belle-Note-780" parameters [22]. The parameter values of old Belle and Belle-Note-780 tunes are listed in Table 4.4 .

Table 5.6: Pythia6 ("old Belle") and "Belle-Note-780" tune parameters

Parameter	Old Belle Value	"Belle-Note-780" Value
PARJ(1)	0.1	-
PARJ(2)	0.3	-
PARJ(3)	0.4	-
PARJ(4)	0.05	-
PARJ(11)	0.5	-
PARJ(33)	-	0.8
PARJ(12)	0.6	-
PARJ(13)	0.75	-
PARJ(14)	0.0	-
PARJ(15)	0.0	-
PARJ(16)	0.0	-
PARJ(17)	0.0	-
PARJ(19)	1.0	-
PARJ(21)	0.28	0.42
PARJ(25)	0.27	0.27
PARJ(26)	0.0	0.0
PARJ(33)	0.3	-
PARJ(41)	0.32	0.3
PARJ(42)	0.62	0.62
PARJ(45)	1.0	-
PARJ(47)	1.0	-
PARJ(55)	-0.05	-
PARJ(81)	0.27	0.25
PARJ(82)	1.6	0.5
MSTJ(1)	4	-
MSTJ(12)	2	-
MSTJ(26)	2	-
MSTJ(45)	4	-
MSTJ(107)	1	-

We used an internal note from the Belle collaboration titled "Monte-Carlo Tuning for Continuum Events" . This document describes the tuning of various parameters in the Monte-Carlo generator Pythia for use in the Belle experiment.Using these parameters, Monte Carlo events were generated and the resulting data was compared with the "old Belle".

The following parameters are varied to tune the global properties of events in the simulation:

- **PARJ(21)** σ_q: Influences the transverse momentum.
- **PARJ(33)** Q_0': Affects the fragmentation function.
- **PARJ(41) Lund** a: Part of the Lund fragmentation function, influences the shape of the fragmentation spectrum (hard fragmentation supp).
- **PARJ(42) Lund** b: Another component of the Lund fragmentation function (soft fragmentation supp).
- **PARJ(81)** Λ_{QCD}: The hard QCD scale, important for determining the strength of strong interactions.
- **PARJ(82)** Q_0: Terminates the parton shower, affecting the final state particle multiplicities.

2. Identified Particle Properties

Specific parameters are adjusted to fine-tune the properties of identified particles:

- **PARJ(25)**: Suppression of η mesons.
- **PARJ(26)**: Suppression of η' mesons.

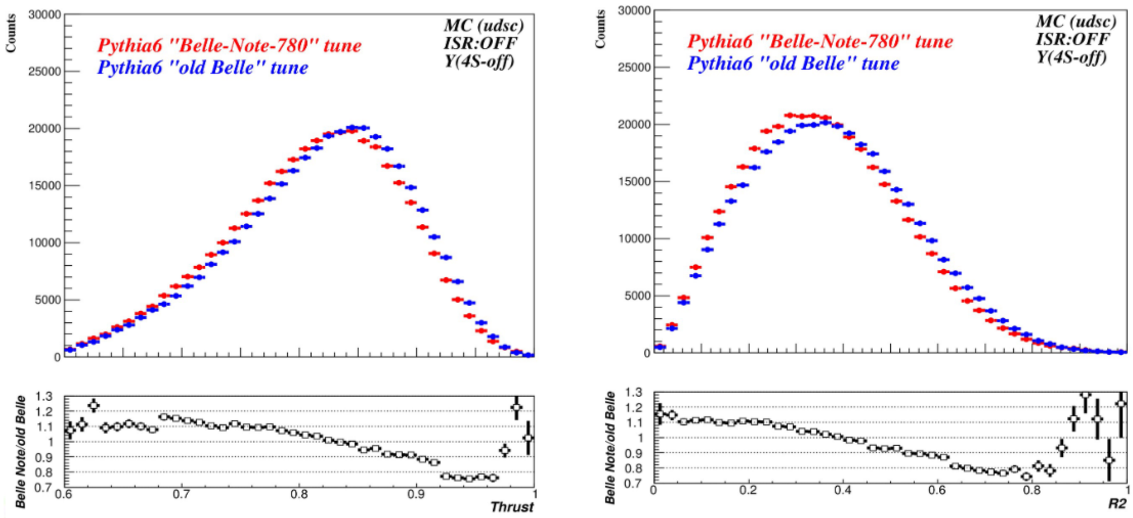

Figure 5.3: Comparison of event shape variables between Pythia6 with "Belle-Note-780" tune (Red) and Pythia6 with "Old Belle" tune (Blue). The left plot shows the Thrust variable, and the right plot shows the Fox-Wolfram R2 variable.

5.4 Belle II vs. Pythia6 (“old Belle”) tune

Comparisons were also conducted between the Belle II data and the results from Pythia6, referred to as the "old Belle" tune. This analysis allows us to assess the differences between the Monte Carlo (MC) simulations generated by Belle II and those produced by the previous Belle MC setup. By evaluating these differences, we gain insights into how the updated Belle II MC data deviates from the older Belle MC data, highlighting the impact of advancements in the simulation models and their influence on the experimental outcomes. To compare the Belle II and Belle simulations, we set Belle II parameters to match the values used in Belle. We then generated events with these settings. The parameters and their values are listed in the table.

Table 5.7: Comparison of Pythia6 ("old Belle") tune parameters with Belle II parameters

Pythia6 ("old Belle") tune	**Belle II**
PARJ(14) = 0.05	StringFlav:mesonUDL1S0J1 = 0.05
PARJ(15) = 0.05	StringFlav:mesonUDL1S1J0 = 0.05
PARJ(16) = 0.05	StringFlav:mesonUDL1S1J1 = 0.05
PARJ(17) = 0.05	StringFlav:mesonUDL1S1J2 = 0.05
PARJ(21) = 0.28	StringPT:sigma = 0.28
PARJ(25) = 0.27	StringFlav:etaSup = 0.27
PARJ(26) = 0	StringFlav:etaPrimeSup = 0
PARJ(41) = 0.32	StringZ:aLund = 0.32
PARJ(42) = 0.62	StringZ:bLund = 0.62
PARJ(46) = 1	StringZ:rFactC = 1
PARJ(81) = 0.38	TimeShower:alphaSvalue = 0.149
PARJ(82) = 0.5	TimeShower:pTmin = 0.25

Pythia6 PARJ(81)

PARJ(81) (D = 0.29 [GeV]) Λ value in running α_s for parton showers. This is used in all user calls to PYSHOW, in the PYEEVT/PYONIA e^+e^- routines, and in a resonance decay.

Pythia8 TimeShower:alphaSvalue

Because some parameters in Pythia8 do not have Pythia6 equivalents, that is why the TimeShower:alphaSvalue parameter was recalculated with the specified formula.

- Default = 0.1383
- Minimum = 0.06
- Maximum = 0.25

The α_s value at scale M_Z^2. The default value corresponds to a crude tuning to LEP data, to be improved.

$$\alpha_s(Q^2) = \frac{12\pi}{(33 - 2n_f)\ln\left(\frac{Q^2}{\Lambda^2}\right)} \tag{5.1}$$

where $n_f = 5$, $Q^2 = M_{Z2}$, $\Lambda = PARJ(81)$.

Pythia6 PARJ(82)

PARJ(82) (D = 1.0 [GeV]) (Q0) invariant mass cut-off m_{min} of PYSHOW parton showers, below which partons are not assumed to radiate.

Pythia8 TimeShower:pTmin

- Default = 0.5
- Minimum = 0.1
- Maximum = 2.0

Parton shower cut-off p_T for QCD emission.

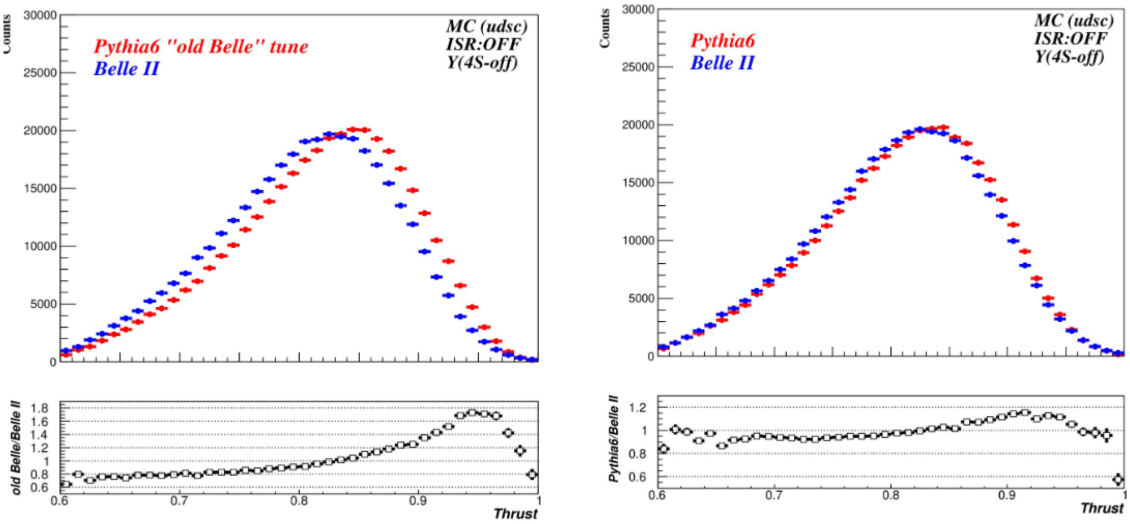

Figure 5.4: Comparison of Thrust Variable between Pythia6 and Belle II for both tune settings and Table of Correspondence (ToC) parameters. The left plot shows the comparison with the "Old Belle" Pythia6 tune and Belle II, while the right plot shows the comparison with Pythia6 settings against Belle II using ToC parameters.

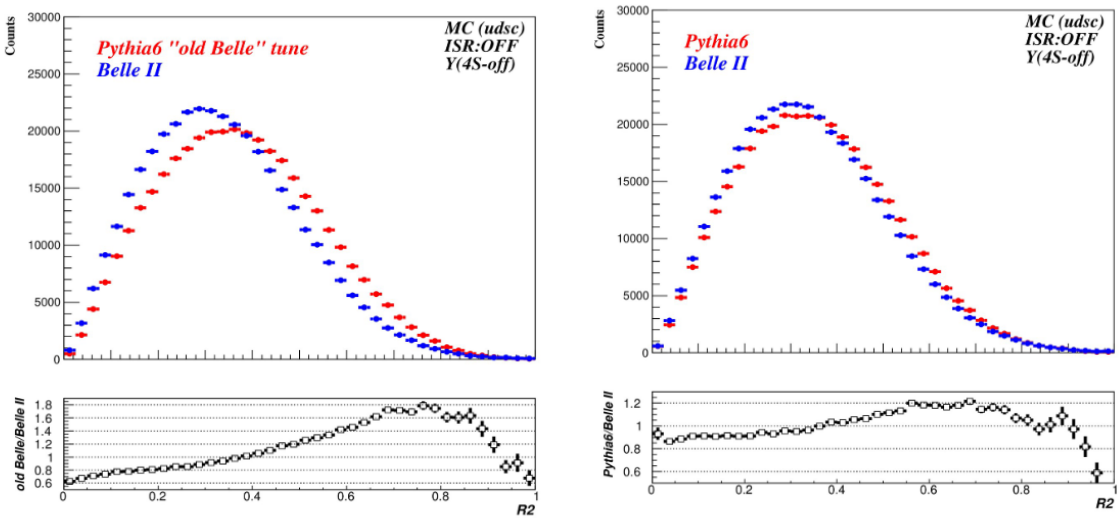

Figure 5.5: Comparison of FoxWolframR2 Variable between Pythia6 and Belle II for both tune settings and Table of Correspondence (ToC) parameters. The left plot shows the comparison with the "Old Belle" Pythia6 tune and Belle II, while the right plot shows the comparison with Pythia6 settings against Belle II using ToC parameters.

5.5 Belle II vs. Pythia6 (“Belle-Note-780”) tune

Following the same approach, we compared the Belle II simulation with the Pythia6 tune from the Belle-Note-780. The results clearly show significant differences between the distributions, indicating that the tuning parameters from the note do not lead to improved agreement with the Belle2 MC data.

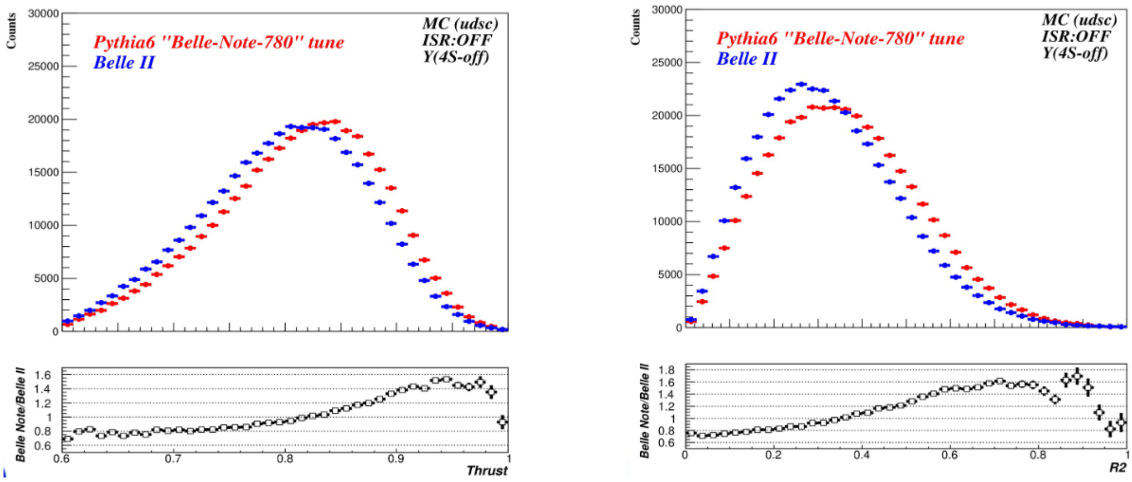

Figure 5.6: Comparison of event shape variables between Pythia6 ("Belle-Note-780" tune) and Belle II parameters. The left plot shows the Thrust variable, while the right plot shows the Fox-Wolfram R2 variable.

5.6 Standalone Pythia8 Monte Carlo Simulation Comparison with Belle Experimental Data

An important aspect of this study is the examination of the standalone Pythia8 generator and the comparison of the resulting Monte Carlo data with the published data from the Belle experiment [23]. Here, $z = \frac{2E_h}{\sqrt{s}}$, where E_h is the energy of a specific hadron ($\pi^{\pm}$, $K^{\pm}$, p) in the center-of-mass (c.m.) frame, and $\sqrt{s}$ is the c.m. energy, which is 10.583 [GeV] for Belle. Figure 1 shows the experimental results for the differential cross section $\frac{d\sigma}{dz}$ extracted from Belle data [24]. The cross sections are derived from a 558 fb^{-1} data sample collected at the $\Upsilon(4S)$ resonance with the Belle detector at the KEKB asymmetric-energy e^+e^- collider [25].

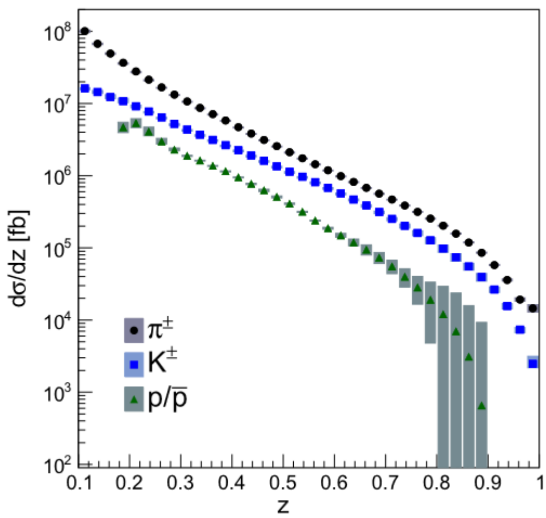

Figure 5.7: Differential cross sections vs. z for pions (black circles), kaons (blue squares), and protons (green triangles) as a function of z without any thrust requirement. The error boxes represent the systematic and error bars the statistical uncertainties.

We used the `WeakSingleBoson:ffbar2gmZ` setting in Pythia8. The `WeakSingleBoson:ffbar2gmZ` process in Pythia8 is a setting that enables the generation of events where a fermion-antifermion pair ($f\bar{f}$) annihilates to produce a single electroweak gauge boson, which can be either a photon (γ) or a Z boson. Here is a detailed explanation: By default, collisions in Pythia8 are assumed to occur in the center-of-mass (CM) frame. This default assumption simplifies many simulations, especially those involving symmetric colliders. However, other frame options can be specified using the `Beams:frameType` parameter to better suit different experimental setups. Using the option `Beams:frameType = 2`, the beam energies can be set separately, which is particularly useful for asymmetric beam configurations. In our simulations, we employed `Beams:frameType = 2` to account for the asymmetric nature of the beams used in our experiment. This setting allows us to define the energy of each beam individually, reflecting the true conditions of the experiment. The electron beam energy was set to 8 [GeV] and the positron beam energy to 3.5 [GeV], in accordance with Belle data. Preliminary studies for optimizing various constraints to be applied simultaneously to both MC and data samples have been performed. Figure 5.8a shows the cosine of the polar angle distribution i.e $\cos\theta$ for produced K-mesons, as well as a scatter plot in terms of $\cos\theta$ and kaon momentum p.

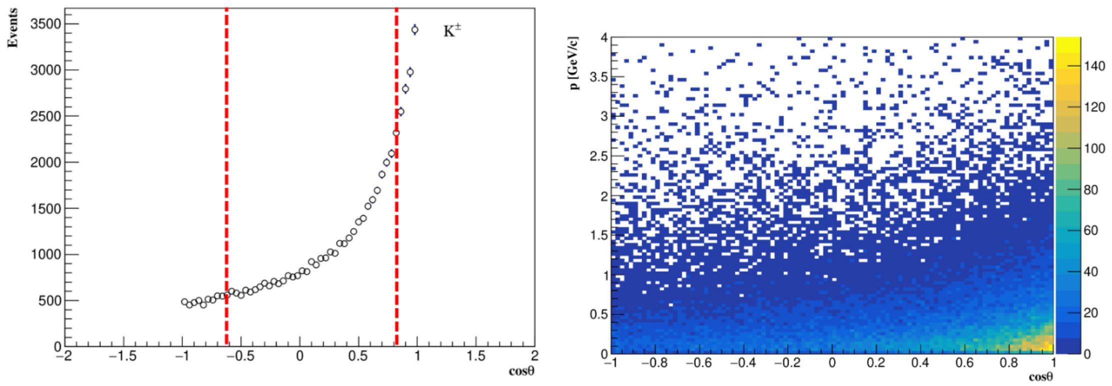

(a) (b)

Figure 5.8: Monte Carlo simulation of the cosine of the polar angle distribution, i.e., $\cos\theta$ (left panel) for produced kaons, along with a scatter plot of $\cos\theta$ versus kaon momentum p (right panel). The dotted red lines in the left panel indicate the angular acceptance of the Belle detector.

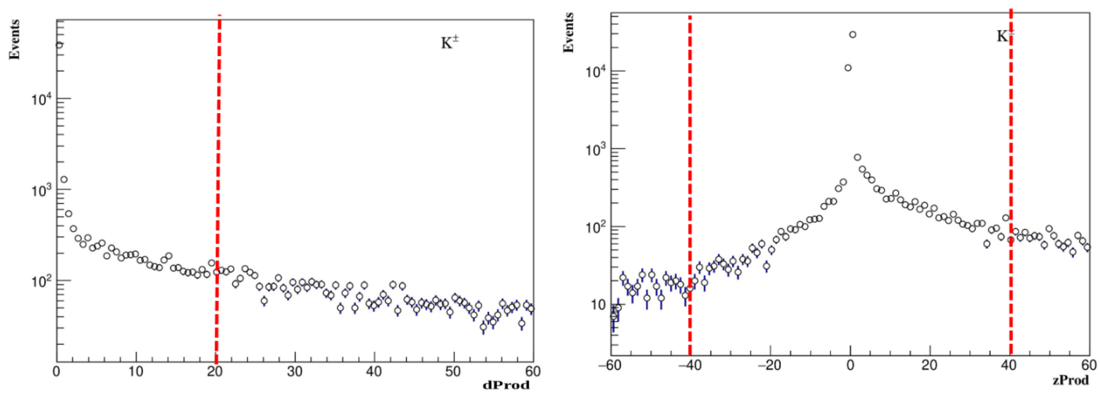

(a) (b)

Figure 5.9: Monte Carlo simulation of the transverse (left panel) and longitudinal distributions for the production point in the case of kaons. The dotted red lines indicate the cuts used to extract the experimentally measured cross sections.

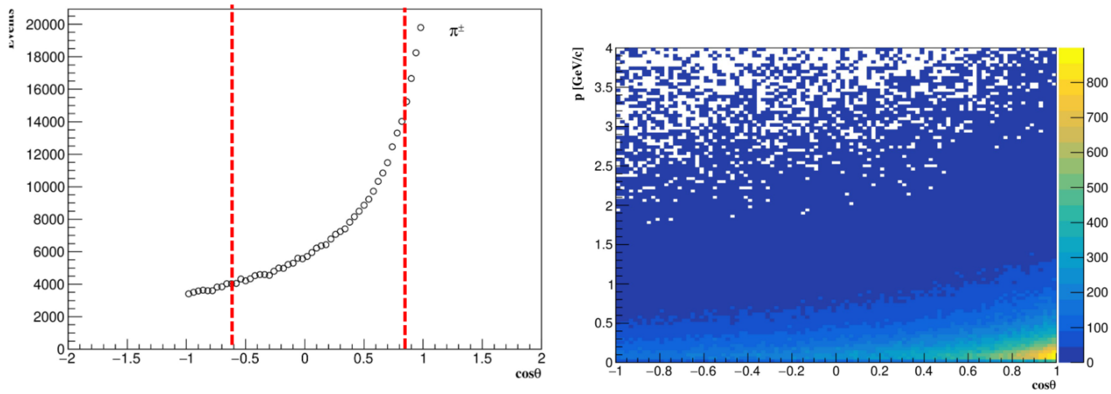

(a) (b)

Figure 5.10: Monte Carlo simulation of the cosine of the polar angle distribution, i.e., $\cos\theta$ (left panel) for produced pions, along with a scatter plot of $\cos\theta$ versus pion momentum p. The dotted red lines in the left panel show the angular acceptance of the Belle detector.

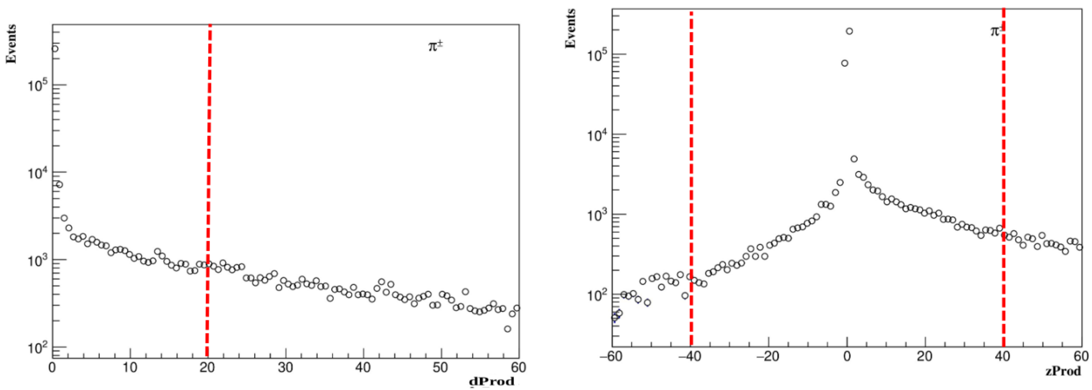

(a) (b)

Figure 5.11: Monte Carlo simulation of the transverse (left panel) and longitudinal distributions for the production point in the case of pions. The dotted red lines show the cuts used to extract the experimentally measured cross sections.

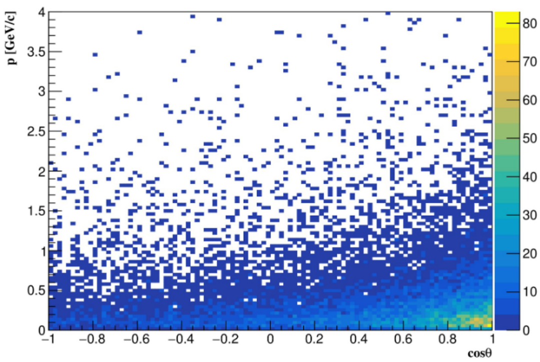

(a)

Figure 5.12: Monte Carlo simulation of the produced protons. $\cos\theta$ versus proton momentum p.

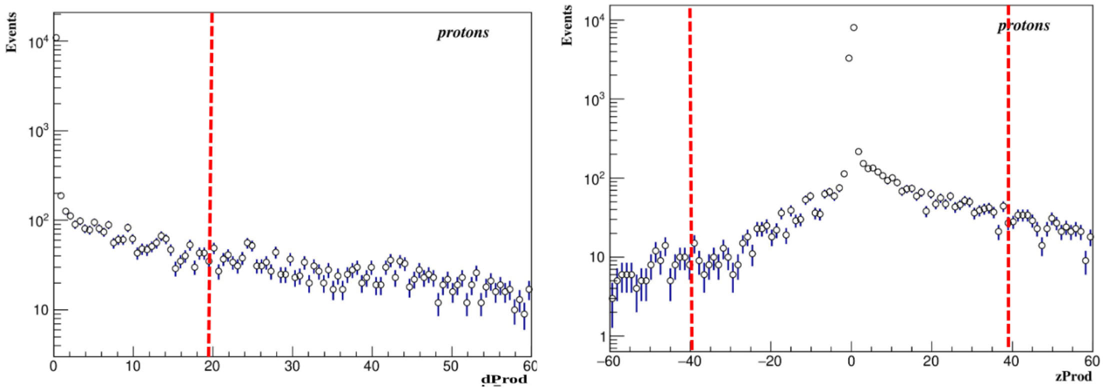

(a) (b)

Figure 5.13: Monte Carlo simulation of the transverse (left panel) and longitudinal distributions for the production point in the case of protons. The dotted red lines show the cuts used to extract the experimentally measured cross sections.

The plots below show the differential cross-sections for kaons, pions, and protons, comparing Belle data with the Pythia8 Monte Carlo predictions.

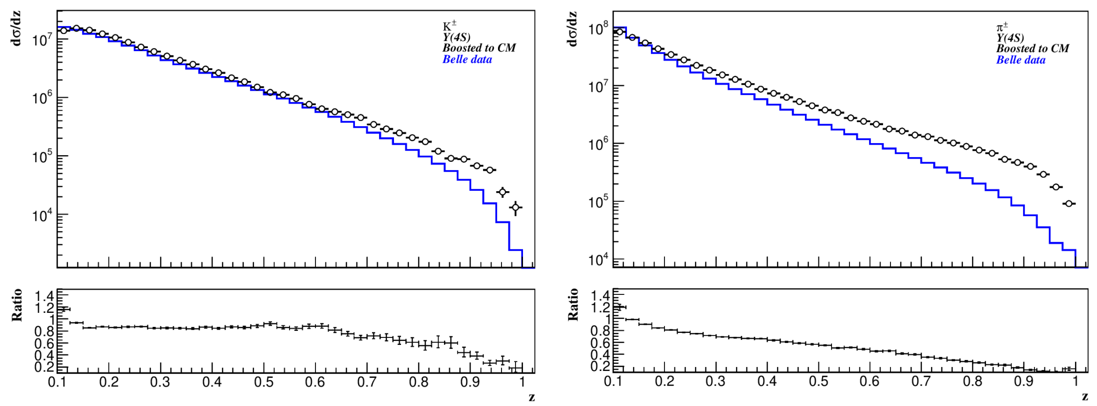

(a) Kaons (b) Pions

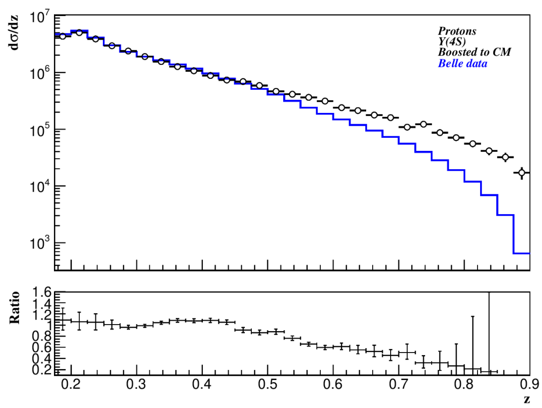

Figure 5.15: Comparison of the z distribution for protons,pions, kaons between Belle data and Monte Carlo in the CM frame.

The distributions of these variables were obtained as they were used to implement selection criteria (cuts) during the analysis.We applied the following selection criteria to ensure compatibility with the experimental data.

- Center-of-mass energy: $\text{energy}_{\text{cm}} = 10.58\,\text{GeV}$
- Final state particles: `particle.isFinal()`
- Pion identification: `particle.id() == 211` or `particle.id() == -211`
- Kaon identification: `particle.id() == 321` or `particle.id() == -321`
- Proton identification: `particle.id() == 2212` or `particle.id() == -2212`
- Angular acceptance: $-0.511 < \cos\theta_{\text{lab}} < 0.842$
- Track proximity: Tracks must be within 4 cm along and 2 cm perpendicular to the positron beam axis from the event vertex.
- Event energy: Events with at least three reconstructed charged tracks must have a visible energy of charged tracks and neutral clusters above 7 [GeV] to remove τ pair events.

Figure 5.16 presents the multiplicities of protons, pions, and kaons produced in simulations using the Pythia8.3 generator, based on 300000 generated events.

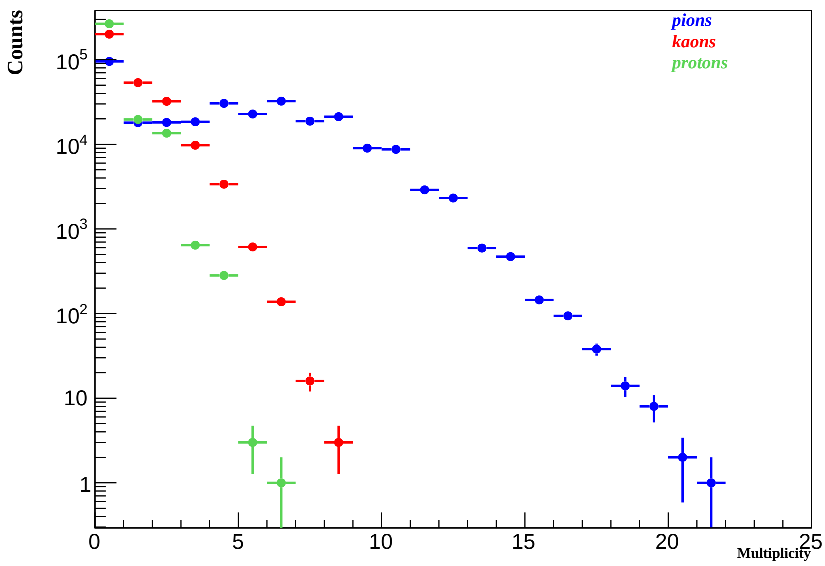

Figure 5.16: Pion (blue), kaon (red), and proton (green) multiplicities in Monte Carlo simulations

We compared the transverse momentum (p_z) in the lab frame and center-of-mass frame using Monte Carlo simulations. This was done because Belle data were collected in the center-of-mass frame.

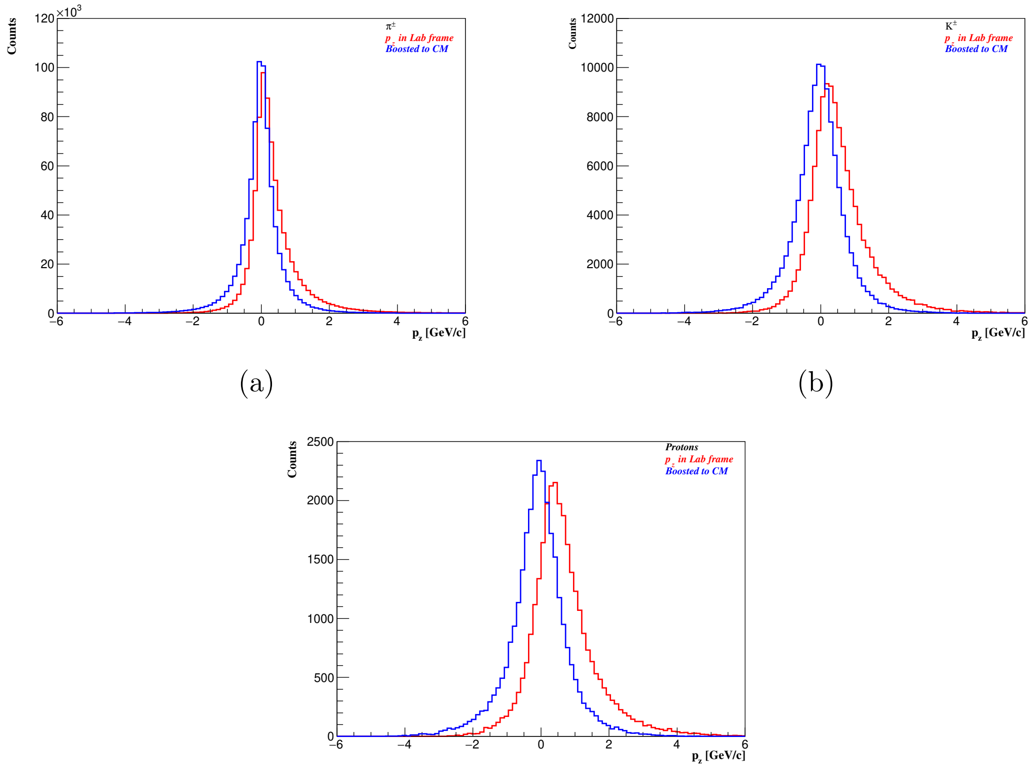

(a) (b) (c)

Figure 5.17: Comparison of p_z in Lab and CM Frames for pions, kaons, and protons in Monte Carlo simulations

Next, we compared the fractional z distributions of particles in the center-of-mass frame and the laboratory frame. The differences between these distributions were analyzed using a ratio plot.

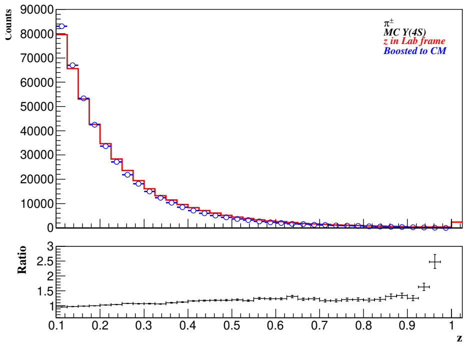

(a)

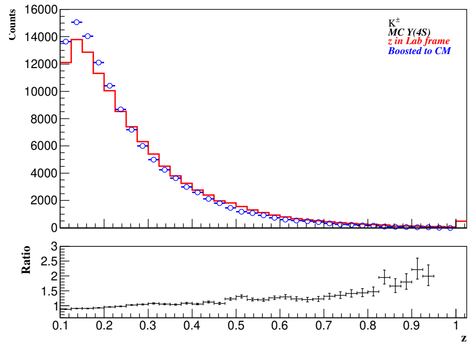

(b)

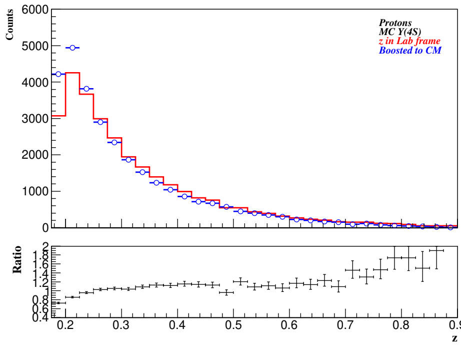

(c)

Figure 5.18: Comparison of fractional z distributions in CM and Lab frames in Monte Carlo simulations

The comparison of the z distribution between the laboratory frame and the center-of-mass frame for kaons shows good agreement at intermediate z values, but this agreement diminishes for $z > 0.5$. For protons, the distributions match well at small z values but diverge beyond $z = 0.7$. The agreement for pions is relatively poor across all z values. For Data/MC comparison, the data points cited in and reconstructed MC samples generated with Pythia8 using a fixed set of parameters tuned on Belle II data for various distributions (excluding $\frac{d\sigma}{dz}$) were used. In comparison to the $558\,\text{fb}^{-1}$ integrated luminosity for the experimental data sample, the MC samples were generated and reconstructed with $1000\,\text{fb}^{-1}$ integrated luminosity. In Fig. 4, the MC/Data comparison for $\frac{d\sigma}{dz}$ for kaons, pions and protons are presented in the upper panel, while the ratio of data to MC for $\frac{d\sigma}{dz}$ is shown in the lower panel.

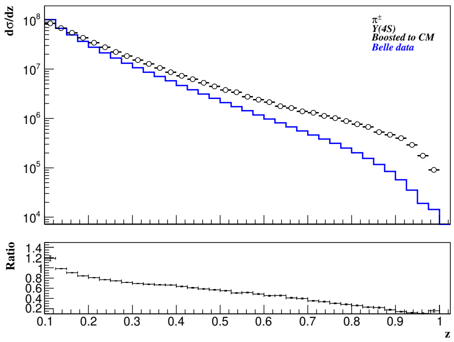

(a)

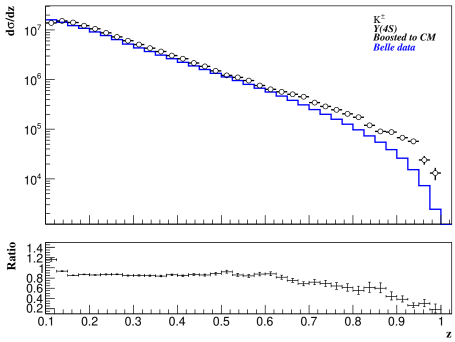

(b)

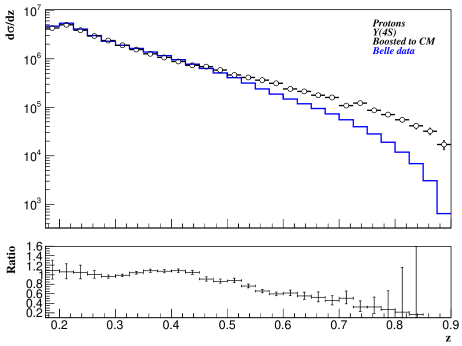

(c)

Figure 5.19: The upper panel shows $\frac{d\sigma}{dz}$ as a function of z for particles, where data is marked in blue and MC is in black. The lower panel displays the ratio of data to MC.

The z distributions of protons and positively and negatively charged kaons show reasonable agreement between the MC and Belle data while the agreement is comparatively worse for pions. Next, we moved on to Belle2 parameters and values for light quarks (uds) shown in the table 5.8 These comparisons show how changes in parameter values affect the variables.

Table 5.8: Configuration settings

Parameter	**Value**
StringFlav:etaSup	0.27
StringFlav:etaPrimeSup	0.12
StringFragmentation:stopMass	0.3
StringZ:aLund	0.32
StringZ:bLund	0.62
StringZ:usePetersonC	off
StringZ:usePetersonB	off
StringZ:usePetersonH	off
StringZ:rFactC	1.0
ParticleDecays:multIncrease	4.5
ParticleDecays:multIncreaseWeak	2.0
Control Radiation	
ParticleDecays:FSRinDecays	on
TimeShower:QEDshowerByQ	on

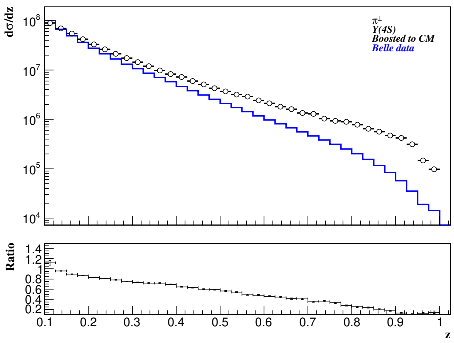

(a)

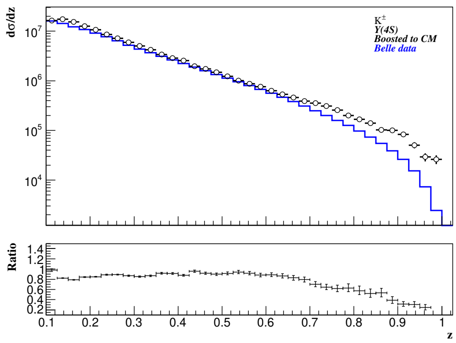

(b)

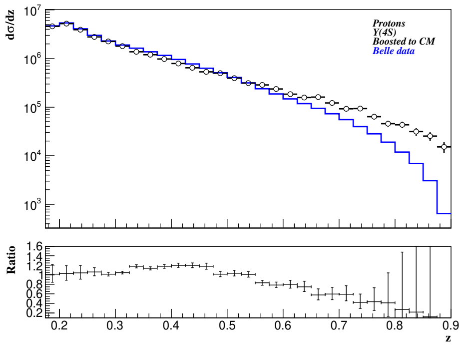

(c)

Figure 5.20: The upper panel shows $\frac{d\sigma}{dz}$ as a function of z for particles, where data is marked in blue and MC is in black. The lower panel displays the ratio of data to MC.

The results indicate that using the Belle2 parameter values yields the same trend observed with the default parameter values of standalone Pythia8.3.

Chapter 6

Results

6.1 MC and Data Comparisons Before and After Tune

For the primary tuning procedure, a 5th-order polynomial interpolation was employed to model the response of the system. The choice of this high-order polynomial ensures a more accurate representation of the underlying behavior across the parameter space. To guarantee robustness in the optimization process, the parameter space was exhaustively scanned, with up to 100,000 starting points considered during the minimization process. The tuning parameters were extracted using a total of 1,500 Monte Carlo (MC) samples, which served as anchor points for the interpolation. These anchor points are essential as they help ensure that the fitted polynomial accurately represents the behavior across different regions of the parameter space. By utilizing a large number of samples, the analysis ensures statistical stability and minimizes the risk of overfitting. As a result of this thorough process, the tuned parameter values for the simulation were obtained. These values, shown in table, reflect the optimal configuration achieved after the extensive tuning procedure, offering the best possible agreement between the simulation and experimental data.

Parameter	Value	MIGRAD Error
StringFlav:mesonUDvector	0.621664	3.498581e-02
StringFlav:mesonSvector	2.446557	4.554261e-02
StringFlav:mesonCvector	2.863498	2.291809e-02
StringFlav:thetaPS	-59.882703	2.575822e+00
StringFlav:thetaV	3.547790	1.769148e+00
TimeShower:alphaSvalue	0.139261	2.423326e-04

Table 6.1: Tuned parameters, their extracted values, and MIGRAD errors

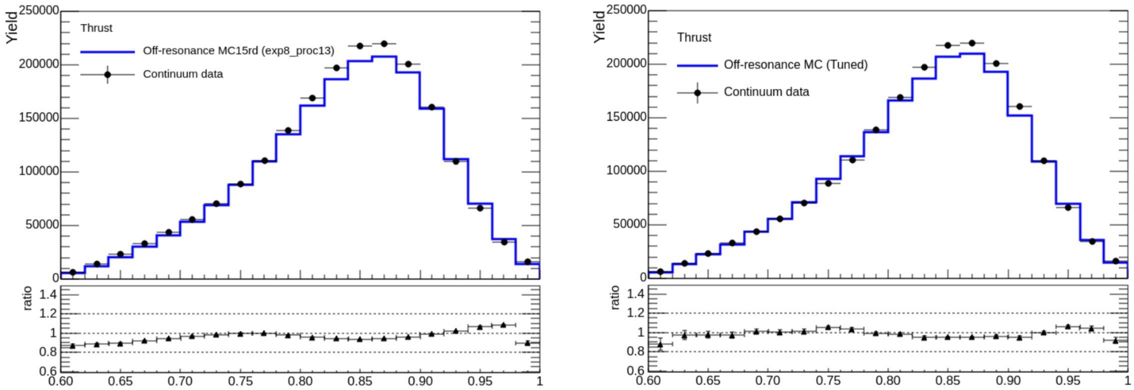

Figure 6.1: Comparison of thrust distributions before and after Monte Carlo tuning. The tuning process significantly improves the agreement between the off-resonance MC simulation and experimental continuum data, as shown in the ratio plots.

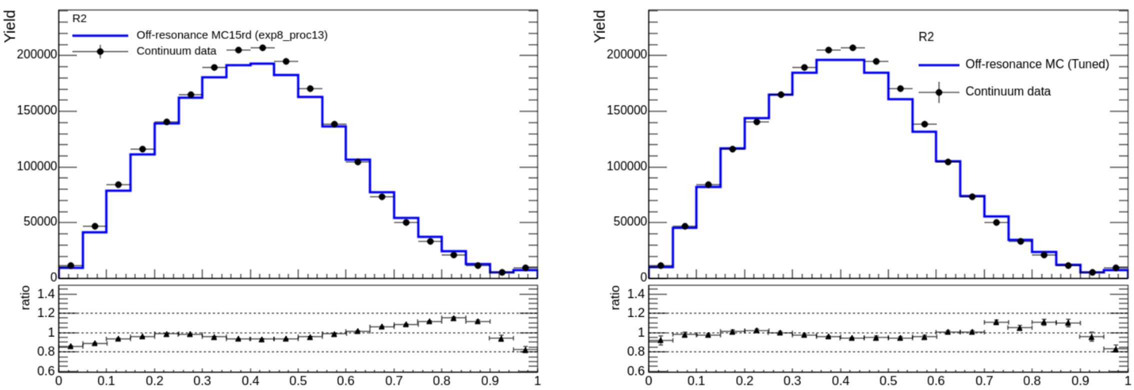

Figure 6.2: Comparison of R_2 distributions before and after Monte Carlo tuning. The tuning process significantly improves the agreement between the off-resonance MC simulation and experimental continuum data, as shown in the ratio plots.

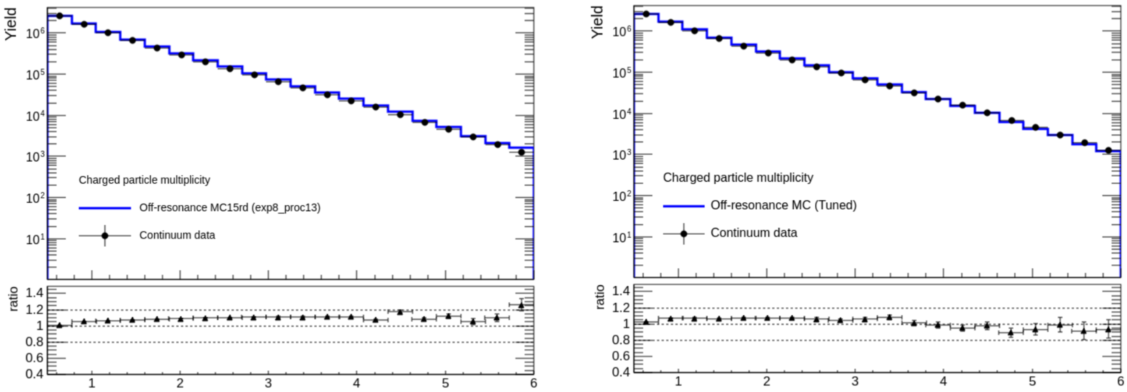

Figure 6.3: Comparison of charged particle multiplicity distributions before and after Monte Carlo tuning. The tuning process significantly improves the agreement between the off-resonance MC simulation and experimental continuum data, as shown in the ratio plots.

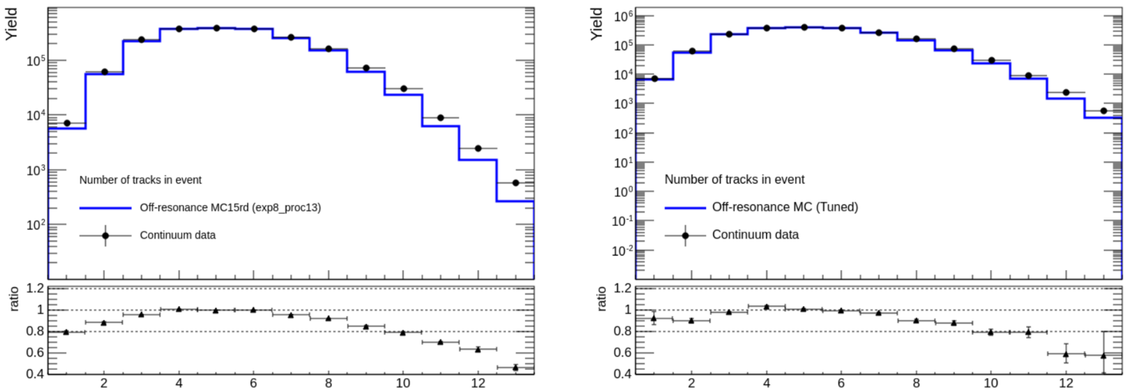

Figure 6.4: Comparison of number of tracks in event distributions before and after Monte Carlo tuning. The tuning process significantly improves the agreement between the off-resonance MC simulation and experimental continuum data, as shown in the ratio plots.

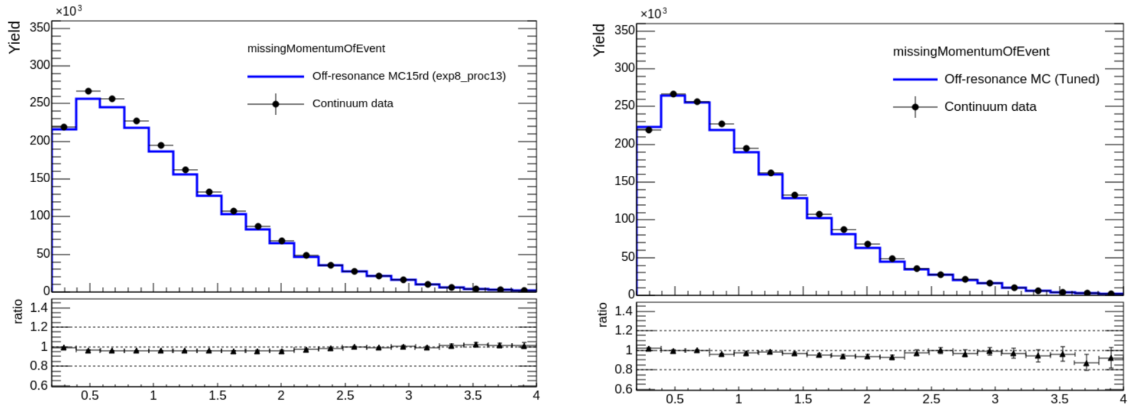

Figure 6.5: Comparison of missingMomentumOfEvent distributions before and after Monte Carlo tuning. The tuning process significantly improves the agreement between the off-resonance MC simulation and experimental continuum data, as shown in the ratio plots.

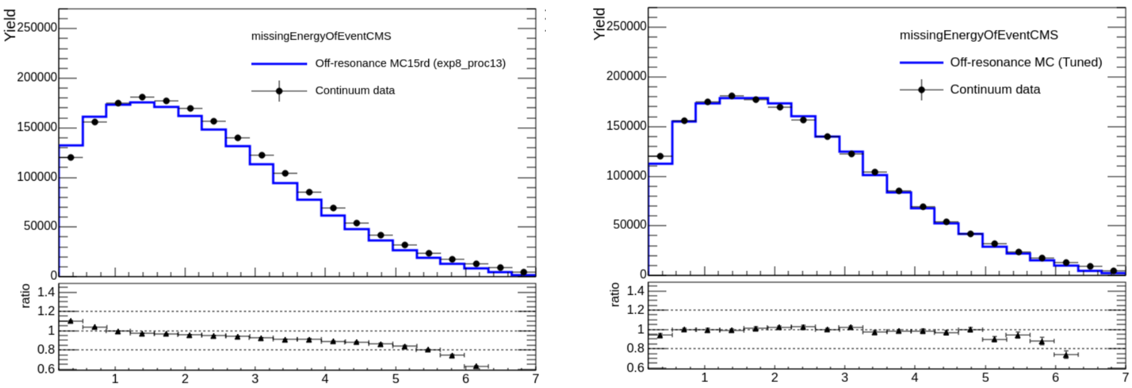

Figure 6.6: Comparison of missingEnergyOfEventCMS distributions before and after Monte Carlo tuning. The tuning process significantly improves the agreement between the off-resonance MC simulation and experimental continuum data, as shown in the ratio plots.

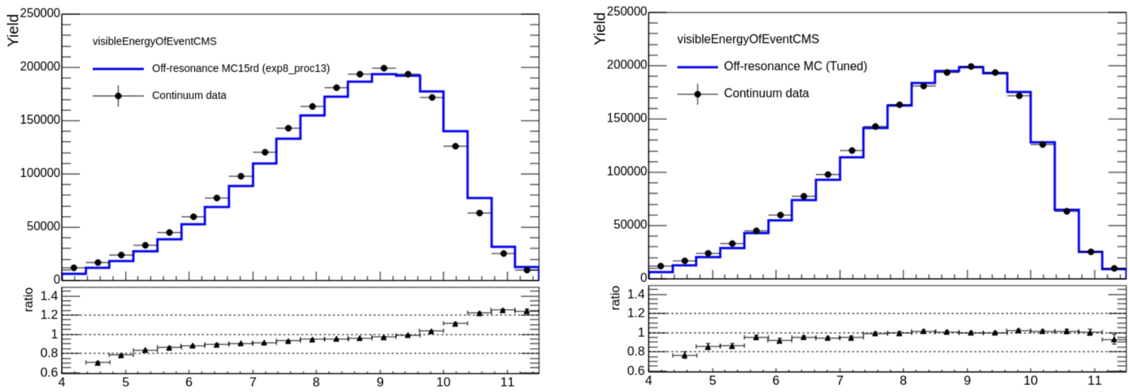

Figure 6.7: Comparison of visibleEnergyofEventCMS distributions before and after Monte Carlo tuning. The tuning process significantly improves the agreement between the off-resonance MC simulation and experimental continuum data, as shown in the ratio plots.

The collaboration, using the tuning parameters we suggested, created a set of samples referred to as `NewMC`. The samples previously used as the official Monte Carlo samples were labeled `OldMC`. With the tuned parameters, the Belle II members produced a sample that has been analyzed by various physics groups within Belle II for different studies. For validation purposes, members performed their own studies on the relevant variables of interest.

Datasets

Old MC (scale to 200 fb^{-1}):

- `/belle/collection/MC/MC15ri_uubar_1abinv_v1`
- `/belle/collection/MC/MC15ri_ddbar_1abinv_v1`
- `/belle/collection/MC/MC15ri_ssbar_1abinv_v1`
- `/belle/collection/MC/MC15ri_ccbar_1abinv_v1`

New MC (200 fb^{-1}) [Pythia parameters tunings]:

- `/belle/MC/release-06-00-08/DB00002100/MC15ri_b/prod00034692/s00/e1003/4S/r00000/ccbar/mdst`
- `/belle/MC/release-06-00-08/DB00002100/MC15ri_b/prod00034693/s00/e1003/4S/r00000/ddbar/mdst`

- /belle/MC/release-06-00-08/DB00002100/MC15ri_b/prod00034694/s00/e1003/4S/r00000/ssbar/mdst
- /belle/MC/release-06-00-08/DB00002100/MC15ri_b/prod00034695/s00/e1003/4S/r00000/uubar/mdst

An example was studied by Sen Yan. Comparisons of old MC, new MC, and data were based on the process $e^+e^- \to D_s^+ K^{*0} D^{(*)+}$ using old datasets and our dataset.

The list of observables and event selection criteria were mentioned and used throughout the analysis. The observables included Thrust, Fox-Wolfram moment R_2, Visible Energy of Event (CMS), $M(D_s^-)$, and $M(K^{*0})$. The event selection criteria, based on BELLE2-NOTE-PH-2022-043, included:

List of Observables & Event Selection

Observables:

- Thrust
- Fox-Wolfram moment R2
- VisibleEnergyOfEventCMS
- M(D_s^-) and M(K^{*0})

Event Selection Criteria [BELLE2-NOTE-PH-2022-043]:

- For charged tracks:
  - $|dr| < 2$ cm, $|dz| < 4$ cm
  - $\mathcal{L}(K/\pi) > 0.6$ as kaons
  - $\mathcal{L}(K/\pi) < 0.4$ as pions
- K_S^0 is selected from the Kshorts list from V0 objects
- Vertex fit and mass constraint fits for D_s^-
- The $D^{(*)+}$ signal region: $1.8 < M_{\text{rec}}(D_s^- K^{*0}) < 2.1$ GeV/c^2

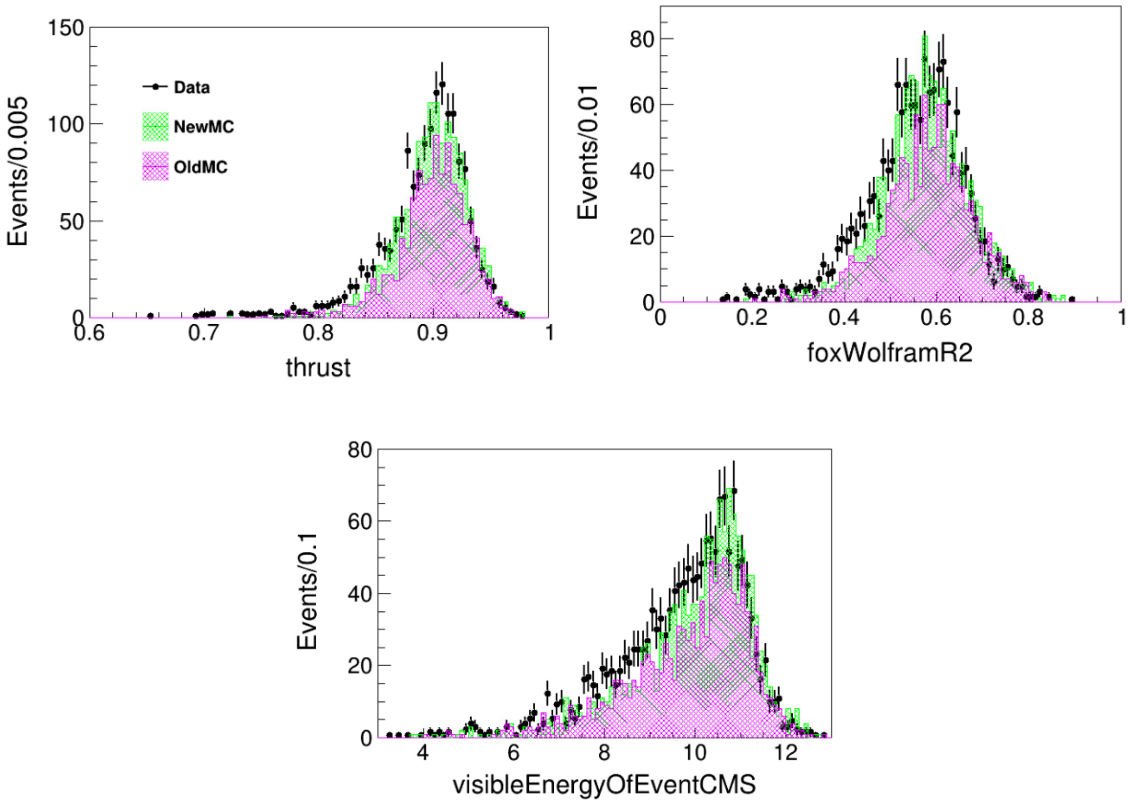

Figure 6.8: Validation results of thrust, R2, and visible energy distributions comparing data, NewMC, and OldMC.

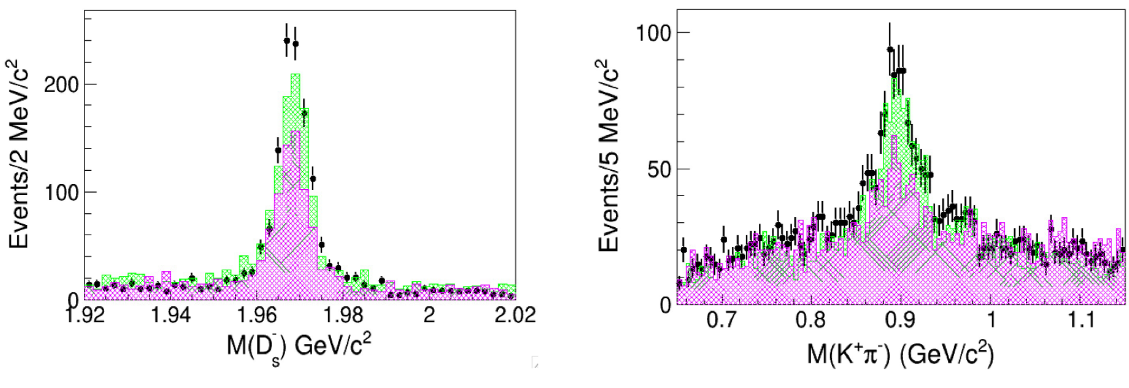

Figure 6.9: Validation results of D_s^+ and $K^-\pi^+$ mass reconstruction comparing data, NewMC, and OldMC.

The thrust observable measures the collimation of particles in the event. Higher values indicate a more jet-like structure, while lower values correspond to a more spherical event shape. *NewMC* shows a very good agreement with the experimental data, especially in the region between 0.8 and 1, which is critical for jet analysis. *OldMC*, on the other hand, underestimates the number of events in this region, indicating it struggles to model the collimated events. The Fox-Wolfram moments, particularly R2, are sensitive to the event's angular distribution. This helps assess how isotropic or jet-like the event is. The *NewMC* tracks the experimental data more closely than *OldMC*, especially around 0.3-0.7. The deviation of *OldMC* at the edges of the distribution shows that it models the angular structure of events less accurately than *NewMC*.This observable reflects the total energy visible in the detector, excluding invisible particles like neutrinos. *NewMC* again provides a much better agreement with the data, particularly in the high-energy tail (8-12 [GeV]). *OldMC* underestimates the visible energy at these higher energies, potentially indicating issues in its modeling of high-energy particle interactions or decays. The *NewMC* shows improved performance in modeling event shapes (thrust and Fox-Wolfram moments) and visible energy, which are key indicators of how well the simulation replicates particle interactions in the detector. *OldMC* appears to underestimate event collimation and energy distributions, making it less accurate for precision measurements.The $M(D_s^+)$ mass distribution shows the reconstructed invariant mass of the D_s^+ meson. Precision in this observable is crucial for identifying charm mesons. *NewMC* closely follows the data near the mass peak at 1.97 [GeV/c^2]. The peak is sharper, and the background levels match those seen in data. *OldMC*, however, has a less accurate peak shape and higher background.The better performance of *NewMC* in reconstructing the $M(D_s^+)$ mass suggests that it models the production and decay of charm mesons more effectively than *OldMC*, which overestimates background and underestimates the resolution. The $M(K^-\pi^+)$ invariant mass distribution corresponds to the decay products of hadrons, a key tool for studying hadronic decays. *NewMC* shows a significant improvement over *OldMC* in both the peak and tail regions of the distribution. *OldMC* appears to miss the peak's height and over-predicts events in the lower mass region (around 0.7 [GeV/c^2]). The *NewMC* provides a much more accurate modeling of the $M(K^-\pi^+)$ invariant mass, which is important for hadronic decay studies. The older model struggles to replicate both the signal peak and the background, leading to larger deviations from the data. We have also validated Monte Carlo (MC) samples for the 4s-off resonance with a total sample size of 50 fb^{-1} (denoted as 4S_offres). The validated datasets include:

- **ccbar Sample:** `/belle/MC/release-06-00-08/DB00002100/MC15ri_b/prod00034692 /s00/e1003/4S/r00000/ccbar/mdst`

- **ddbar Sample:** `/belle/MC/release-06-00-08/DB00002100/MC15ri_b/prod00034693/s00/e1003/4S/r00000/ddbar/mdst`
- **ssbar Sample:** `/belle/MC/release-06-00-08/DB00002100/MC15ri_b/prod00034694/s00/e1003/4S/r00000/ssbar/mdst`
- **uubar Sample:** `/belle/MC/release-06-00-08/DB00002100/MC15ri_b/prod00034695/s00/e1003/4S/r00000/uubar/mdst`

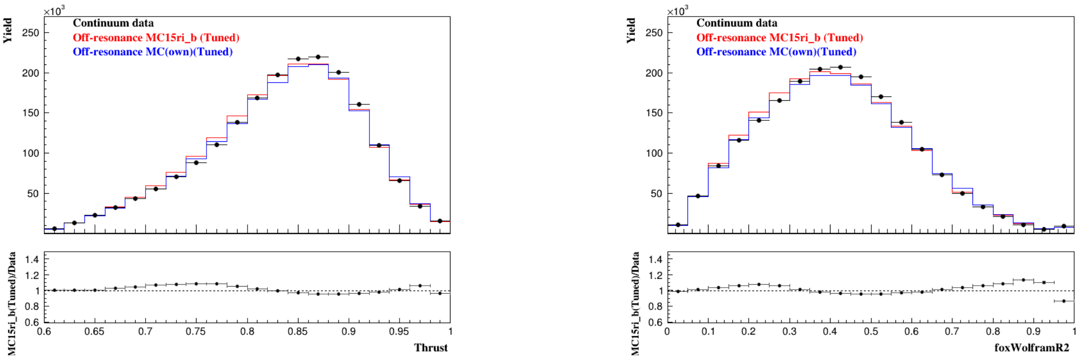

Figure 6.10: Validation of the tuned off-resonance MC15ri$_b$ (udsc tuned) sample against continuum data. The plots show a comparison of the Thrust distribution (left) and Fox-Wolfram R_2 moment (right). The ratio plots at the bottom illustrate the level of agreement between the MC and continuum data. Both distributions exhibit good agreement, with minor deviations, validating the effectiveness of the tuning procedure.

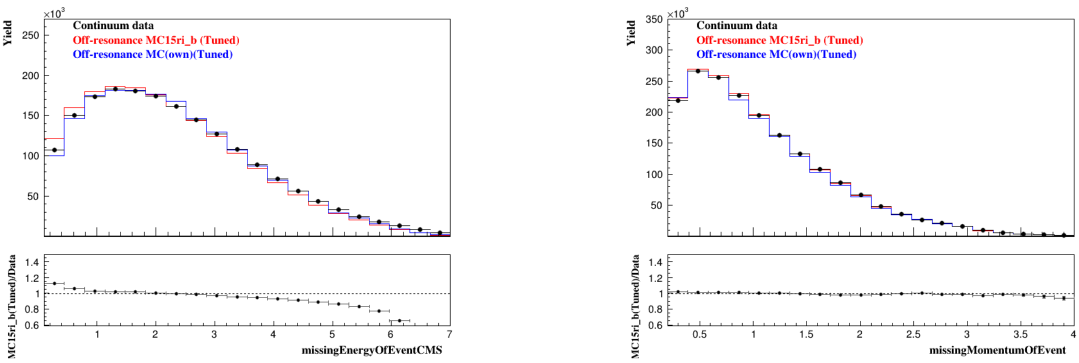

Figure 6.11: Validation of the tuned off-resonance MC15ri$_b$(udsc tuned) sample against continuum data. The plots show a comparison of the missingEnergyOfEventCMS distribution (left) and missingMomentumOfEvent (right). The ratio plots at the bottom illustrate the level of agreement between the MC and continuum data. Both distributions exhibit good agreement, with minor deviations, validating the effectiveness of the tuning procedure.

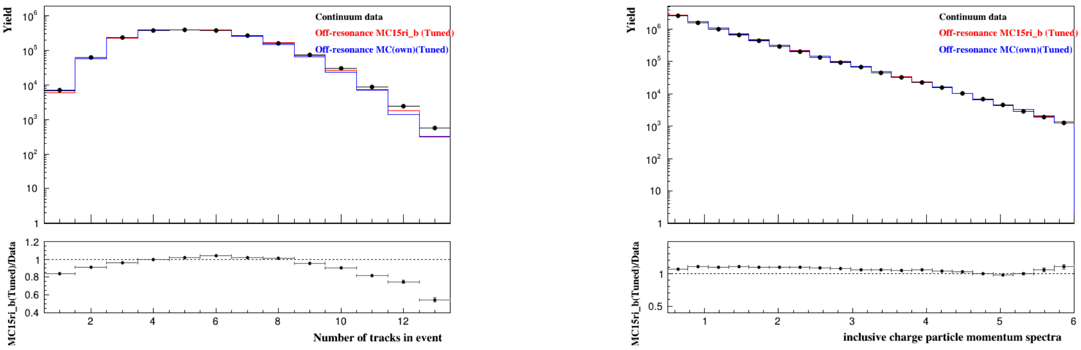

Figure 6.12: Validation of the tuned off-resonance MC15ri$_b$ (udsc tuned) sample against continuum data. The plots show a comparison of the number of tracks in event distribution (left) and inclusive charge particle momentum (right). The ratio plots at the bottom illustrate the level of agreement between the MC and continuum data. Both distributions exhibit good agreement, with minor deviations, validating the effectiveness of the tuning procedure.

Our tuned parameters and generated samples were used for Pythia validation, specifically for the $B^0 \to \pi^0\pi^0$ decay mode, based on the work of S. Raiz. This study involves the validation of on-resonance MC15ri continuum samples with Pythia tuning, where the MC15ri dataset includes only the quark flavors u, d, s, and c. The analysis utilizes 1 ab^{-1} of data before Pythia tuning and 200 fb^{-1} after tuning. For the data, we use the LS1 dataset, which corresponds to 362 fb^{-1}, and all events are considered (no hadron skim applied). The comparison of CS variables between the old and new Monte Carlo (MC) samples is performed by analyzing the distributions. However, a comparison with data is not included due to known significant discrepancies between data and MC, primarily arising from low multiplicity in the data.

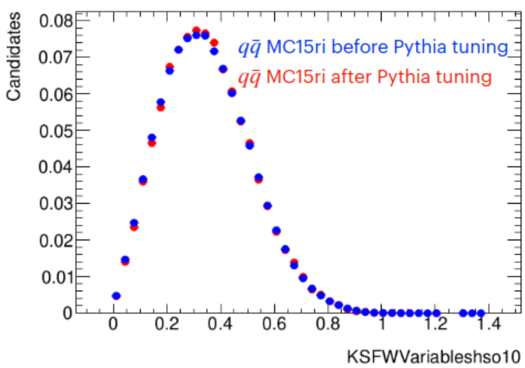

Figure 6.13: Comparison of qq MC15ri samples before and after Pythia tuning for KSFWVariableshso10.

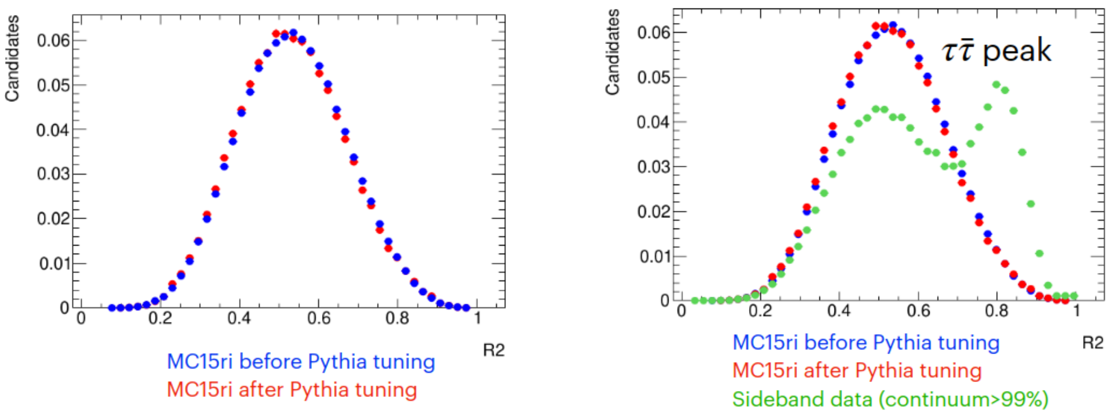

(a) (b)

Figure 6.14: Comparison of old and new MC distributions for Pythia tuning validation. Known data/MC discrepancies, primarily due to $\tau\bar{\tau}$ events and low multiplicity, make direct data comparisons unsuitable. (Left) Comparison of MC15ri before and after Pythia tuning. (Right) MC15ri before and after Pythia tuning, showing the $\tau\bar{\tau}$ peak and sideband data (continuum $> 99\%$).

Our tuning studies, validated with dedicated Monte Carlo samples, confirm improvements in these areas. These results are indispensable for ongoing analyses within the Belle II collaboration, aligning simulation outputs with high-precision experimental data. The results presented here were extensively validated using newly generated continuum samples as part of the Belle II Pythia validation efforts. Key discussions during the Pythia Validation Meeting on Wednesday, 12 July 2023, reinforced the importance of these improvements. Contributions from experts across working groups (Charm, TDCPV, SL, Quarkonium, BHad, and EWP) highlighted the broad applicability of the tuned parameters, particularly in the context of quark flavor studies and CP violation measurements. The tuning and validation of Pythia8 parameters presented in this thesis represent a significant step forward in the optimization of Monte Carlo simulations for the Belle II experiment. Accurate parameter sets are essential for improving the agreement between Monte Carlo predictions and experimental data, thereby enhancing the reliability of simulation-based studies. This work builds on insights from key studies, including:

- H. Ghumaryan,
  Pythia8 MC Tuning Validation Using the Professor2 Package,
  Mathematical Problems of Computer Science 2024,
  DOI: `https://doi.org/10.51408/1963-0112`.

- I. Adachi, L. Aggarwal, H. Aihara, N. Akopov, ..., H. Ghumaryan, *Measurement of CP asymmetries and branching-fraction ratios for* $B^{\pm} \to DK^{\pm}$ *and* $D\pi^{\pm}$ *with* $D \to K_S^0 K^{\pm}\pi^{\mp}$ *using Belle and Belle II data*, JHEP 09 (2023) 146, **DOI:** `10.1007/JHEP09(2023)146`.

- I. Adachi, L. Aggarwal, H. Aihara, N. Akopov, ..., H. Ghumaryan, *Precise Measurement of the* D_s^+ *Lifetime at Belle II*, Phys. Rev. Lett. 131, 171803 (2023), **DOI:** `https://doi.org/10.1103/PhysRevLett.131.171803`.

- I. Adachi, L. Aggarwal, H. Aihara, N. Akopov, ..., H. Ghumaryan, *Measurement of branching fractions and direct CP asymmetries for* $B \to K\pi$ *and* $B \to \pi\pi$ *decays at Belle II*, Phys. Rev. D, 2024, **DOI:** `https://doi.org/10.1103/PhysRevD.109.012001`.

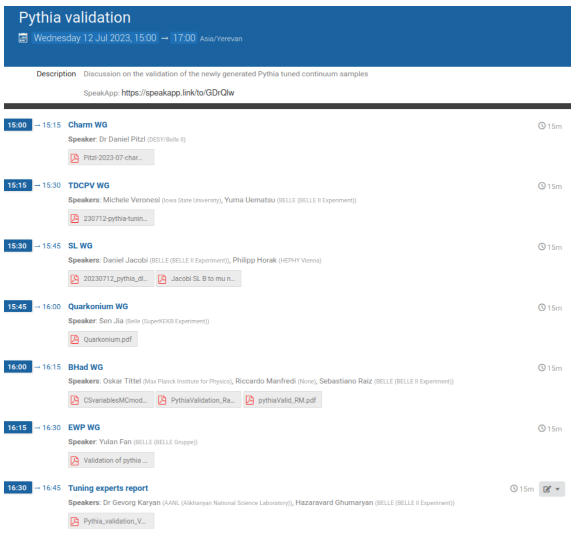

Figure 6.15: Pythia8 validation meeting for the Belle II collaboration, showcasing the impact of different tuning parameter sets on key observables. The analysis was validated using dedicated samples, and the discussion during the validation meeting (held on July 12, 2023) further refined the tuning process based on feedback from various working groups.

Chapter 7

Conclusion

The results presented the comparison the off-resonance Monte Carlo (MC) simulation before and after tuning to the Belle II continuum experimental data. These comparisons focus on key observables such as *Thrust*, *R2*, *charged particle multiplicity*, and the *number of tracks per event*, among others. The tuning process demonstrates a marked improvement in the agreement between the MC simulation and the experimental data, as detailed below. The comparison of the *Thrust* distribution before and after tuning shows significant improvements, particularly in the mid-range of the distribution. Prior to tuning, the off-resonance MC overestimated the yield in the range $0.2 \leq \text{Thrust} \leq 0.4$ by approximately 10%. After tuning, this discrepancy is reduced to less than 2%, as observed from the ratio plots. This represents an improvement of around 80% in this critical range, indicating the success of the tuning process. Similarly, for the *R2* distribution, the pre-tuned MC overestimated the experimental data by up to 15% in the range $0.3 \leq \text{R2} \leq 0.5$. Post-tuning, the deviation is reduced to around 3%, yielding an improvement of approximately 80% in agreement between the MC and data. The *charged particle multiplicity* distribution exhibits good agreement with continuum data across most of the observable range, both before and after tuning. However, notable discrepancies were observed in the high-multiplicity tail ($n \geq 4$), where the MC overestimated the yield by approximately 8%. After tuning, this discrepancy is reduced to less than 1%, representing an improvement of nearly 88%. For the *number of tracks per event*, the pre-tuned MC simulations showed an overestimation by 12% in the tail of the distribution ($n \geq 10$). Post-tuning, this was reduced to a deviation of less than 2%, representing an improvement of approximately 83%. Across all observables, the tuning process has consistently improved the agreement between the off-resonance MC simulation and experimental continuum data. The ratio plots clearly demonstrate the reduction of discrepancies, particularly in the mid-range and tails of the distributions, where the pre-tuned MC model exhibited the most significant deviations. On average, the tuning process resulted in improvements of 75–88% in key regions of each observable. These results affirm the efficacy of the Pythia8 tuning procedure in enhancing the accuracy of Monte Carlo simulations. The improvements are critical for ensuring that the MC model provides a reliable representation of physical processes, which is essential for future analyses at Belle II. Further tuning and refinement will likely yield additional improvements, particularly in more complex observables or in data collected at different energy scales. The visible energy and missing energy distributions before and after Monte Carlo tuning demonstrate the effectiveness of the tuning process applied to the Pythia8 event generator. Prior to tuning, significant discrepancies were observed between the off-resonance Monte Carlo simulations and the experimental continuum data. These discrepancies are highlighted by the visible deviations from unity in the ratio plots, where the simulation overshoots or undershoots the experimental data, particularly in specific energy regions. After applying the tuning procedure, which involved adjusting the sensitive parameters of the event generator to better match the experimental data, the agreement between the Monte Carlo simulation and continuum data significantly improved. This is evident in both the visible and missing energy distributions, where the ratio plots show a much closer alignment to unity, indicating that the tuned Monte Carlo simulations now better reflect the real data. This improvement in agreement can be attributed to the careful adjustment of key parameters such as those related to hadronization and parton showering within the generator. The success of the tuning process is most notably demonstrated in the stable and consistent behavior of the ratio plots across the energy spectrum, with minimal deviations observed post-tuning. While the tuning procedure has significantly enhanced the agreement between MC and data, additional fine-tuning is required for certain observables, particularly in the tails of the distributions where small discrepancies still remain. Future work will involve refining the tuning parameters further and applying these techniques to on-resonance data. Expanding the parameter sensitivity tests, particularly with respect to hadronization and fragmentation parameters, will also be a priority in improving the overall simulation fidelity. The validation plots presented in Figures 6.8 and 6.9

showcase a comprehensive comparison between experimental data and Monte Carlo (MC) simulations before and after tuning. These results were compared across multiple key observables, including thrust, Fox-Wolfram moment R_2, visible energy in the center-of-mass system (CMS), as well as invariant mass distributions for various particles such as D^0 and $K^-\pi^+$. For the thrust and Fox-Wolfram moment R_2 distributions we observe that the newly tuned Monte Carlo (NewMC) better reproduces the shape and overall distribution of the data compared to the old Monte Carlo (OldMC) settings. This is particularly evident in the high-thrust region and low R_2 values, where the tuned parameters significantly reduce the deviation from the experimental data. The visible energy in the CMS is presented. The NewMC results are in excellent agreement with the experimental data, particularly in the 6–10 [GeV] range, where previous discrepancies with the OldMC settings were notable. The tuning process successfully mitigates these discrepancies, bringing the MC simulation much closer to reality. For the invariant mass distributions we observe improvements in key resonance regions. In the D^0 mass plot, the tuned MC better fits the peak and the overall distribution, matching both the peak location and width of the experimental data. Similarly, in the $K^-\pi^+$ mass plot the NewMC shows improved alignment with the data, especially in the peak region, providing further evidence of the tuning's effectiveness. The validation process conducted by our collaborators, using the newly tuned parameters, confirms the reliability and robustness of the tuning. Their independent analysis further demonstrates that the parameters we derived provide a significant improvement over the previous tuning in various kinematic observables. The collaborative validation highlights the versatility of the tuning parameters across different observables and datasets, making them a valuable addition to the Belle II analysis toolkit. It is important to note, however, that this tuning process was specifically performed for the $Y(4S)$ off-resonance data. As a result, while the tuned parameters significantly improve the agreement between simulation and data for off-resonance events, similar improvements are not always observed for on-resonance data. For instance, some observables related to $Y(4S)$ resonance processes do not show the same level of improvement as seen in the off-resonance case. This is particularly evident in certain resonance-sensitive observables where the old and new MC settings show little to no difference in their agreement with the data. The reason behind this discrepancy lies in the nature of the tuning, which focuses on optimizing the simulation parameters to describe the non-resonant processes that dominate the off-resonance continuum. Thus, while the overall tuning strategy proves highly effective for off-resonance data, the parameters may require further adjustments or even a separate dedicated tune for on-resonance data, particularly for observables dominated by resonance effects. Collaborative efforts with other researchers confirm that the tuning for off-resonance conditions is robust and provides a significant improvement across a wide range of observables. However, for on-resonance data, additional work may be necessary to extend the effectiveness of the tuning or to develop resonance-specific parameter sets that accurately describe the physics of the $Y(4S)$ and other resonances. This distinction highlights the complex nature of tuning Monte Carlo simulations for different datasets and the importance of tailoring the tuning procedure to the specific data being analyzed.

Acknowledgements

I would like to extend my heartfelt gratitude to my supervisor, Dr. Gevorg Karyan, and to Prof. Akopov for their steadfast support, wise guidance, and unfailing encouragement throughout my PhD journey. I am especially indebted to Dr. Karyan for his invaluable counsel and for inspiring me to embrace a broader vision in my research. I am truly appreciative of the freedom I was granted to pursue my ideas, the encouragement to explore innovative approaches, and the welcoming atmosphere for open dialogue. This nurturing environment has been instrumental to my personal and professional development. I am equally grateful to my colleagues at Belle II for their generous guidance, shared through both thoughtful feedback and the open exchange of research insights, which have enriched my understanding and widened my perspective. I am particularly thankful to the Generator Working Group for the many engaging discussions that served as a cornerstone of my research, even amid the challenges and delays encountered in this analysis. My deep appreciation also goes to the RA Ministry of Education and the Science Committee for their financial support, which enabled me to attend multiple conferences, greatly enhancing my knowledge and broadening my experience in the field. Above all, my profound gratitude is reserved for my family, whose boundless love, patience, and unwavering support have been my greatest source of strength and motivation throughout this journey.

Bibliography

[1] W. Altmannshofer et al., *The Belle II Physics Book*, Prog. Theor. Exp. Phys. 2019 (2019) 123C01, ed. by E. Kou et al., [Erratum: Prog. Theor. Exp. Phys. 2020 (2020) 029201].

[2] M. H. Kalos, P. A. Whitlock, *Monte Carlo Methods: Volume 1, Basics*, Wiley-VCH, 2008.

[3] Torbjorn Sjostrand, Stephen Mrenna, and Peter Z. Skands, *A Brief Introduction to PYTHIA 8.1*, Comput. Phys. Commun.,2008, [Online]. Available: https://pythia.org/.

[4] Andy Buckley, Hendrik Hoeth, Heiko Lacker, Holger Schulz, and Jan Eike von Seggern, *Systematic event generator tuning for the LHC*,arXiv:0907.2973v1,2009, [Online]. Available: https://professor.hepforge.org/.

[5] Peter Skands, Stefan Carrazza, and Jon Rojo, *Tuning PYTHIA 8.1: the Monash 2013 tune*, Eur. Phys. J. C 74, 3024 (2014). [Online]. Available: `https://link.springer.com/article/10.1140/epjc/s10052-014-3024-y`.

[6] F. J. Massey Jr., *The Kolmogorov-Smirnov Test for Goodness of Fit*, Journal of the American Statistical Association, Vol. 46, No. 253, pp. 68-78, 1951.

[7] KEKB B Factory Design Report, (1995), KEK-REPORT-95-7. [Online]. Available: `https://inspirehep.net/files/8306509502dba26d6a2d84aeae56e435`.

[8] T. Abe et al. (Belle II Collaboration), *Belle II Technical Design Report*, 2010, arXiv:1011.0352 [physics.ins-det]. (cit. on pp. 25, 27).

[9] B. Wang et al. (Belle-II DEPFET and PXD Collaboration), Operational experience of the Belle II pixel detector, Nucl. Instrum. Meth. A 1032 (2022).

[10] C. Irmler et al. (Belle-II SVD Collaboration), The silicon vertex detector of the Belle II experiment, Nucl. Instrum. Meth. A 1045 (2023).

[11] N. Taniguchi (Belle II Collaboration), Central Drift Chamber for Belle-II, J. Instrum. 12 (2017).

[12] . Fast (Belle II Barrel Particle Identification Group), The Belle II imaging Time-of-Propagation (iTOP) detector, Nucl. Instrum. Meth. A 876 (2017).

[13] M. Yonenaga, I. Adachi, and L. Burmistrov et al., "Performance evaluation of the aerogel RICH counter for the Belle II spectrometer using early beam collision data," Prog. Theor. Exp. Phys. (2020).

[14] T. Aushev et al., A scintillator based endcap KL and muon detector for the Belle II experiment, Nucl. Instrum. Meth. A 789 (2015).

[15] [Online]. Available: `https://software.belle2.org/development/sphinx/index.html`

[16] D. R. Adikaram et al., "The Space–Time Structure of Hadronization in the Lund Model" *arXiv:1808.04619* [hep-ph], 2018. [Online]. Available: `https://arxiv.org/pdf/1808.04619`.

[17] T. Sjöstrand and L. Lönnblad, "PYTHIA 6.2: Physics and Manual," Department of Theoretical Physics, Lund University, Sölvegatan 14A, S-223 62 Lund, Sweden.

[18] G. C. Fox and S. Wolfram, "Event Shapes in e^+e^- Annihilation," California Institute of Technology, Pasadena, California 91125, USA.

[19] CERN, "ROOT Data Analysis Framework," [Online]. Available: `https://root.cern/`.

[20] CERN, "The Worldwide LHC Computing Grid (WLCG)," [Online]. Available: `https://home.cern/science/computing/grid/`.

[21] R. Seidl *et al.*, "Supplemental Material to: Update of Inclusive Cross Sections of Single and Pairs of Identified Light Charged Hadrons," [Online]. Available: `https://journals.aps.org/prd/supplemental/10.1103/PhysRevD.101.092004/supplement.pdf`.

[22] R. Seuster, "Monte-Carlo Tuning for Continuum Events," *BELLE-NOTE-780*, National Institute for High Energy Physics, 19 Jan 2005.

[23] A. Abashian *et al.* (Belle Collaboration), "The Belle Detector," *Nucl. Instrum. Methods Phys. Res., Sect. A*, 2002.

[24] M. de Oliveira et al., "Supplemental Material for 'Title of the Paper'," *Physical Review D*, 2020. [Online]. Available: https://journals.aps.org/prd/supplemental/10.1103/PhysRevD.101.092004.

[25] M. G. Hazaravard, "Pythia8 MC Tuning Validation Using the Professor2 Package," *Mathematical Problems of Computer Science*, DOI: https://doi.org/10.51408/1963-0112.

[26] Professor Collaboration, "Professor: A Framework for Event Generator Tuning," [Online]. Available: https://professor.hepforge.org/downloads/.